

Garnet-Type Solid-State Electrolytes: Materials, Interfaces, and Batteries

Chengwei Wang,[¶] Kun Fu,[¶] Sanoop Palakkathodi Kammampata, Dennis W. McOwen, Alfred Junio Samson, Lei Zhang, Gregory T. Hitz, Adelaide M. Nolan, Eric D. Wachsman, Yifei Mo, Venkataraman Thangadurai,^{*} and Liangbing Hu^{*}



Cite This: *Chem. Rev.* 2020, 120, 4257–4300



Read Online

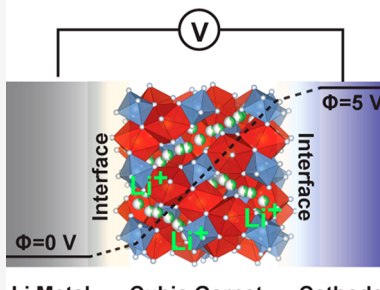
ACCESS |

Metrics & More

Article Recommendations

ABSTRACT: Solid-state batteries with desirable advantages, including high-energy density, wide temperature tolerance, and fewer safety-concerns, have been considered as a promising energy storage technology to replace organic liquid electrolyte-dominated Li-ion batteries. Solid-state electrolytes (SSEs) as the most critical component in solid-state batteries largely lead the future battery development. Among different types of solid-state electrolytes, garnet-type Li₇La₃Zr₂O₁₂ (LLZO) solid-state electrolytes have particularly high ionic conductivity (10^{-3} to 10^{-4} S/cm) and good chemical stability against Li metal, offering a great opportunity for solid-state Li-metal batteries. Since the discovery of garnet-type LLZO in 2007, there has been an increasing interest in the development of garnet-type solid-state electrolytes and all solid-state batteries. Garnet-type electrolyte has been considered one of the most promising and important solid-state electrolytes for batteries with potential benefits in energy density, electrochemical stability, high temperature stability, and safety. In this Review, we will survey recent development of garnet-type LLZO electrolytes with discussions of experimental studies and theoretical results in parallel, LLZO electrolyte synthesis strategies and modifications, stability of garnet solid electrolytes/electrodes, emerging nanostructure designs, degradation mechanisms and mitigations, and battery architectures and integrations. We will also provide a target-oriented research overview of garnet-type LLZO electrolyte and its application in various types of solid-state battery concepts (e.g., Li-ion, Li–S, and Li–air), and we will show opportunities and perspectives as guides for future development of solid electrolytes and solid-state batteries.

Garnet-Based Solid-State Batteries



Li Metal Cubic Garnet Cathode

CONTENTS

1. Introduction	4258
2. Fundamentals of Garnet-Type Solid-State Electrolytes	4259
2.1. Overview of Solid-State Electrolytes and Recent Development of Garnet-Type Solid-State Electrolytes	4259
2.2. Design Principle of Garnet-Type Solid-State Electrolytes	4261
2.3. Li-Ion Conduction Mechanism in Garnet-Type Solid-State Electrolytes	4262
2.4. Li-Ion Conductivity of Bulk and Thin-Film Garnet-Type Oxides	4263
2.5. Mechanical Properties of Garnet-Type Oxides	4264
3. Chemical and Electrochemical Stability of Garnet-Type Solid-State Electrolytes	4265
3.1. Chemical and Electrochemical Stability of Garnet-Type Electrolytes	4265
3.2. Chemical and Electrochemical Stability with Anode Materials	4266

3.3. Chemical and Electrochemical Stability with Cathode Materials (Conversion Cathodes; Intercalation Cathodes)	4266
3.4. Chemical and Electrochemical Stability with Liquid Electrolytes (Organic Electrolytes; Aqueous Electrolytes)	4268
4. Interface Challenges in Solid-State Electrolytes and Electrodes	4269
4.1. Strategies to Address Interfacial Challenges	4269
4.1.1. Artificial Solid–Electrolyte Interface	4269
4.1.2. Nanoscale Interfacial Engineering	4270
4.1.3. Emerging Processing Techniques	4271
4.2. Characterization Techniques for Garnet-Based Solid-State Batteries	4272
4.2.1. EIS Analysis (AC)	4272

Received: July 3, 2019

Published: April 9, 2020



4.2.2. Symmetric Li Cycling (DC)	4273
4.2.3. Solid-State Li Nuclear Magnetic Resonance (NMR) Study	4273
4.2.4. <i>In Situ</i> Characterizations	4274
5. Emerging Nanostructured Solid Electrolyte Design	4275
5.1. Nanogarnet Solid Electrolyte Synthesis	4275
5.2. Transport Mechanism in Garnet-Based Composite Electrolytes	4276
5.3. Nanostructure Design toward Flexibility and High Conductivity	4278
6. Batteries Using Solid-State Electrolytes	4279
6.1. Architectures	4279
6.1.1. Thin Film Planar Structure	4279
6.1.2. Ordered LLZO Scaffold Structure	4279
6.1.3. Random LLZO Scaffold Structure	4280
6.2. Degradation and Failure: Mechanisms, <i>In Situ/Ex Situ</i> Characterizations, and Mitigations	4283
6.2.1. Failure Modes and Causes	4283
6.2.2. Plating through Existing Pores (Pinholes or Other Physical Flaws)	4283
6.2.3. Plating through Grains (Decomposition or Mechanical Failure of Material)	4284
6.2.4. Plating through Grain Boundaries (Decomposition or Mechanical Failure of Grain Boundary)	4284
6.2.5. Electronic Conduction through Material (Breakdown of Material)	4284
6.2.6. Electronic Conduction through Grain Boundaries (Breakdown of Grain Boundary)	4284
6.2.7. Cracking of Ceramic Separator (Mechanical Failure of Material or Grain Boundary)	4284
6.3. Proof-of-Concept Batteries with Garnet Electrolyte	4285
6.3.1. Oxide Cathodes	4286
6.3.2. Sulfur Cathode	4286
6.3.3. Oxygen/Air Cathode	4289
7. Conclusions and Future Perspective	4290
Author Information	4291
Corresponding Authors	4291
Authors	4291
Author Contributions	4291
Notes	4291
Biographies	4291
Acknowledgments	4292
References	4292

1. INTRODUCTION

Advanced energy storage technologies with high energy, good safety, and low cost have been facing promising opportunities and unprecedented challenges. Traditionally, lithium-ion battery technology has been widely used and almost dominated every aspect of our e-life including portable electronics and electric vehicles. With the increasing demand and deployment of batteries, great attention has been paid to achieving battery technologies with higher energy and power densities, better safety, and lower cost.^{1–3} Current lithium-ion battery technology has almost reached its limit in terms of capacity, energy density, cycle life, and safety. In a lithium-ion system,

liquid electrolyte provides a high ionic conductivity and good wetting for electrodes, but the complexity of electrolyte constituents including salts, multiple solvents, and additives inevitably produces many challenges closely related to their unstable components. Those challenges are, for example, solid–electrolyte interphase (SEI), electrode dissolution and corrosion, and electrolyte flammability. All these challenges limit the further development of high energy batteries, with safer fabrication and operation, and low-cost manufacturing technology. Since so many challenges have been identified in liquid electrolyte-based lithium-ion battery chemistry, it motivates us to explore beyond lithium-ion battery technology and focus on nonliquid electrolytes to achieve high energy, good safety, and low cost for future battery technology and deployment.

In this scenario, solid-state battery technology shows its promising position as an advanced technology to outperform current lithium-ion battery technology in the three aspects of merit (energy density, safety, and cost).^{4,5} Solid-state batteries are designed using solid electrolytes instead of liquid electrolytes. The solid electrolyte is either a solid polymer, inorganic solid, or a hybrid, to carry out ion transport and maintain the overall electrochemical and mechanical stability. Since solid-state battery technology largely relies on the solid electrolyte, in the past decades, extensive research activities have been carried out experimentally and computationally to explore new types of solid electrolytes, fundamentally investigate their ion transport mechanism, electrochemical stability window, and mechanical properties, and find ways to improve performances.⁶ Therefore, the development of solid-state batteries is naturally emphasized on the exploration and optimization of suitable solid electrolytes to match with desirable electrodes and electrochemistry.

In solid-state battery design, the prerequisite for selecting a good solid electrolyte is high ionic conductivity,⁷ a large electrochemical window, good chemical stability with both cathode and anode materials, and good mechanical properties.^{1,8} On the basis of these considerations, most of the current well-studied solid electrolytes could possibly be excluded due to the difficulty of meeting all the three criteria. Among the inorganic solid–electrolyte materials, which range from sulfides to oxides and oxynitrides, they either have a relatively low ionic conductivity, exhibit an unstable interface against electrodes resulting in a low electrochemical window, or show an impractical and unscalable synthesis and battery fabrication pathway. Even for solid polymer electrolytes, a very narrow selection of polymers can be used to allow fast ion transport, the mechanical performance and ionic conductivity are always a pair of counteractions, and the low lithium-ion transference number is usually actively neglected in most of research work.⁹ Although extensive work has been carried out with great efforts to reach every aspect of solid electrolyte studies, it is a great challenge to decide which electrolyte is more appropriate for solid battery application. $\text{Li}_{10}\text{GeP}_2\text{S}_{12}$ (LGPS), a sulfide-type material, has a high ionic conductivity (10^{-2} S/cm), but is highly sensitive to moisture and is unstable against Li metal anodes. $\text{Li}_x\text{La}_{2/3-x}\square_{(1/3)-2x}\text{TiO}_3$ ($0 < x < 0.16$) (LLTO) has a high bulk ionic conductivity (10^{-3} S/cm)^{10,11} but is not suitable for Li metal as well. $\text{Li}_x\text{PO}_y\text{N}_z$ ($x = 2y + 3z - 5$) (LiPON) has a good stability with Li metal by forming a protection layer at the interface but exhibits a low ionic conductivity (10^{-6} S/cm).¹² $\text{Li}_6\text{PS}_5\text{X}$ ($\text{X} = \text{Cl, Br, I}$), an argyrodite lithium superionic conductor, has a high ionic conductivity (10^{-2} – 10^{-3} S/cm) but tends to easily form an interface when it is in contact with Li or different cathode materials.¹³ Moreover, materials synthesis

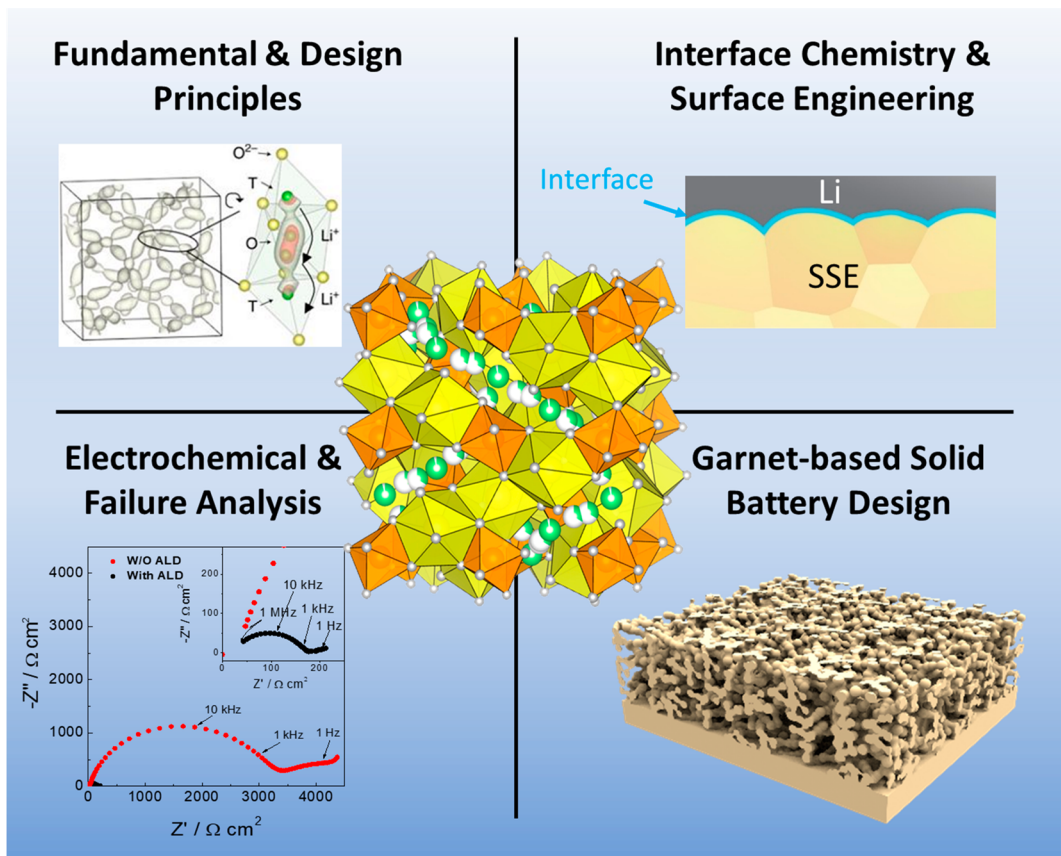


Figure 1. Overview of opportunities and challenges in garnet-type LLZO solid electrolyte and batteries, including fundamentals and design principles for garnet-type solid electrolytes, their interface chemistry and stability with electrodes as well as surface engineering strategies, electrochemical evaluation and failure analysis, and battery structural design based on garnet-type solid electrolytes for high energy and high power. Reproduced with permission from refs 22, 23, and 24. Copyright 2017 Springer Nature. Copyright 2017 Royal Society of Chemistry.

strategies and battery processing are critical factors that should be taken into consideration for solid-state battery development. Therefore, selecting a proper electrolyte to study and focus on with a series of continued research activities becomes important.

Among the different types of solid-state electrolytes, recent development of garnet-type $\text{Li}_7\text{La}_3\text{Zr}_2\text{O}_{12}$ (LLZO) solid-state electrolytes has emerged as the most promising solid electrolyte, with a high ionic conductivity (10^{-4} to 10^{-3} S/cm),¹⁴ good stability against Li metal, large electrochemical window, and easy ambient environment handling, offering a great opportunity for solid-state batteries.^{15–17} Since its discovery in 2007, there has been an increasing interest in the development of LLZO garnet-type solid-state electrolytes. Garnet-type LLZO electrolyte has been considered one of the most promising and important solid-state electrolytes for batteries with potential benefits in energy density, electrochemical stability, temperature stability, and safety. Recently, studies about garnet-type LLZO solid-state electrolytes, such as synthesis strategies and modifications, stability of garnet solid electrolytes/electrodes, degradation mechanisms and mitigations, and battery architectures and integrations, have been extensively reported.^{18–21} Therefore, it is important and timely to review the recent development of garnet solid electrolytes and batteries, discuss their challenges and opportunities, and provide a perspective as a guide for future development of solid electrolytes and solid-state batteries.

In this Review, we will survey the fundamentals of garnet-type solid electrolytes, including the history and recent development of garnet-type solid electrolytes, and their design principles to

guide the future electrolyte development (Figure 1). We will show the Li-ion conduction mechanism and the relationship of chemical composition and structure in garnet-type oxide materials. We will discuss the mixed electronic/ionic conductor concept and design, and the mechanical properties of garnet-type electrolytes. Second, we will show the chemical and electrochemical stability of garnet-type solid electrolytes, mainly focusing on the stability with different types of anode and cathode materials and liquid electrolytes including organic and aqueous electrolytes. Third, we will discuss the origin and computational studies of the interfacial challenges derived from garnet-type solid electrolytes and show strategies to address interfacial challenges and corresponding characterization techniques. Fourth, we will discuss the recent emerging nanostructured solid electrolyte design principle, synthesis methods, and ion transport mechanism. Fifth, we show how garnet-type solid electrolyte functions in a full battery, discuss the degradation and failure mechanism and analysis, and the solid-state battery design for $\text{Li}-\text{S}$ and $\text{Li}-\text{O}_2$ concept. In the end, we provide perspective and discuss opportunities for solid electrolyte and battery development.

2. FUNDAMENTALS OF GARNET-TYPE SOLID-STATE ELECTROLYTES

2.1. Overview of Solid-State Electrolytes and Recent Development of Garnet-Type Solid-State Electrolytes

Solid-state ionics (SSI) is a multidisciplinary research area concerned with the rapid transport of mobile ions and mixed

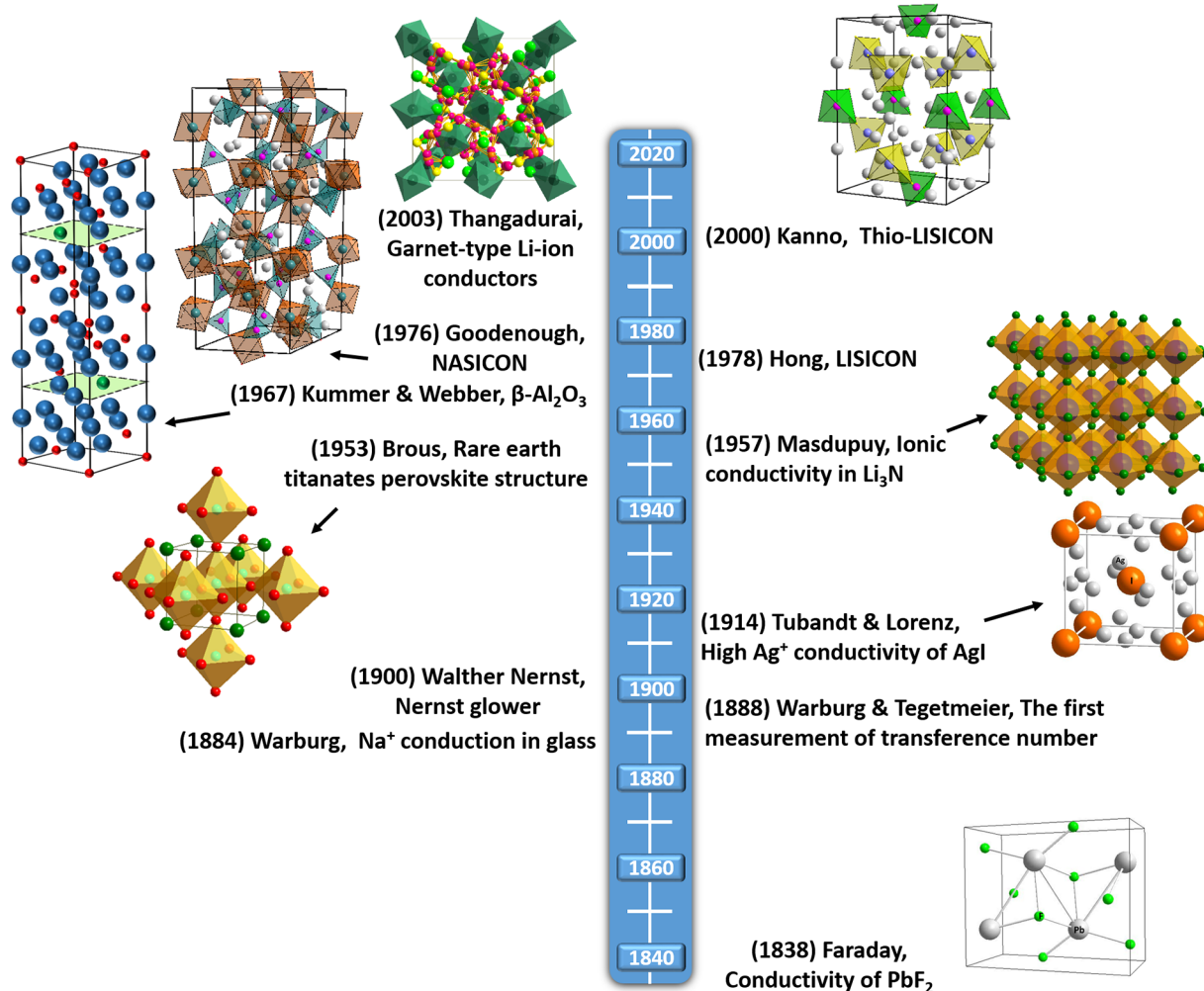


Figure 2. Historical development of solid electrolytes.

ions and electrons in solid materials and their physical and chemical properties. The term SSI was first introduced by Takahashi in the early 1970s;²⁵ however, the phenomenon was known since early 1800 when Michael Faraday discovered mass transport in Ag_2S and PbF_2 .^{26,27} Funke²⁷ and Yamamoto²⁵ have reviewed the development of solid-state ionics in the European and Japanese perspective, respectively. Faraday observed an exponential increase in conductivity with increasing temperature in Ag_2S .²⁸ In the study of ionic conductors, the attainment of good Na^+ ion mobility in a glass by Warburg²⁹ and the first Na^+ ion transference number measurements by Warburg and Tegetmeier³⁰ are significant contributions.

In 1897, Walther Nernst made fundamental contributions by deriving the Nernst equation and detecting ionic conduction in aliovalent-doped zirconia.³¹ Nernst utilized his findings in developing the Nernst lamp by using yttria-stabilized zirconia (YSZ) as the filament.^{27,31} The more efficient tungsten filament lamps later replaced these lamps. Although Nernst realized the mass transport in zirconia, he could not have possibly known the structural details of the material and the transport mechanism, as these came to be known only decades later when Wagner illustrated the underlying mechanism of oxygen ion conduction in doped ZrO_2 using oxygen concentration EMF measurements in 1943.^{27,32}

Another key milestone in SSI was the discovery of the surprising properties of $\alpha\text{-AgI}$ by Tubandt and Lorenz at Halle in

1914.³³ During 1930s, Tubandt observed ionic conductivity of several metal halides by using new experimental methods to measure the ionic and electronic contributions to conductivity. Tubandt used electrodes that allowed the inward and outward movement of mobile ion(s) through the sample and determined the total current that passed through the sample using simple DC measurements and thus estimated electronic contribution to the total conductivity. The number of ions that were transferred through AgI was measured by the change in masses of the two electrodes and thereby determined ionic contributions to the conductivity.

In 1925, Frenkel suggested two basic diffusion mechanisms through interstitials and vacancies separately assuming the presence of point defects.³⁴ During 1920–1930, the concept of point defects was established by Frenkel, Walter Schottky, and Carl Wagner including the development of point-defect thermodynamics by Schottky and Wagner^{35,36} that helped in visualizing ionic and electronic transport in solids. In 1950s, there were a number of contributions from Wagner, which included the Hebb-Wagner direct-current polarization technique in which a blocking electrode is capable of distinguishing the partial ionic and electronic current carriers in predominantly ionic conducting solids.^{37,38} This method is still being used to determine the ionic and electronic conductivity of a wide range of solid electrolytes.^{39–42} In 1957, Kiukkola and Wagner

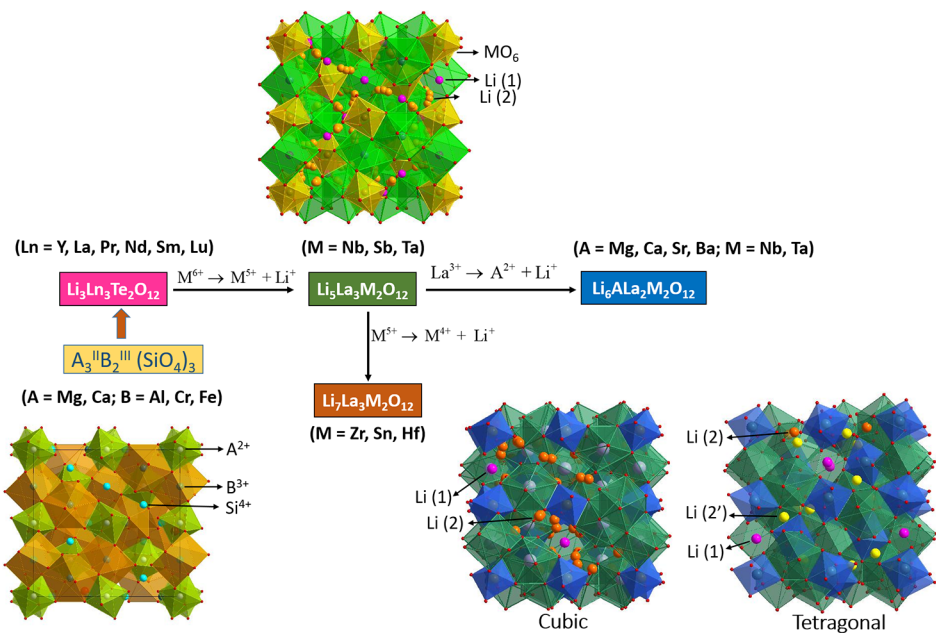


Figure 3. Different chemical compositions possible in garnet-type Li-ion conductors.

used solid electrolyte-based electrochemical sensors and conducted extensive potentiometric measurements.⁴³

In the 1960s, silver ion conducting solids such as $\text{Ag}_3\text{Si}_{11}$ and RbAg_4I_5 were introduced, and their use in electrochemical cells was demonstrated by Takahashi and Yamamoto,⁴⁴ and Argue and Owens, respectively.^{45,46} Takahashi et al. synthesized a Cu^+ ion super conductor, $\text{Rb}_4\text{Cu}_{16}\text{I}_7\text{Cl}_{13}$, with the highest room temperature ionic conductivity (0.34 S/cm) ever observed among solid electrolytes.⁴⁷ Yao and Kummer discovered high ion mobility in alkali metal substituted β -alumina in 1967.⁴⁸ Kummer and Weber successfully applied Na- β -alumina in Na-S batteries.⁴⁹ The discovery of β -alumina led to the synthesis of newer superionic conductors such as gallates (Al replaced by Ga) and ferrites (Al replaced by Fe).^{50,51}

In 1976, Goodenough and Hong reported a sodium super ionic conductor, now popularly known as NASICON.^{52,53} They synthesized a compound with the general formula $\text{Na}_{1+x}\text{Zr}_2\text{P}_{3-x}\text{Si}_x\text{O}_{12}$, where $0 < x < 3$, in which $\text{Na}_3\text{Zr}_2\text{PSi}_2\text{O}_{12}$ showed the highest conductivity, 0.2 S/cm at 300 °C, which is comparable to Na- β -alumina. Hong demonstrated the possibility of ionic substitutions in NASICON (with elements like Li, Ag, and K), and this led to the synthesis of a large number of compounds.⁵³

Because of the small ionic radii of the Li^+ ion and its lower weight, lithium-ion conductors gained increased attention since the 1970s. The ionic conductivity of single and polycrystalline lithium nitride was reported during the late 1970s.⁵⁴ Incorporation of Al_2O_3 into LiI showed a conductivity which is 50-times higher than that of LiI alone.⁵⁵ In 1980, Alan et al. demonstrated the use of LiI as the electrolyte in cardiac pacemakers.⁵⁶ Hong⁵⁷ developed another class of lithium super ionic conductor called LISICON with general formula $\text{Li}_{16-2x}\text{M}_x(\text{TO}_4)_4$, where M is a divalent cation (M = Mg^{2+} , Zn^{2+}), T is a tetravalent cation (T = Si^{4+} , Ge^{4+}), and $0 < x < 4$.

In 2000, Kanno et al. introduced another lithium-ion conductor, thio-LISICON, and $\text{Li}_{3.25}\text{Ge}_{0.25}\text{P}_{0.75}\text{S}_4$ showed the highest conductivity in the series.⁵⁸ The lithium-ion conductivity of garnet type $\text{Li}_5\text{La}_3\text{M}_2\text{O}_{12}$ (M = Ta, Nb) was

reported in 2003 by Thangadurai et al.⁵⁹ The main advantage of garnet type electrolytes is that they can directly contact Li metal without any damage. Another class of solid electrolytes called Li-rich antiperovskite was reported by Zhao et al. in 2012.⁶⁰ In this series, $\text{Li}_3\text{OCl}_{0.5}\text{Br}_{0.5}$ showed a room temperature conductivity of 1.94×10^{-3} S/cm. In the last few decades, there has been immense progress in discovering and exploring novel solid electrolytes, particularly in advanced solid-state battery systems, fuel cells, and sensors and this progress is given in the Figure 2.

2.2. Design Principle of Garnet-Type Solid-State Electrolytes

Garnet-type Li-ion conductors have been intensively studied as solid electrolytes for LIBs following the first report by Thangadurai et al.⁵⁹ Garnet-type electrolytes are considered as the prospective electrolytes for all-solid-state LIBs due to their stability toward Li metal, wide electrochemical stability window (>6 V vs Li/ Li^+ from CV studies and ~3 V from computational analyses), and high ionic conductivity.^{12,17,61,62} Ideal garnets are a group of orthosilicates having the general formula of $\text{A}_3^{\text{II}}\text{B}_2^{\text{III}}(\text{SiO}_4)_3$ (A = Ca, Mg; B = Al, Cr, Fe) where A, B, and Si cations occupy the eight, six, and four coordination sites, which generally crystallize in cubic structure (space group $I\bar{a}3d$).^{17,63} Li containing garnets $\text{Li}_x\text{M}_2\text{M}'_3\text{O}_{12}$ are derived from the structural prototype $\text{Ca}_3\text{Al}_2\text{Si}_3\text{O}_{12}$. Each unit formula of $[\text{Ca}_3][\text{Al}_2](\text{Si}_3)\text{O}_{12}$ consists of two octahedral AlO_6 , three antiprismatic CaO_8 , and three tetrahedral SiO_4 polyhedra. The analogous Li containing garnet-type structure is $\text{Li}_3\text{La}_3\text{Te}_2\text{O}_{12}$ where Li replaces the tetrahedral Si^{4+} .⁶⁴ However, $\text{Li}_3\text{La}_3\text{Te}_2\text{O}_{12}$ exhibits poor Li-ion conductivity. Therefore, it is required to increase the Li content, forming the so called “Li-stuffed” garnet compositions. Various chemical compositions possible in a garnet-type structure by doping at different sites are shown in Figure 3.

Garnet-type electrolytes can be classified into four different subtypes, Li3, Li5, Li6, and Li7. The general trend is that the ionic conductivity of Li containing garnets increases almost exponentially with Li content in a wide Li content scale. To examine the relationship between Li site occupation and Li-ion

conductivity, O'Callaghan et al. developed garnet-type $\text{Li}_3\text{Ln}_3\text{Te}_2\text{O}_{12}$ ($\text{Ln} = \text{Y, Pr, Nd, Sm-Lu}$).⁶⁵ It was suggested that Li ions in $\text{Li}_3\text{Ln}_3\text{Te}_2\text{O}_{12}$ are located solely in the tetrahedral sites. These compounds showed a low ionic conductivity with a high activation energy proposing that these Li ions at tetrahedral positions are less mobile. Partial substitution of the trivalent La^{3+} with divalent ions in $\text{Li}_5\text{La}_3\text{M}_2\text{O}_{12}$ results in Li_6 phase, and the general formula can be represented as $\text{Li}_6\text{ALa}_2\text{M}_2\text{O}_{12}$ ($\text{A} = \text{Mg, Ca, Sr, Ba, and M = Nb, Ta}$).⁴⁰ Murugan et al. synthesized the cubic-structured $\text{Li}_7\text{La}_3\text{Zr}_2\text{O}_{12}$ in 2007, which has the highest conductivity of $3 \times 10^{-4} \text{ S/cm}$ and the lowest activation energy of 0.3 eV for garnet structure materials.⁶¹ The Li_7 phase is obtained by replacing M with Zr in $\text{Li}_5\text{La}_3\text{M}_2\text{O}_{12}$ along with excess Li^+ stuffing for charge balancing.

2.3. Li-Ion Conduction Mechanism in Garnet-Type Solid-State Electrolytes

The crystal structure and Li-ion transport properties of Li-stuffed garnet-type oxides have been reviewed by Cussen in 2010, and it was confirmed that cubic garnet has a space group $Ia\bar{3}d$.⁶⁶ Using neutron diffraction studies, Cussen confirmed that Li-ions in garnet structures are distributed in three different interstitial sites, namely, (i) tetrahedral (24d), (ii) octahedral (48g), and (iii) off-centered octahedral (96h). In Li_3 phases, all Li-ions are tightly bound to the tetrahedral (24d) positions. Figure 4 shows the variation of Li occupancy of tetrahedral and

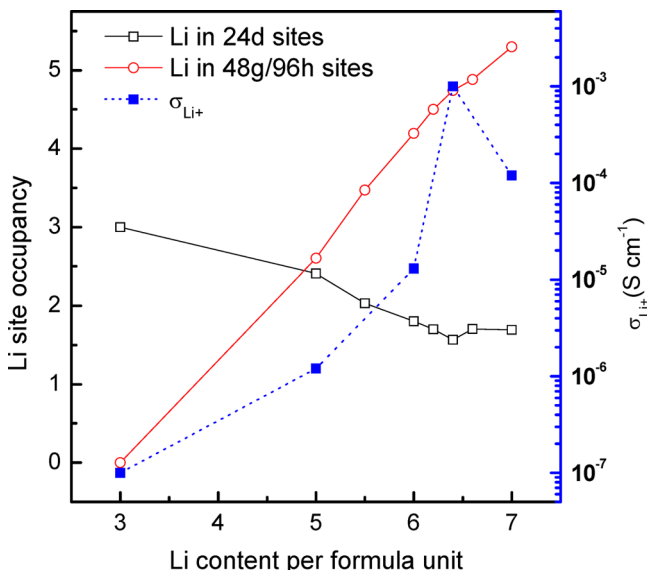


Figure 4. Variation of Li occupancy of tetrahedral and octahedral sites and room temperature conductivity as a function of Li content in the garnet structure. Reproduced with permission from ref 17. Copyright 2014 Royal Society of Chemistry.

octahedral sites and room temperature conductivity as a function of Li concentration in cubic garnets.^{17,66} The Li-stuffed garnets, such as Li_5 , Li_6 , and Li_7 (cubic) subtypes, have Li content higher than three per unit formula. The excess Li-ions are incorporated into the octahedral sites, resulting in tetrahedral vacancy formation. Li^+-Li^+ interaction due to the increased octahedral population displaces Li-ions at central octahedral 48g site to off-centered 96h site near the opposite face, which is shared with the adjacent tetrahedra.⁶⁶ As shown in Figure 4, the ionic conductivity of lithium-stuffed garnets increases exponentially as lithium content increases. From the neutron diffraction studies, it has been shown that the maximum

Li content in a cubic garnet phase can reach 7.5 per formula. However, the highest Li-ion conductivity has been achieved at a Li content of 6.4 ± 0.1 .^{67,68}

$\text{Li}_7\text{La}_3\text{Zr}_2\text{O}_{12}$ crystallizes in two stable phases: a cubic phase with a space group $Ia\bar{3}d$, which exhibits a disordered lithium-ion distribution, and a tetragonal form, with the $I4_1/acd$ space group, which contains ordered lithium-ion distribution.^{61,69} Among these phases, the tetragonal polymorph has a conductivity two orders of magnitude lower than that of cubic form. In contrast to cubic polymorph, in tetragonal $\text{Li}_7\text{La}_3\text{Zr}_2\text{O}_{12}$, the tetrahedral Li sites are completely filled.

To understand the conduction mechanism in Li garnets, a number of studies have been conducted by X-ray and neutron diffraction analysis, along with computational modeling.⁷⁰⁻⁷⁵ Li nuclear magnetic resonance (NMR) spectroscopy has also been used to provide information about garnet structure and Li dynamics.⁷⁶⁻⁸⁰ However, the very narrow range of Li chemical shifts (δ_{iso}) and the presence of lithium-containing impurities in garnet materials makes it challenging to characterize them using NMR spectroscopy.⁷⁷ As shown in Figure 5, 24d tetrahedra and 48g/96h octahedra are face shared to each other and form the 3D network structure due to which fast Li-ion conduction is observed in the garnet structure.

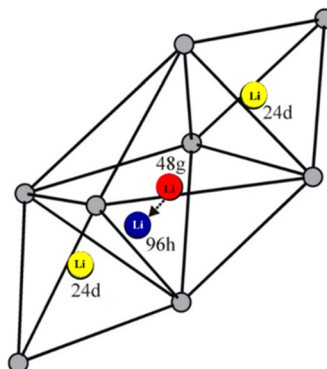


Figure 5. Distribution of Li-ions in tetrahedral (24d) and octahedral (48g and 96h) sites.

Using *ab initio* calculations, Xu et al. have proposed two distinct mechanisms of Li-ion transport in garnet-type materials (Route A and Route B).⁷¹ Li-ions are occupied at tetrahedral sites [Li(1), 24d sites] and the octahedral sites [Li(2), 48g/96h sites]. Li-ions will be redistributed over the Li(1) and Li(2) based on the total Li concentration. Li-ions can migrate either between two octahedral sites (Li(2)) (path 1), bypassing the tetrahedral site (Li(1)), or through the shared triangular faces that separate the polyhedra around Li(1) and Li(2) (path 2). Path 1 is preferred when Li concentration is lower, whereas path 2 is preferred in Li-stuffed garnets.⁷¹ The latest computational modeling studies have shown that the nearest-neighbor tetrahedral–octahedral Li pairs and (octahedral,□)–tetrahedral–(octahedral,□) Li clusters appear to be the most advantageous for conduction of these lithium-stuffed garnet oxides.⁸¹ Multiple groups have studied the diffusion mechanism in $\text{Li}_7\text{La}_3\text{Zr}_2\text{O}_{12}$ using *ab initio* molecular dynamics (AIMD) simulations.^{22,73} These studies show that fast diffusion in superionic conductors occurs through a concerted migration of multiple ions with low energy barriers rather than isolated ion hopping, which is typical in solids. The concerted migration of Li ions in $\text{Li}_7\text{La}_3\text{Zr}_2\text{O}_{12}$, which is extracted from AIMD

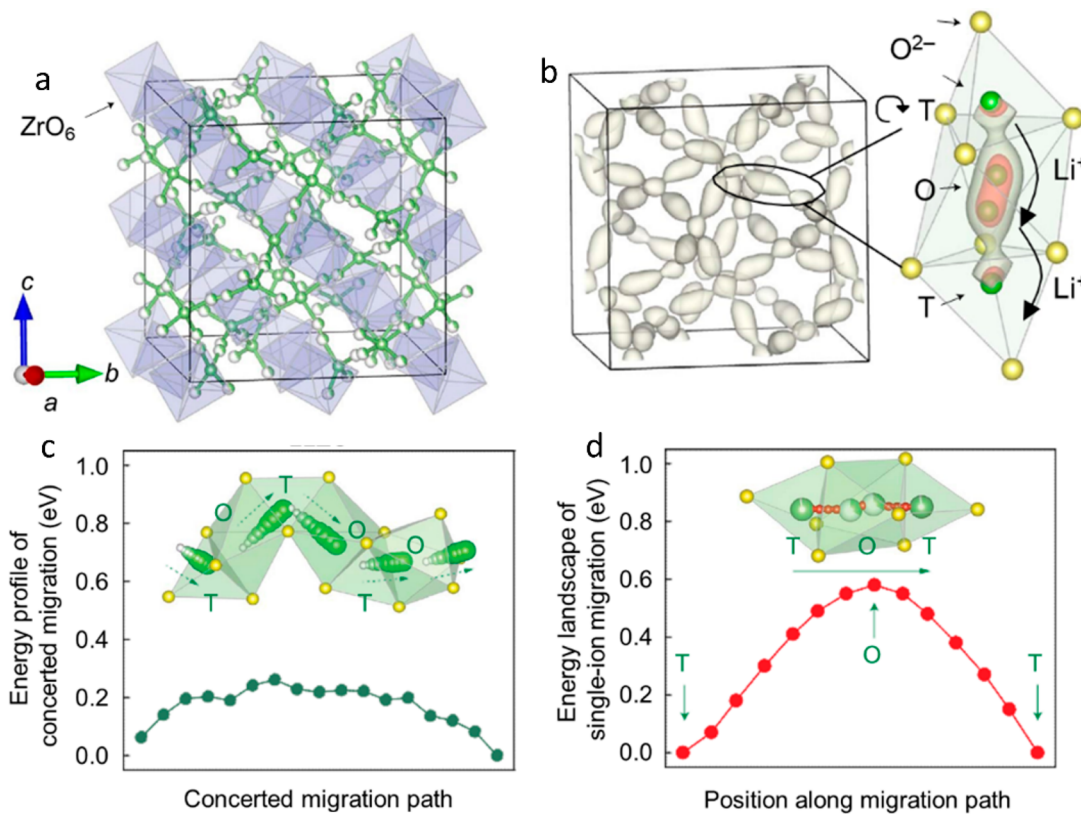


Figure 6. Li-ion diffusion in $\text{Li}_7\text{La}_3\text{Zr}_2\text{O}_{12}$. (a) Crystal structure of $\text{Li}_7\text{La}_3\text{Zr}_2\text{O}_{12}$, (b) probability density of Li^+ spatial occupancy during AIMD simulations. The zoom-in subset shows the elongation feature of probability density along the migration channel (Li, green; O, yellow), (c) migration energy barrier in $\text{Li}_7\text{La}_3\text{Zr}_2\text{O}_{12}$ for concerted migration of multiple Li ions hopping into the next sites along the diffusion channel. Inset show the Li^+ path (green spheres) and O ions (yellow spheres), (d) energy landscape of single Li^+ along the migration channel (shown in inset) across multiple Li sites (partially filled green sphere) and Li^+ pathway (red spheres). Reproduced with permission from ref 22. Copyright 2017 Springer Nature.

simulations, is shown in Figure 6. As shown in Figure 6, concerted hopping of multiple Li ions takes place when tetrahedral Li ions hop to the nearest-neighbor octahedral sites and the Li ions occupying these octahedral sites hop into their nearest neighbor tetrahedral sites.²²

2.4. Li-Ion Conductivity of Bulk and Thin-Film Garnet-Type Oxides

Figure 7 shows selected Li-garnet compositions^{40,61,68,69,82–113} in bulk or pellet form that exhibit the highest conductivity from each year following the first report by Thangadurai et al. in 2003 on fast Li-conducting garnet $\text{Li}_5\text{La}_3\text{M}_2\text{O}_{12}$ ($\text{M} = \text{Nb}, \text{Ta}$).⁵⁹ For a more extensive list until 2014, and a complete literature review on garnet solid electrolytes, the reader is referred to Thangadurai et al.¹⁷ As already noted in literature,^{17,94} the Li7 -phases ($\text{Li}_7\text{La}_3\text{M}_2\text{O}_{12}$ ($\text{M} = \text{Zr}, \text{Sn}$)) generally exhibit higher conductivity than Li5 - ($\text{Li}_5\text{La}_3\text{M}_2\text{O}_{12}$ ($\text{M} = \text{Nb}, \text{Ta}, \text{Sb}$)) or Li6 -phases ($\text{Li}_6\text{Al}_2\text{M}_2\text{O}_{12}$ ($\text{A} = \text{Mg}, \text{Ca}, \text{Sr}, \text{Ba}; \text{M} = \text{Nb}, \text{Ta}$)) due to higher Li-ion concentration. Specifically, the optimal Li content for the highest conductivity appears to be at $x \approx 6.5$ (below the theoretical limit of 7.5), while the optimal lattice constant is around $12.90\text{--}12.95 \text{ \AA}$.¹¹⁴

Despite almost two decades of targeted efforts to increase the ionic conductivity of Li-garnets, the current highest attained room temperature Li-ion conductivity of $2.06 \times 10^{-3} \text{ S cm}^{-1}$ ($\text{Li}_{6.55}\text{Ga}_{0.15}\text{La}_3\text{Zr}_2\text{O}_{12}$)¹¹⁵ is still lower than organic electrolytes ($1 \times 10^{-2} \text{ S cm}^{-1}$ at RT for 1 M LiPF_6 in ethylene carbonate:dimethyl carbonate).⁷ One analysis¹¹⁴ pointed out that Li-content and structural data show that an optimized limit

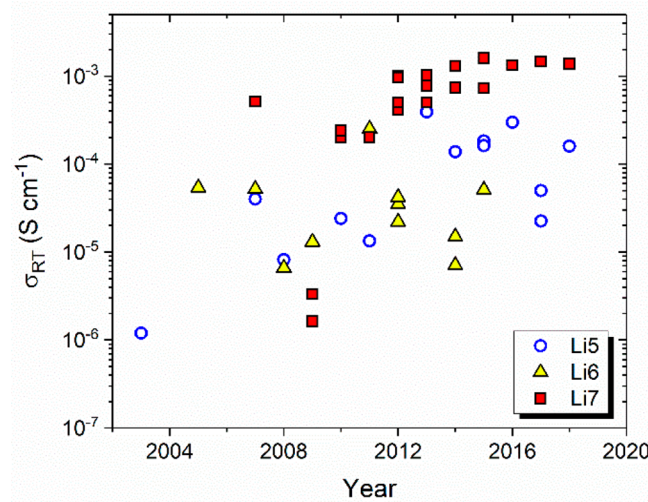


Figure 7. Selected high conductivity Li-garnet compositions since Thangadurai et al. reported the fast Li-conducting garnet $\text{Li}_5\text{La}_3\text{M}_2\text{O}_{12}$ ($\text{M} = \text{Nb}, \text{Ta}$) in 2003.⁵⁹ $\text{Li}_5\text{La}_3\text{M}_2\text{O}_{12}$ ($\text{M} = \text{Nb}, \text{Ta}, \text{Sb}$) (Li5-phases),¹⁰⁸ $\text{Li}_6\text{Al}_2\text{M}_2\text{O}_{12}$ ($\text{A} = \text{Mg}, \text{Ca}, \text{Sr}, \text{Ba}; \text{M} = \text{Nb}, \text{Ta}$) (Li6-phases), and $\text{Li}_7\text{La}_3\text{M}_2\text{O}_{12}$ ($\text{M} = \text{Zr}, \text{Sn}$) (Li7-phases).^{40,61,68,69,82–113}

in lithium-ion conductivity has possibly been reached. Still, a lot more possible substitutions can be explored with the aid of numerical simulation¹¹⁶ to find the composition with the highest possible Li-ion conductivity.

To compensate for the lower Li-ion conductivity of Li-garnets compared to the currently used liquid electrolyte, researchers have explored the possibility of thin film fabrication for Li-garnets using various deposition techniques. Figure 8 summarizes

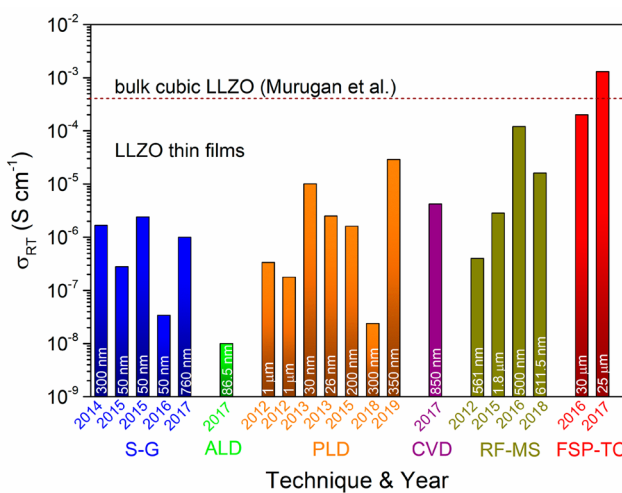


Figure 8. Thin film garnet development by year and technique and the resulting conductivities at room temperature. The thicknesses of the films are also indicated in the bar. Only $\text{Li}_3\text{La}_3\text{Zr}_2\text{O}_{12}$ (LLZO) compositions are studied by researchers. The dashed line represents the value of $\text{Li}_3\text{La}_3\text{Zr}_2\text{O}_{12}$ (LLZO)¹³⁵ in bulk or pellet form. S-G, sol-gel + spin/dip coating;^{117–120} ALD, atomic layer deposition;¹²¹ PLD, pulsed laser deposition;^{105–107,109,110} CVD, chemical vapor deposition;¹²⁸ RF-MS, radio frequency magnetron sputtering;^{129,130} FSP-TC, flame spray pyrolysis + tape casting.^{133,134}

rizes the current attempts by several groups to obtain thin film garnets using techniques such as sol-gel + spin or dip coating,^{117–120} atomic layer deposition (ALD),¹²¹ pulsed laser deposition (PLD),^{122–127} chemical vapor deposition (CVD),¹²⁸ radio frequency magnetron sputtering (RF-MS),^{129–132} and flame spray pyrolysis + tape casting.^{133,134} Note that all the

available thin film development data are obtained from the high-conducting $\text{Li}_3\text{La}_3\text{Zr}_2\text{O}_{12}$ (LLZO) garnet.

In general, the total conductivity of the films is lower than that found for LLZO obtained in bulk form. The possible reasons for lower conductivity are porous or cracked films and not phase-pure garnet films.¹³⁶ The technique or the method influences the microstructure and phase content, which in turn affects the lithium-ion conductivity of the film. It is also evident from Figure 8 that films of thicknesses less than several micrometers usually exhibit lower conductivity than films that are thicker (e.g., 25–30 μm).

2.5. Mechanical Properties of Garnet-Type Oxides

Because of the rigid nature of ceramic garnet-type materials, they are seen as a potential separator to block lithium dendrite in lithium metal batteries. The effectiveness to block lithium dendrite during operation is tied to the mechanical properties of the garnet-type material. Further, the knowledge of mechanical properties is essential to forecast mechanical degradation during operation, especially since volume changes during cycling is one of the critical factors that affect the lifetime of all-solid-state lithium batteries.^{137–139} The mechanical properties of these materials may be influenced by the processing and assembly of solid-state batteries.

Mechanical properties determine the material's response to stress and may be affected by various factors such as the microstructure, defects, and temperature. A range of mechanical properties can be measured or calculated, but the most common that are considered are Young's modulus, E , shear modulus, G , hardness, H , and fracture toughness, K_c . Young's modulus is the measure of the stiffness, or material's resistance to elastic deformation (nonpermanent deformation) under uniaxial stress, while shear modulus is the same measure of stiffness but under shear stress. Hardness is a measure of a material's resistance to localized plastic deformation (permanent deformation). Finally, fracture toughness is the material's resistance to brittle fracture when a crack is present. For most situations, that is, the specimen thickness is much greater than the crack dimensions and the crack is in an opening or tensile mode

Table 1. Mechanical Properties of Li-Stuffed Garnets Reported in Literature^a

composition	Young's modulus, E (GPa)	shear modulus, G (GPa)	hardness, H (GPa)	fracture toughness, K_c (MPa m ^{0.5})
$\text{Li}_{6.24}\text{La}_3\text{Zr}_2\text{Al}_{0.24}\text{O}_{11.98}$ ¹⁴⁸				0.86–1.63
$\text{Li}_{6.24}\text{La}_3\text{Zr}_2\text{Al}_{0.24}\text{O}_{11.98}$ ¹⁴¹	149.8 ± 0.4 (RUS)	59.6 ± 0.1	6.4 ± 0.4 (V:2.9 N)	
$\text{Li}_{6.91}\text{La}_3\text{Zr}_{1.98}\text{Al}_{0.13}\text{O}_{12}$ ¹³⁹	145.6 ± 7.3 (nanoindentation, micropillar splitting)		8.5 ± 0.4	1.19 ± 0.13 ; 0.99 ± 0.05 (micropillar)
$\text{Li}_{6.19}\text{Al}_{0.27}\text{La}_3\text{Zr}_2\text{O}_{12}$ ¹⁵⁰	140		9.1 (V:0.3 N) or (B: 125 μN)	0.97 ± 0.1
$\text{Li}_{6.17}\text{Al}_{0.28}\text{La}_3\text{Zr}_2\text{O}_{12}$ ¹⁴²	162.6 (DFT, 0 K) 154.5 (DFT extrapolated, 298 K) 146.1 ± 0.8 (Impulse excitation, 298 K) 150.3 ± 0.8 (Dynamic nanoindentation)	64.6 61.4 58.1 ± 0.3 59.8 ± 0.9		
$\text{Li}_{6.5}\text{La}_3\text{Zr}_{1.5}\text{Ta}_{0.5}\text{O}_{12}$ ¹⁴²	154.9 (DFT, 0 K) 147.2 (DFT extrapolated, 298 K) 139.9 ± 2.1 (impulse excitation, 298 K) 153.8 ± 2.7 (dynamic nanoindentation)	62.5 59.4 55.7 ± 0.8 61.2 ± 1.1		
Li ¹⁴²	4.9–13.0	4.0–5.0		
$\text{Li}_{1.3}\text{Al}_{0.3}\text{Ti}_{1.7}(\text{PO}_4)_3$ ¹⁵¹	115			1.1 ± 0.3
$\text{Li}_{0.33}\text{La}_{0.57}\text{TiO}_3$ ¹⁵²	200 \pm 3	~77	9.2 ± 0.2	1.0

^aMechanical properties of other electrolytes and lithium metal are listed for comparison. RUS, resonant ultrasound spectroscopy; DFT, density functional theory; V = Vickers indenter; B = Berkovich indenter.

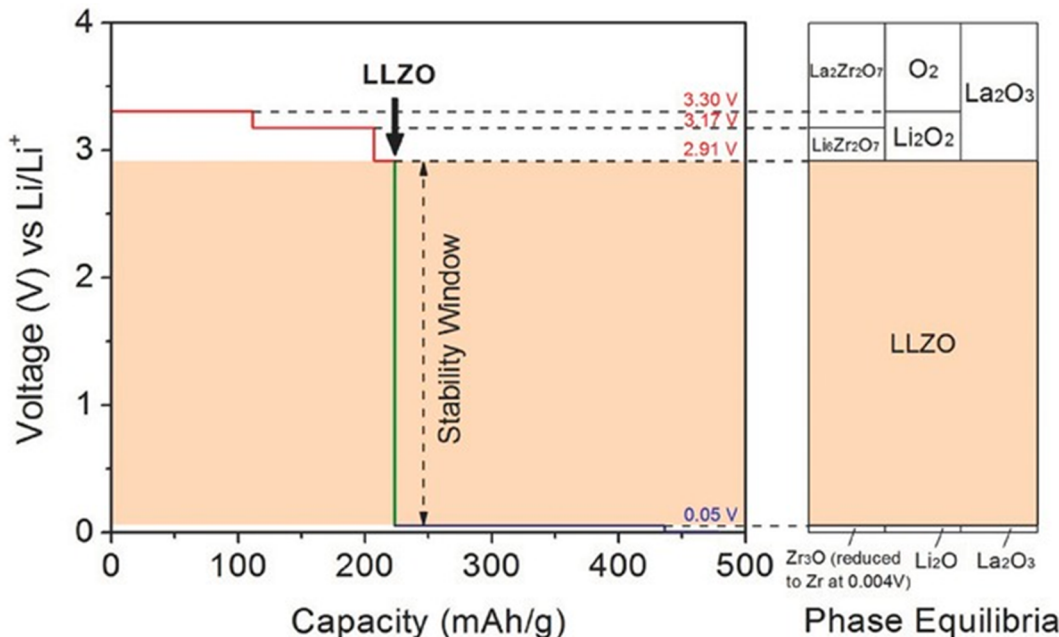


Figure 9. Calculated equilibrium potential profile and phase equilibria of LLZO. Reproduced with permission from ref 158. Copyright 2016 WILEY-VCH.

(mode I), the fracture toughness is cited as plain strain fracture toughness, K_{Ic} .

Mechanical property studies of garnet-type materials have only started several years ago (2012), so the information for garnet-type materials are currently limited. A brief review of the available mechanical property data of Li-ion conducting crystalline oxide-based solid electrolytes, which includes an example of garnet is available recently.¹⁴⁰ Ni et al. were the first to report the mechanical properties of Li-garnet, a hot-pressed cubic phase $\text{Li}_{6.4}\text{Al}_{0.24}\text{La}_3\text{Zr}_2\text{O}_{11.98}$.¹⁴¹ The material was confirmed to exhibit a high Young's (~ 150 GPa) and shear (~ 60 GPa) modulus. For comparison, the Young's and shear modulus of Li metal are 4.9–13.0 and 4.0–5.0 GPa.¹⁴² Monroe and Newman, in their work on modeling the mechanical aspects of the lithium metal and polymer interface stability, have suggested that the instability at lithium/polymer interfaces causing dendrite formation can be suppressed if the shear modulus of the polymer separator (with a Poisson's ratio similar to poly(ethylene oxide)) is about twice that of lithium.¹⁴³ The shear moduli of Li-garnets are an order of magnitude larger than that of Li metal. Thus, Li-garnets may sufficiently suppress Li dendrite growth.¹⁴² However, Monroe and Newman acknowledge that their assumptions limit the accuracy of their analysis and that extrapolating the shear modulus criteria to ceramics like Li-garnets may be inaccurate. Still, looking into Li-garnets with high shear modulus for dendrite suppression continues to intrigue battery researchers.

Shear modulus alone may not be sufficient as a lone selection guide for a solid electrolyte.¹³⁹ In several studies, dendrite formation has been observed in LLZO at current densities $> 0.3 \text{ mA cm}^{-2}$.^{144–147} One of the aspects that has been highlighted is the formation of microcracks during charging cycles.¹³⁹ Microcrack formation is related to the fracture toughness of the material, so it is important to study fracture toughness and fracture mechanisms in Li-garnets. So far, only a few studies have reported fracture toughness values, as shown in Table 1. The K_{Ic} values for LLZO are within the typical range exhibited by

polycrystalline ceramics (1–7 MPa $\text{m}^{0.5}$).¹⁴⁸ For comparison, glasses have K_{Ic} of 0.5–1, while most polymers exhibit K_{Ic} of 1–3 MPa $\text{m}^{0.5}$.¹⁴⁹ Aluminum alloys and steel exhibit much higher K_{Ic} at 20–50 and 30–200 MPa $\text{m}^{0.5}$, respectively.¹⁴⁹ A study of hot-pressed LLZO has shown that fracture toughness increases as relative density decreases, which was explained by weak grain boundaries deflecting the crack trajectories away from the direction of maximum driving force in low-density samples.¹³⁹

3. CHEMICAL AND ELECTROCHEMICAL STABILITY OF GARNET-TYPE SOLID-STATE ELECTROLYTES

3.1. Chemical and Electrochemical Stability of Garnet-Type Electrolytes

Garnet-type solid electrolytes have been widely reported to have good stability and compatibility with Li metal and oxidation stability at high voltages. Several groups have performed first-principles computations based on density functional theory (DFT) energies to evaluate the thermodynamic phase equilibria of solid electrolytes such as LLZO as a function of potential referenced to Li (Figure 9).^{153–155} From these calculations, the garnet LLZO phase has been shown to be stable in potentials ranging from 0.05 to 2.9 V, which corresponds to the thermodynamic intrinsic electrochemical window.^{153–155} It should be noted that the studies referenced here refer to the intrinsic thermodynamic stability of garnet with respect to the chemical potential of Li metal. Other criteria used to define the theoretical electrochemical window yield different window widths.¹⁵⁶ At potentials outside the electrochemical window, the most thermodynamically favorable state is the lowest energy phase equilibria, that is, a combination of phases formed by the lithiation and delithiation reactions of the original LLZO composition.¹⁵⁷ However, these phases may not necessarily form due to various kinetic limitations during electrochemical cycling.

These thermodynamic calculations revealed that LLZO garnet is not thermodynamically stable with Li metal, and

instead the phase equilibria is predicted to be Zr, La₂O₃, and Li₂O. The lithiation reaction of LLZO to form this phase equilibria has a small reaction energy of -0.021 eV/atom. Since this reaction energy is around the magnitude of typical DFT errors¹⁵⁹ and because of other approximations made in these calculations,¹⁶⁰ these calculation results may be inconclusive as to whether LLZO garnet is stable with Li metal. In addition, given the large energy barrier required to fully reduce Zr bonded with O into metallic Zr and the small reaction energy between garnet LLZO and Li metal, this reduction reaction may be kinetically constrained. The small reaction energy and low reduction potential of garnet suggests that garnet possesses good resistance to Li reduction, and that garnet exhibits the best Li metal stability among current oxide and sulfide SEs, including NASICON-type LATP, LLTO, LGPS, and LPS, which all have high reduction potentials greater than 1 V against Li metal.^{154,155} Indeed, computational evaluation of the conduction band minimum of LLZO has suggested that the band edge is high enough to prevent electron injection by Li metal.¹⁵⁶ The computation results on garnet stability corroborate experimental reports of garnet compatibility with Li metal anodes.

3.2. Chemical and Electrochemical Stability with Anode Materials

For full battery application, the electrolytes have to be chemically stable with both anode and cathode materials or be able to form a stable SEI. Additionally, the electrolytes also need to possess excellent electrochemical stability to ensure a stable battery performance. Garnet SSEs are among the most stable SSEs with both the Li metal anode and cathode materials. The wide electrochemical window (>6 V vs Li/Li⁺ from CV studies and ~ 3 V from computational analyses) of garnet SSEs makes it possible to achieve high voltage batteries. However, according to the computational results based on bulk-phase thermodynamic data, garnet SSEs may be thermodynamically unstable with Li metal and some cathode materials. Nevertheless, garnet SSEs are still one of the most stable and promising SSEs for potential practical applications. Some reported reactions happened under some extreme conditions required for battery fabrication and assembly, which may be avoided if the processing is improved.

One of the most attractive features of garnet SSEs is the ability to directly use Li metal anodes. The previous studies demonstrated that garnet SSEs can maintain stability to both the solid Li metal at room temperature and the molten Li at high temperature up to 300 °C.¹⁶¹ However, depending on the dopants and the temperatures, side reactions between Li metal and garnet SSEs have been reported. Chi et al. reported that even at room temperature, the contact between the Li metal and Al-doped cubic garnet phase can quickly form the less conductive tetragonal garnet interphase.¹⁶² When in contact with molten Li at high temperature up to 300 °C, a gray to black surface layer was also noticed on the garnet SSEs. The relatively less stable dopants such as Al and Nb can result in poor chemical stability of garnet SSEs against Li metal or molten Li.^{158,163,164}

To improve the compatibility of garnet SSEs with Li metal anode, surface coatings or alloy anodes can be used. Surface modification can improve the wettability of molten Li on garnet SSEs, which enables a lower coating temperature and shortens processing time for the Li metal anode. The details on surface modifications will be discussed in the following section. It has also been reported that Li alloy anodes can improve the stability between SSEs and Li metal anode. For thermodynamically unstable SSEs such as LPS and LATP, Li-In alloys have been

used as the anode. Note that a thin layer of alloying metal coating cannot improve the chemical stability of the SSEs against the Li metal anode as most of the anode is still Li metal. Pure alloys can improve the stability, however, the potential of the whole anode will increase, which is undesirable.

In addition to chemical stability with electrodes, electrochemical stability is also critical to achieve stable battery performance. The electrochemical stability is highly related to the current density, mechanical properties, interface, and ionic and electrical conductivities.¹⁶⁵ High mechanical strength can potentially block dendritic Li growth. On the basis of the calculations, the mechanical strength of garnet SSEs should be high enough to block Li dendrite growth.^{143,166} However, a recent experimental study indicated that Li dendrites can grow into single crystal garnet SSEs at high current densities.¹⁶⁷ Good contact between electrodes and SSEs can also significantly improve the cycling stability due to the improved interface and uniformly distributed Li-ion transport. From another point of view, an alloy interface layer can provide a stable interface during cycling. For garnet SSEs, it has been reported that Li-Al or Li-Mg alloy interface can improve the electrochemical stability between SSEs and Li metal anode.^{168,169} In these cases, Li will deposit on the alloy layer and pushes the layer away from the interface instead of passing through the metallically conductive alloy interface layer because of the lack of driving force.^{170,171} Therefore, it is highly probable that the improved electrochemical stability from introducing the alloy interface is mainly due to the good wettability.

The ionic and electrical conductivities of SSEs are also important for electrochemical stability. It has been suggested that an ionic conductivity greater than 10^{-4} S/cm and electronic conductivity less than 10^{-10} S/cm are necessary for potential practical applications.¹⁷² Poor ionic conductivity can increase the overpotential and cause voltage breakdown at high current densities. High electronic conductivity can lead to high self-discharge rates and potentially cause Li dendrite growth from the interior of the SSEs.¹⁷¹ Recently, Han et al. proposed that internal Li deposition due to high electronic conductivity causes short-circuit formation in garnet SSEs.¹⁷³ The results indicated that it is easier for Li dendrites to form at high temperature because the electronic conductivities of garnet SSEs increase with temperature.¹⁷³ However, the ionic conductivity of garnet SSE increases about 1 order of magnitude while the electronic conductivity only increases about 2 times from 6×10^{-8} S/cm to 1×10^{-7} S/cm when the temperature increases from 20 to 100 °C.¹⁷³ The ratio of the electronic leaking current to ionic current should be smaller at higher temperature, which should result in less internal Li deposition.

3.3. Chemical and Electrochemical Stability with Cathode Materials (Conversion Cathodes; Intercalation Cathodes)

On the cathode side, LLZO garnet does not show thermodynamic stability at high voltages or in Li-poor environments. In the same first-principles studies based on thermodynamic DFT energies discussed in Section 3.1,^{153–155} LLZO is predicted to have an oxidation potential of 2.9 V and an equilibrium potential of 3.3 V, which corresponds to fully delithiated LLZO. This oxidation potential corresponds to the reaction of oxygen gas evolution, which is known to be kinetically difficult as in the charging reactions of Li–O₂ batteries, and is expected to exhibit a high overpotential.¹⁷⁴ This may explain the good oxidation stability observed for LLZO garnet.

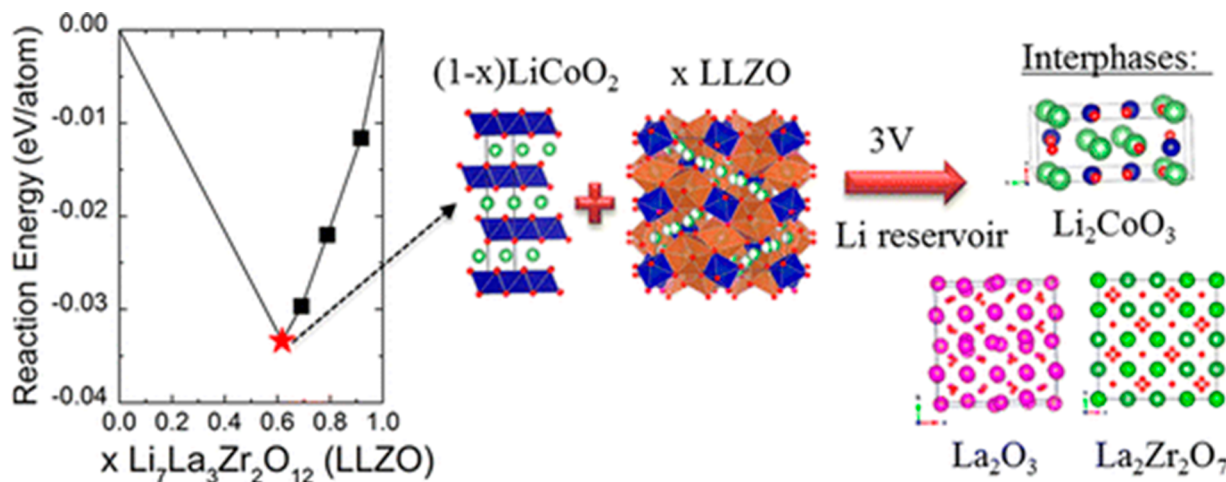


Figure 10. Schematic showing theoretical thermodynamic calculations of decomposition energies and phase equilibria at the cathode-garnet interface. Reproduced with permission from ref 116. Copyright 2015 American Chemical Society.

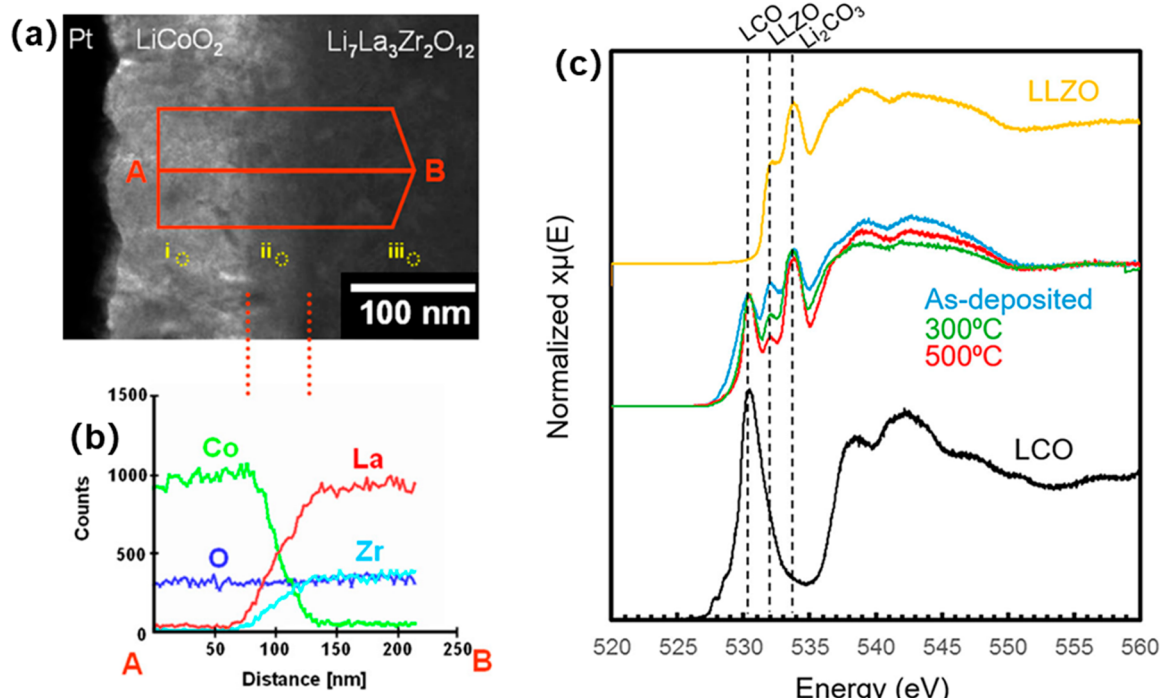


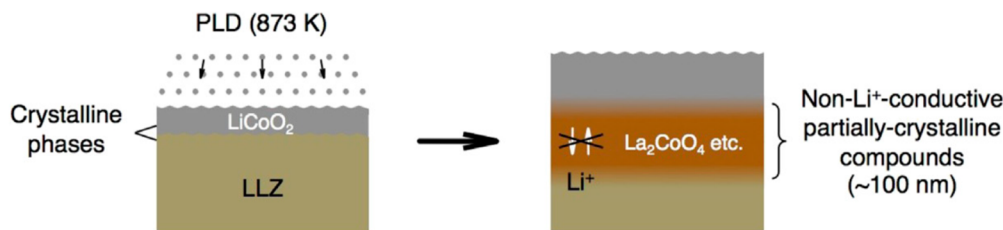
Figure 11. (a) Cross-sectional TEM image of an LLZO/ LiCoO_2 thin film interface and (b) EDS line profile obtained from the region indicated by the red arrow in the direction A–B. The broken red lines indicate the reaction layer at the LLZO/ LiCoO_2 interface. Points i, ii, and iii indicate locations used for NBD analysis. Reproduced with permission from ref 175. Copyright 2010 Elsevier. (c) O K-edge X-ray absorption spectroscopy data (partial fluorescence yield mode) for LLZO, LCO, and 60 nm-thick LCO film on LLZO in the as-deposited state after annealing at 300 and 500 °C. Reproduced with permission from ref 176. Copyright 2016 American Chemical Society.

The same thermodynamic scheme is applied to evaluate the interface stability of garnet SSE and cathode by constructing their pseudobinary.^{116,153} At an interface with the common oxide cathode LiCoO_2 (LCO), LLZO garnet is reported to have a very small reaction energy for decomposition (Figure 10).¹¹⁶ This small energy may explain both the stable interfaces, where the reaction is kinetically inhibited, and interfacial reactions reported in different experimental studies. As described in section 4.1, interfacial engineering strategies have been predicted to stabilize the interface of garnet with Li metal and high-voltage cathodes. The introduction of an interfacial coating

layer may play a key role in providing interface compatibility and low resistance.

Because of the kinetic inhibition, garnet SSEs are normally stable to most common cathode materials at room temperature. However, to achieve good contact and interface, high temperature treatment or cosintering is necessary for oxide cathode materials. For LCO cathode, many studies have demonstrated that high temperature treatment can form an intermediate reaction layer at the garnet SSEs/LCO interface (Figure 11a,b).¹⁷⁵ After cosintering of LCO and garnet SSEs, garnet SSEs suffer from color changing to green or blue, indicating cross-doping of Co. The EDS line profile in Figure 11b indicates

Non-modified interface



Nb-modified interface

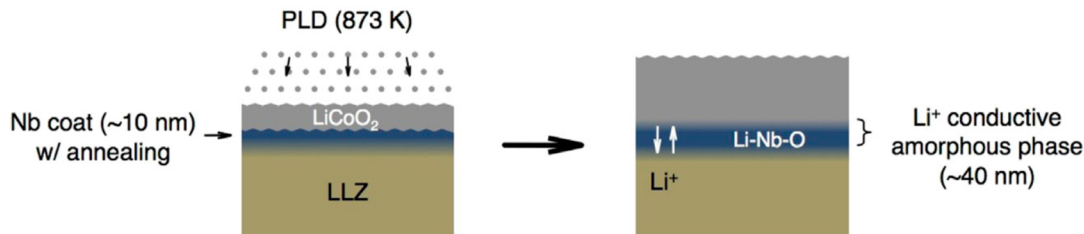


Figure 12. Schematic illustrations of nonmodified and Nb-modified LLZO/LiCoO₂ interfaces. The mutual diffusion between LLZO and LiCoO₂ produces non-Li conductive phases such as a crystalline La₂CoO₄. Nb-modified LLZO/LiCoO₂ interface suppresses the mutual diffusion and produces a Li-conductive amorphous phase. Reproduced with permission from ref 183. Copyright 2014 Elsevier.

a 50 nm thick intermediate layer formed by mutual diffusion of elements between garnet and LCO at high temperature. Recent work by Yildiz and co-workers indicated that the Li blocking interface layer starts to form at temperatures as low as 300 °C.¹⁷⁶ The O K-edge X-ray absorption spectroscopy (XAS) shown in Figure 11c indicates that as the annealing temperature increases, the LCO peak and Li₂CO₃ peak did not change in intensity. However, the peak intensity associated with LLZO decreased during annealing, indicating the decomposition of LLZO near the interface with LCO. Therefore, decreasing the annealing temperature and time is necessary to avoid or minimize side reactions and cross-doping.

Another strategy to avoid cross-reactions is to apply a stable protecting layer. Because of low melting temperature (~700 °C) and relatively high ionic conductivity (2×10^{-6} S/cm), Li₃BO₃ has been demonstrated as a successful cosintering additive that can help decrease cross-diffusion during annealing at temperatures up to 700 °C and improves the cycling performance for LCO cathode in garnet based solid-state batteries.^{177–181} On the basis of a similar mechanism, Wang et al. applied Li_{2.3}C_{0.7}B_{0.3}O₃ as the sintering additive to prevent side reactions and improve the LCO cathode interface with garnet SSEs.¹⁸² Li_{2.3}C_{0.7}B_{0.3}O₃ has a similar melting temperature with Li₃BO₃ but has a much higher ionic conductivity than Li₃BO₃. Another benefit of using Li_{2.3}C_{0.7}B_{0.3}O₃ is that Li_{2.3}C_{0.7}B_{0.3}O₃ can consume the Li₂CO₃ insulating layer on garnet SSEs and LCO by forming a solid solution. Besides the low-melting-point Li conductive sintering additives, Iriyama et al. has demonstrated that a 10 nm Nb layer coating can also prevent the formation of the non-Li-ion conductive La₂CoO₄ interface at high temperature.¹⁸³ Instead, a Li-ion conductive Li–Nb–O amorphous phase can form (Figure 12), which significantly improves the cycling performance of LCO all solid-state batteries.

3.4. Chemical and Electrochemical Stability with Liquid Electrolytes (Organic Electrolytes; Aqueous Electrolytes)

Liquid electrolytes are generally still necessary in solid-state batteries to improve the interface between electrodes and SSEs, especially on the cathode side. Garnet SSEs are stable to most traditional commercial organic electrolytes. The potential side reaction is a proton exchange if the liquid electrolyte has trace water or other protic impurities. Zhong et al. has demonstrated that the n-BuLi superbase additive can greatly improve the interface stability between organic electrolyte and garnet SSEs.¹⁸⁴ With n-BuLi additive, the interfacial resistance has little change after 400 cycles, while the interfacial resistance of the cell without additive increased from ~1056 to ~2419 Ω cm² after 1 week. They proposed that superbase additive can retard the decomposition of liquid electrolyte and suppress the proton exchange of garnet SSEs due to the trace protic impurities.

In fact, proton exchange is the main concern for garnet SSEs when working with liquid electrolytes. There have been several works studying the stability of garnet SSEs during proton exchange.^{80,185–194} Depending on the composition, garnet SSEs have different proton exchange behavior and structure evolution. Nb-, Ta-, and Sn-based garnet SSEs have been demonstrated to undergo structural transition after proton exchange.^{185,190} For LLZO garnet SSEs, Chi et al. has demonstrated reversible Li⁺/H⁺ exchange in aqueous solutions.¹⁹⁴ The selected area electron diffraction (SAED) patterns of LLZO SSEs before and after proton exchange indicated that LLZO preserved its structure during proton exchange. On the basis of their electron energy loss spectroscopy (EELS) study, they concluded that 24d sites are still occupied by Li, 48 g sites are occupied by Li and a small amount of H, while 96 h sites are solely occupied by H in the proton exchanged garnet (Figure 13). Even though the proton exchange can partially replace Li, garnet SSEs still show some stability to aqueous electrolytes. Takeda and co-workers studied the stability of LLZO garnet SSEs in different aqueous electrolytes and found that LLZO is

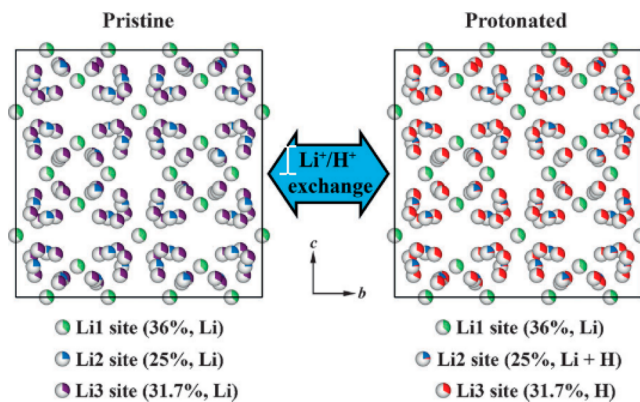


Figure 13. Schematic illustration for the Li^+/H^+ exchange process of cubic LLZO in water. Li1, Li2, and Li3 represent the 24d, 48g, and 96h sites, respectively. Reproduced with permission from ref 194. Copyright 2015 WILEY-VCH.

stable in saturated LiCl aqueous solution and is unstable in water, acid, and LiOH solutions with respect to the structure and conductivity.¹⁸⁶ Chi and co-workers' recent work indicated that even though the high-degree proton-exchange ($\sim 75\%$ Li exchanged) LLZO has a slight structural distortion and a decreased ionic conductivity, H^+ is immobile at temperatures below 400 K, which makes LLZO a promising separator layer in aqueous Li batteries.¹⁹⁵

4. INTERFACE CHALLENGES IN SOLID-STATE ELECTROLYTES AND ELECTRODES

4.1. Strategies to Address Interfacial Challenges

The high interfacial resistance originating from the poor solid–solid contact between SSE and electrodes is the main challenge that hinders the development of solid-state batteries. For garnet based solid-state batteries, the excellent chemical stability of garnet SSE against Li metal enables the use of Li metal anode directly. As a metallic anode, Li metal has a high electrical conductivity. Therefore, the anode interfacial problem in garnet-based solid-state Li metal batteries can be simplified to Li-ion transport behavior across the interface. If the Li metal anode can have a conformal and stable contact with garnet SSE, allowing continuous Li-ion transport, the interfacial problem at anode side can be addressed. As many strategies have been developed to improve the contact between garnet and Li metal, the interfacial resistance at the anode has been significantly decreased. However, recent work has indicated that contact loss can occur during long-term cycling, particularly at high current densities due to the vacancy diffusion limitation in Li metal.^{196,197} To maintain a stable interface, an external pressure may be necessary to prevent contact loss.¹⁷⁹ The interfacial problem at cathode side can be much more complicated and challenging due to the poor electrical and ionic conductivities of cathode materials. In batteries with liquid electrolytes, the slurry-coated cathode particles are conformally surrounded by the electrolytes. Most Li ions just need to diffuse in a single particle, and the length of diffusion is only submicrometer scale. In solid-state batteries, the rigid SSE and granular cathode materials can only have poor point contact, and Li ions need to diffuse between cathode particles. This problem results in huge cathode–SSE interfacial resistance and greatly hinders the development of garnet based solid-state batteries. In this section, we will review the typical strategies of addressing interfacial

challenges in garnet based solid-state batteries and give some perspectives.

4.1.1. Artificial Solid–Electrolyte Interface. A common strategy to address interfacial problem in solid-state batteries is to apply an artificial interface layer between the SSE and electrodes. Because of the flexibility and softness, polymer-based SSEs are normally used as the interfacial buffer layer.¹⁹⁸ Soft polymer electrolytes can conformally coat SSEs and electrodes like liquid electrolytes, and are also conducive to scalable processing. Goodenough and his co-workers have demonstrated polymer/ceramic/polymer sandwich electrolytes with a cross-linked polymer for stable $\text{Li}/\text{LiFePO}_4$ cell cycling (Figure 14a,b).^{199,200} The polymer layer not only improves the contact

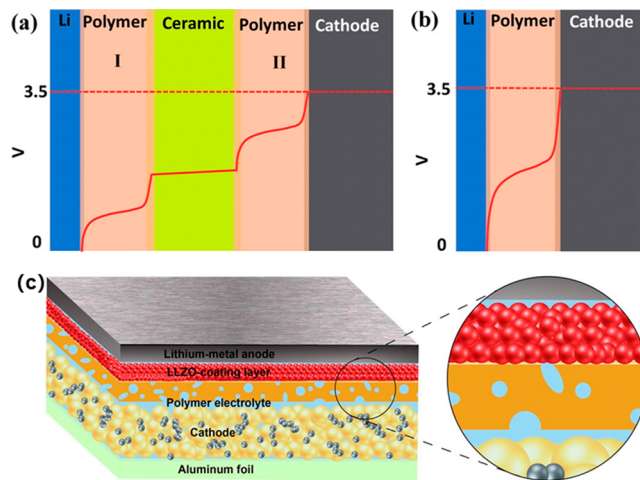


Figure 14. Illustration of the electric potential profile across the (a) sandwich electrolyte and (b) individual polymer electrolyte in the charge process of a hybrid full cell. Reproduced with permission from ref 199. Copyright 2016 American Chemical Society. (c) Schematic diagrams of solid Li-metal battery with solid polymer electrolytes (SPEs). Reproduced with permission from ref 201. Copyright 2017 American Chemical Society.

between electrodes and garnet electrolytes but also provides a more uniform Li-ion flux at the interface, which significantly improves the cycling stability of the full cells. On the basis of a similar idea, Guo et al. developed a thin asymmetric solid electrolyte with a soft polymer layer formed by *in situ* polymerization on cathode side to improve the contact between cathode and garnet electrolytes (Figure 14c).²⁰¹ Although the polymer buffer layer can significantly improve the contact and interface between garnet SSEs and electrodes, the ionic conductivity of polymer SSEs are only about 10^{-5} S/cm, three orders of magnitude lower than that of liquid electrolytes and one to two orders of magnitude lower than that of garnet SSEs. This significantly limits the charge transfer at high rate cycling. Therefore, even though the polymer SSEs can improve the contact properties, the interfacial resistance of this additional layer is still too high for full cell cycling. Another issue associated with polymer SSEs is their low electrochemical stability compared to garnet SSEs, which will sacrifice the advantages of garnet SSEs.

Another strategy to address the cathode interface is to apply low melting point ion-conductive inorganics. Because of the low melting point and moderate ionic conductivity, Li_3BO_3 has been used as the interface and binder to improve the contact between cathode and garnet SSEs (Figure 15a).¹⁷⁷ By forming a

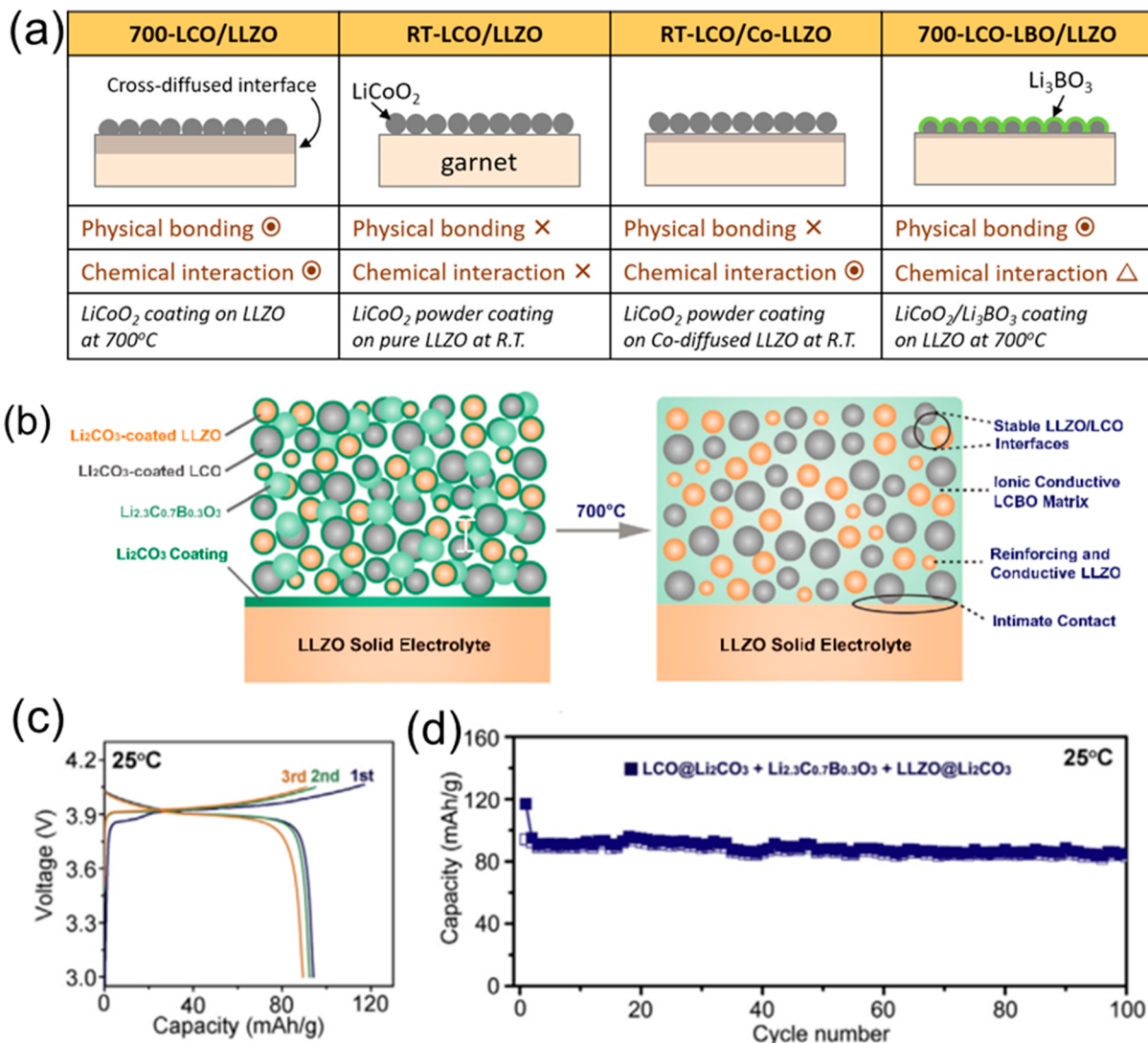


Figure 15. (a) LiCoO_2 /LLZO cathode configurations with different degree of physical and chemical interactions. Reproduced with permission from ref 177. Copyright 2016 American Chemical Society. (b) Schematics of the Interphase-Engineered All-Ceramic Cathode/Electrolyte. (c) Charge/discharge profiles of the interphase-engineered all-ceramic Li/LLZO/LCO cell for the first three cycles at 0.05 C at 25 °C. (d) Cycling performance of the interphase-engineered all-ceramic Li/LLZO/LCO cell at 0.05 C at 25 °C. Reproduced with permission from ref 182. Copyright 2018 Elsevier.

composite with Li_2CO_3 , the ionic conductivity can be further improved while the low melting point is still maintained (Figure 15b–d).¹⁸² The glass state inorganic binder can also prevent direct contact and the potential cross doping reaction between garnet SSEs and metal oxide cathodes at high temperature. The challenges associated with the inorganic binder are microcracks or other defects formation during cycling. Even though there are some “zero-strain” electrode materials, such as $\text{Li}_4\text{Ti}_5\text{O}_{12}$,²⁰² most electrode materials demonstrate volume change during lithiation and delithiation. Since the inorganic binders have rigid contact with the electrode materials, the volume change of the electrode materials can cause the contact loss between electrode materials and the SSEs. Therefore, in solid-state battery design, how to form both electronic and ionic contacts between electrode materials and SSEs, while saving additional empty space to accommodate the volume change of electrode materials during cycling is challenging and needs additional study.

4.1.2. Nanoscale Interfacial Engineering. The interface between Li metal anode and garnet SSEs highly depends on the wettability of garnet SSEs against the molten Li. Li metal does

not readily wet the surface of garnet due to the formation of Li carbonate and hydroxide on garnet surfaces exposed to air. These products cause poor physical contact and high interface resistance at the garnet-Li metal interface, which have been confirmed by multiple computational and experimental studies.^{23,203} Wettability and interfacial contact can be improved by introducing an additional interface layer on garnet surface. Hu group has demonstrated that with an alumina ALD coating, the wettability of garnet SSEs against molten Li was significantly improved (Figure 16a,b). The interfacial resistance decreased from $1710 \Omega \text{ cm}^2$ to $34 \Omega \text{ cm}^2$ (Figure 16c), while the cycling stability was also greatly improved (Figure 16d).²³ A similar effect is also observed with other coating materials, such as Si, Al, Au, and ZnO , etc.,^{204–208} which can alloy or react with the molten Li to improve the wettability. The driving force of the chemical reaction between the coating layer and molten Li can even help infiltrate Li into high-tortuosity porous garnet (Figure 16e–k), which is critical to developing ionic framework supported Li metal anodes.²⁰⁴ Therefore, for the highly electrically conductive Li metal anode, it is much easier to

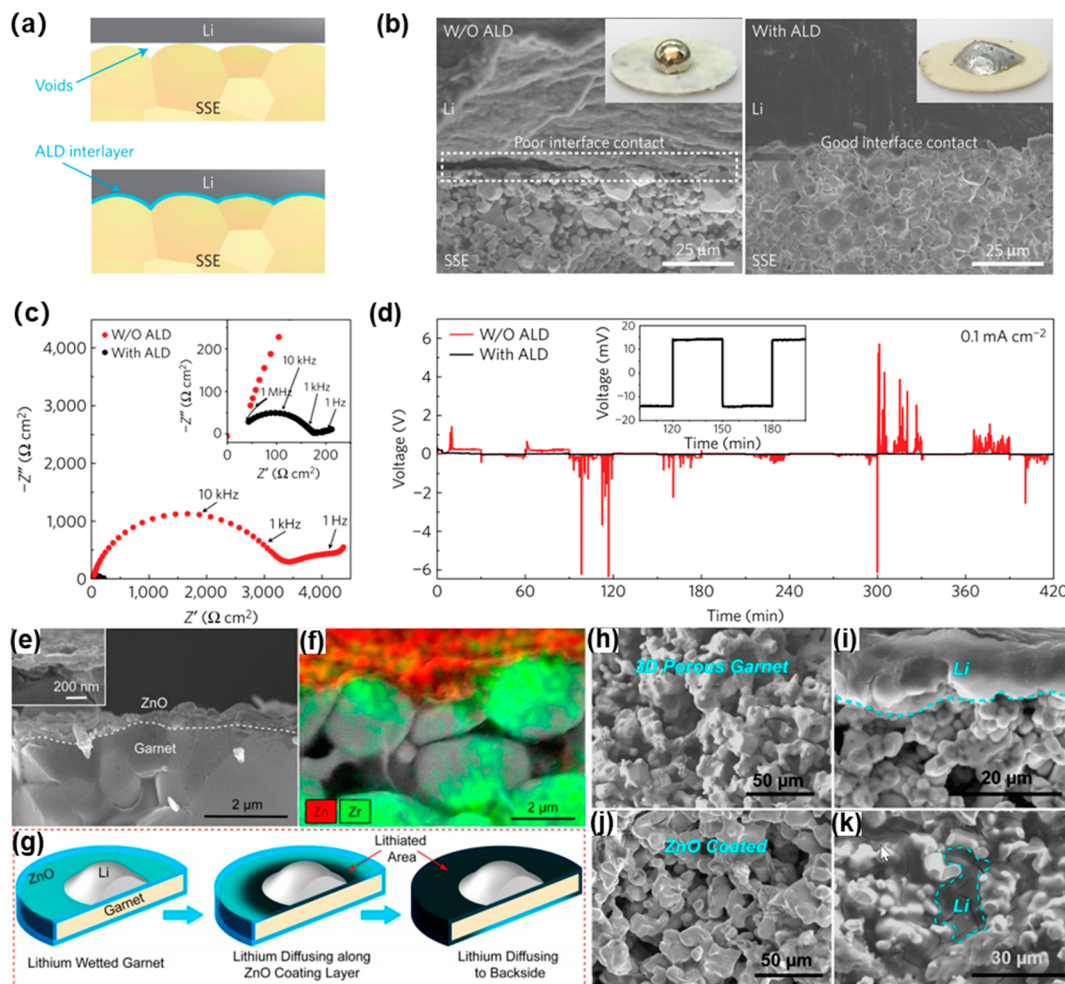


Figure 16. Characterizations of garnet solid-state electrolyte/Li metal interface. (a) Schematic of the wetting behavior of garnet surface with molten Li. (b) SEM images of the garnet solid-state electrolyte/Li metal interface. Without ALD- Al_2O_3 coating, garnet has a poor interfacial contact with Li metal even on heating. With the help of ALD- Al_2O_3 coating on garnet, Li metal can uniformly bond with garnet at the interface on heating. Insets are photos of melted Li metal on top of the garnet surface clearly demonstrating classical wetting behavior for the ALD-treated garnet surface. (c) Comparison of EIS profiles of the symmetric Li nonblocking garnet cells. Inset shows the enlarged impedance curve of the ALD-treated garnet cell. (d) Comparison of d.c. cycling for symmetric cells of Li/bare garnet/Li (black curve) and Li/ALD-treated garnet/Li (red curve) at a current density of 0.1 mA cm^{-2} . The inset is the magnified curve of the ALD-treated cell. Reproduced with permission from ref 23. Copyright 2017 Springer Nature. (e) SEM images and (f) elemental mapping of the garnet electrolyte coated with a 50 nm ALD ZnO layer. (g) Schematic of the lithium diffusion process along the ZnO coating layer on the garnet surface. (h) the pristine and (i) the lithium infiltrated porous garnet with a porosity of 60%–70%. (j) SEM image of the porous garnet coated with conformal ZnO. (k) SEM images of lithium infiltrated porous garnet with ZnO surface treatment, where almost all pores have been filled with lithium metal. Reproduced with permission from ref 204. Copyright 2016 American Chemical Society.

address the interfacial problem after solving the wetting problem.

4.1.3. Emerging Processing Techniques. Besides applying an artificial layer on the surface of garnet SSEs, several groups have reported that the removal of Li_2CO_3 can also significantly improve wettability of molten Li against garnet SSEs and decrease the interfacial resistance. ^{203,209–211} Sakamoto and his co-workers have demonstrated that wet polishing followed by high temperature treatment can effectively remove the Li_2CO_3 surface contamination. The molten Li exhibits a much smaller contact angle on the Li_2CO_3 -free garnet surface (Figure 17a), and the interfacial resistance also decreased to single digits (Figure 17b). ²⁰³ With carbothermal reduction, Goodenough's group successfully removed Li_2CO_3 from both the surface and grain boundary of garnet pellets (Figure 17c), and the resulted garnet SSEs have significantly decreased interfacial resistance for both anode and cathode sides (Figure 17d). ²⁰⁹ Hu and co-

workers applied a high temperature thermal pulse technique to remove the contamination on both the surface and grain boundaries of garnet SSEs in less than 2 s, and the cycling performance of garnet SSEs was significantly improved. ²¹⁰

Instead of applying an artificial coating or other special treatment, Hu and co-workers also demonstrated a universal soldering technique, which can directly coat Li metal to various substrates in several seconds. ²¹² In this technique, they addressed the wetting problem by tuning the surface tension and viscosity of the molten Li. The addition of alloy elements, such as Si, Al, Sn, and Zn, can significantly improve the wettability of the molten Li to many substrates including garnet SSEs (Figure 17e). The garnet pellets without any surface coating or treatment can be fully coated with the alloyed molten Li in 10 s (Figure 17f). The same effect applies to the molten Na system, and the fundamentals of this technique can be ascribed to the well-studied metal-ceramic joining. Therefore, the

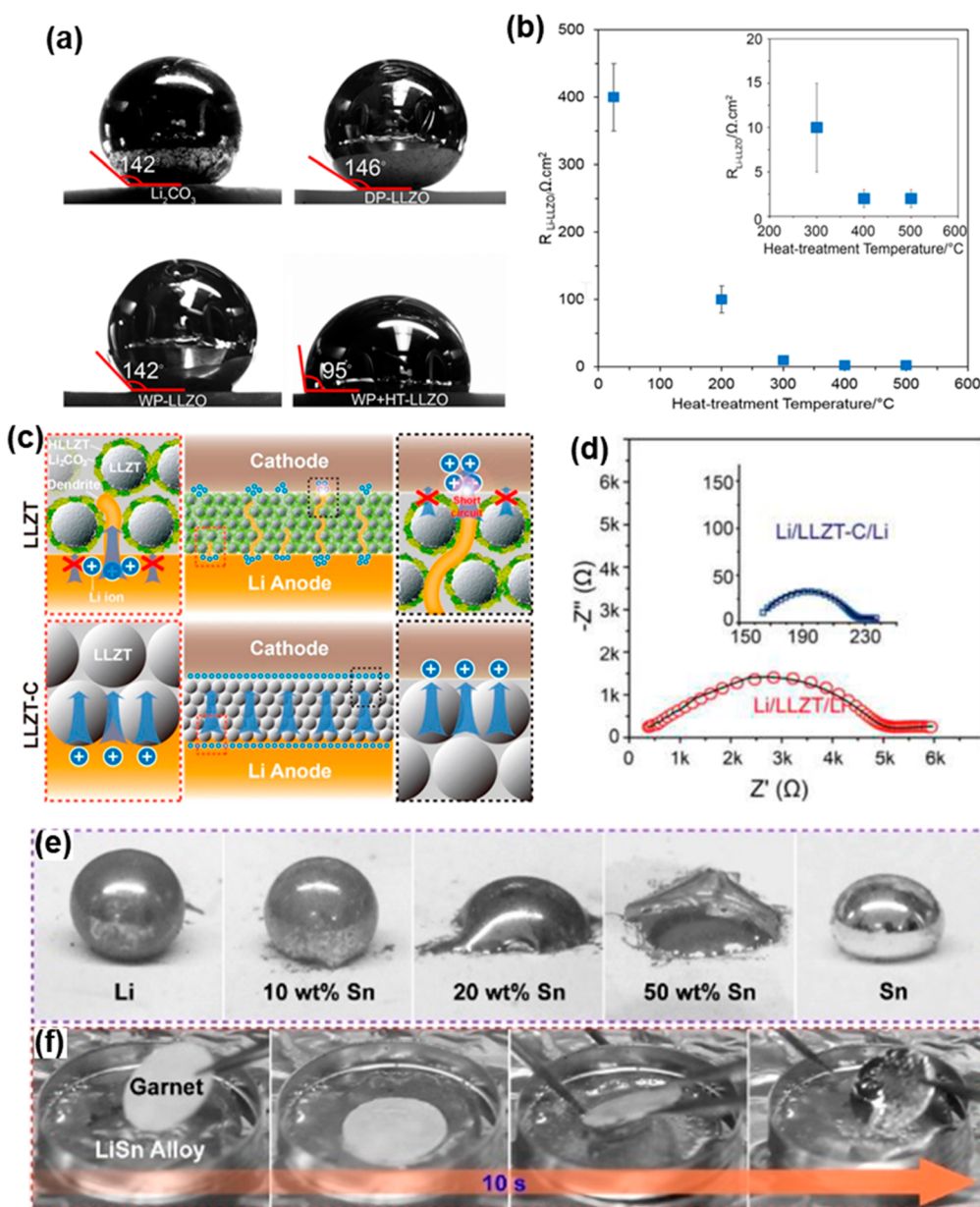


Figure 17. (a) Contact angle measurements of molten metallic Li on Li_2CO_3 , DP-LLZO, WP-LLZO, WP+HT-LLZO after heat treatment at 500 °C. (b) Li–LLZO interfacial resistance after preconditioning at 175 °C versus the heat-treatment temperature. Reproduced with permission from ref 203. Copyright 2017 American Chemical Society. (c) Schematic of Li-metal batteries with garnet LLZT and LLZT-C. (d) Electrochemical impedance plots of LLZT-C with symmetric Li electrodes at 65 °C. Reproduced with permission from ref 209. Copyright 2018 American Chemical Society. (e) Wettability of molten Li–Sn alloys with different ratios of Sn on alumina substrates. The increasing content of Sn significantly improves the wettability of molten Li against alumina. (f) In less than 10 s, the polished garnet pellet was successfully coated with uniform Li–Sn alloy. Reproduced with permission from ref 212. Copyright 2017 WILEY-VCH.

interfacial problem at the Li metal anode in garnet-based solid-state batteries directly relates to the contact and the surface contamination, which both have been addressed with multiple strategies.

4.2. Characterization Techniques for Garnet-Based Solid-State Batteries

The complicated fabrication and rigidity of the components makes the characterization of solid-state batteries more challenging than liquid batteries. In garnet-based solid-state Li metal batteries, the interfacial properties and the electrochemical stability of the SSEs and electrodes are of the most importance. To characterize interfacial properties, the thickness

of the electrode and SSEs is critical for many techniques, including X-ray photoelectron spectroscopy (XPS), Raman, time-of-flight secondary ion mass spectrometry (ToF-SIMS), etc.

4.2.1. EIS Analysis (AC). One of the most common and useful characterization techniques for solid-state batteries is electrochemical impedance spectroscopy (EIS), which can provide enough information about the ionic conductivity of SSEs and interfacial charge transport. To measure the ionic conductivity of garnet based SSEs, Li-ion blocking electrodes including Au and Ag can be coated or deposited on both sides of the pellets. A semicircle at high frequency corresponding to the bulk ionic conductivity of the SSEs and a long blocking tail at low

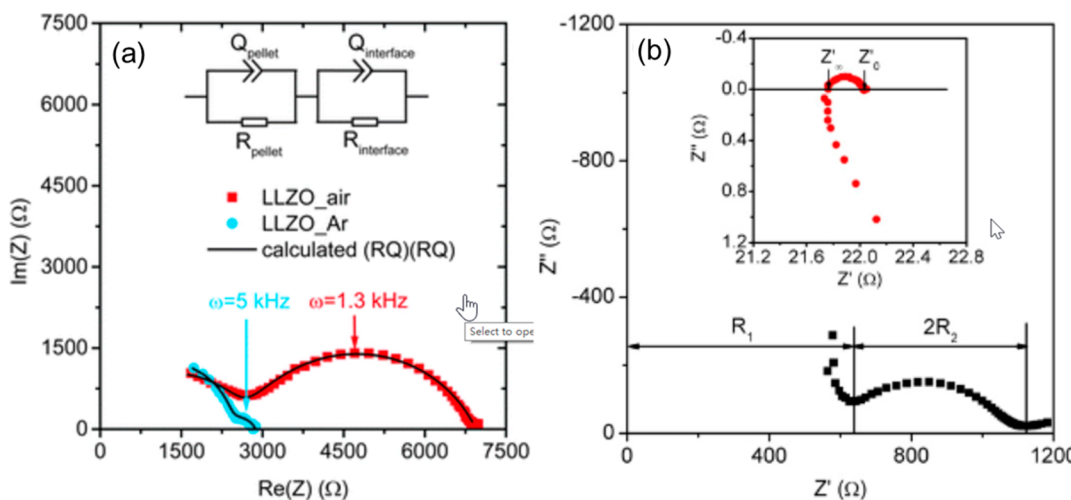


Figure 18. (a) Nyquist plots of symmetrical cells containing pellets sandwiched between lithium electrodes. (Figure inset: $(R_{\text{pellet}}Q_{\text{pellet}})(R_{\text{interface}}Q_{\text{interface}})$ equivalent circuit). Reproduced with permission from ref 213. Copyright 2014 The Royal Society of Chemistry. (b) Initial and short-circuited (inset) impedance spectra of Li/LLZTO/Li symmetric cell. Reproduced with permission from ref 147. Copyright 2015 Elsevier.

frequency can be identified on the EIS curve. When the Li metal is used as the electrodes, there is no diffusion tail in Li-garnet-Li symmetric cells but there could be an additional semicircle if the interface resistance is significant (Figure 18a).²¹³ If the grain boundary resistance is significant, a semicircle at midfrequency range will also be visible. The capacitance values can be analyzed to distinguish between the grain boundary and interface resistance. The semicircle corresponding to the interface resistance at low frequency can be used to study the influence of surface modification on the contact between the Li metal anode and SSEs. In a full cell, if the interface resistance at the cathode is significant, there will be a third semicircle associated with the cathode/garnet interface resistance, which is different from the resistances corresponding to garnet bulk and Li/garnet interface on the EIS curve.^{180,214,215} The semicircles corresponding to the interface resistances between electrodes and SSEs can also be used to study the interface stability after cycling. In Li-garnet-Li symmetric cells, EIS can also be used to diagnose short-circuits. The fully short-circuited EIS spectra has much lower resistance than the initial spectra, and a tail corresponding to inductance will appear below the real axis (Figure 18b).¹⁴⁷

4.2.2. Symmetric Li Cycling (DC). The high interface resistance at the cathode side makes cycling of full cells challenging for garnet based solid-state batteries. To evaluate the electrochemical stability and cycling properties of garnet SSEs, the easiest configuration is the Li symmetric cell, especially after the wetting problem between the molten Li and garnet has been addressed by multiple surface modification techniques. The low interface resistance between Li anodes and garnet SSEs enables high current density cycling with low over potential, while the Li metal provides enough Li for high capacity cycling. Therefore, symmetric Li cycling has almost become the standard electrochemical measurement for garnet SSEs. However, as the cycling current density gets close to the critical current density (where the cell becomes short-circuited), the diagnosis of short-circuit for the symmetric cell becomes super challenging. Since both sides are Li metal, the open circuit voltage is always zero, which makes the voltage profile of symmetric cell act like a resistor. Even though the cell is short-circuited, the feature of the voltage profile is still the same.

A possible electrochemical method to diagnose a short-circuit in symmetric cells is EIS. Ideally, the EIS curve normally contains one or more semicircles above the real axis for a cell without a short-circuit, while a short-circuited symmetric cell only has an inductance component below the real axis on the Nyquist plot. However, short-circuits in solid-state batteries are more complicated, as a “soft” short circuit state can exist. Soft short circuit is a state where the SSEs have both ionic and electrical conductivity, and these two types of conductivities are comparable to each other. At the soft short state, the EIS curve of the symmetric cell can have similar features as that of the cell without short circuit. In some cases, EIS curves can even recover from the soft short state to the pristine state, which makes the EIS technique unreliable for diagnosing a short circuit in symmetric cells. Because of this issue, Albertus et al. proposed a depletion test to prove that cell have no short-circuit after high current cycling.²¹⁶ Theoretically, if the cell is not short-circuited, the voltage will increase after one side is fully depleted of Li. However, this method is not practical for real tests. Since Li does not have a uniform coating on the garnet, when the Li is almost depleted, some areas may lose contact with the garnet SSEs, which will result in an increase of the local current density. Even though the cell is not short-circuited during the high current cycling, the short-circuit may form during the depletion test due to increased local current density. Moreover, if the cell is in the soft short state, Li can still be potentially depleted, or the soft short Li filament can be dissolved during the depletion process. In any situation, the depletion test is not a reliable technique for determining short circuits. Recently, Janek's group applied galvanostatic electrochemical impedance spectroscopy (GEIS) to measure operando changes of the impedance during Li stripping/plating, which can be a reliable tool to monitor Li dendrite growth, soft short circuits, and changes in the interface contact.^{171,197}

4.2.3. Solid-State Li Nuclear Magnetic Resonance (NMR) Study. Since both ^7Li and ^{6}Li are NMR active isotopes, NMR can be a powerful tool to detect Li in SSEs. NMR has been widely used to study Li-ion transport pathways and proton exchange mechanism in garnet SSEs. The ^6Li NMR results for the $\text{pH} \approx 3$ treated $\text{Li}_3\text{La}_3\text{Ta}_2\text{O}_{12}$ and $\text{Li}_3\text{La}_3\text{Nb}_2\text{O}_{12}$ garnet SSEs indicated that the Li ions in the nonmobile site undergo proton

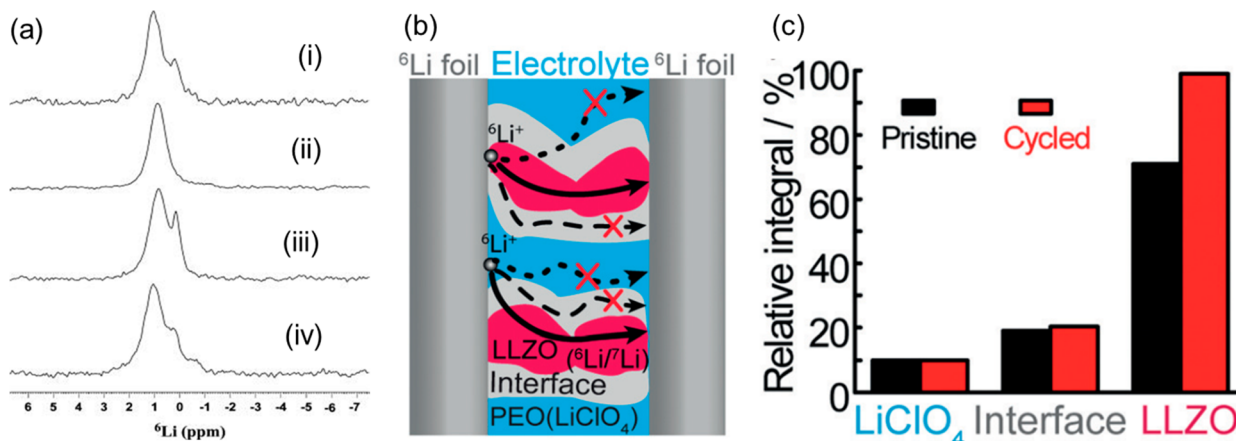


Figure 19. (a) The ${}^6\text{Li}$ MAS NMR spectra for the $\text{H}^+ \rightarrow \text{Li}^+$ exchanged LiLaTa and LiLaNb ($\text{pH} \approx 3$) garnet materials: (i) LiLaTa -white, (ii) LiLaTa -tan, (iii) LiLaNb -pink, and (iv) LiLaNb -tan. Reproduced with permission from ref 80. Copyright 2010 American Chemical Society. (b) Illustration of the symmetric ${}^6\text{Li}$ foil/composite electrolyte/ ${}^6\text{Li}$ foil battery and possible Li^+ transport pathways within the composite electrolyte upon cycling the symmetric battery. (c) Quantitative analysis of ${}^6\text{Li}$ amount in LiClO_4 interface, and LLZO of the LLZO-PEO (LiClO_4) before and after cycling. Reproduced with permission from ref 218. Copyright 2016 WILEY-VCH.

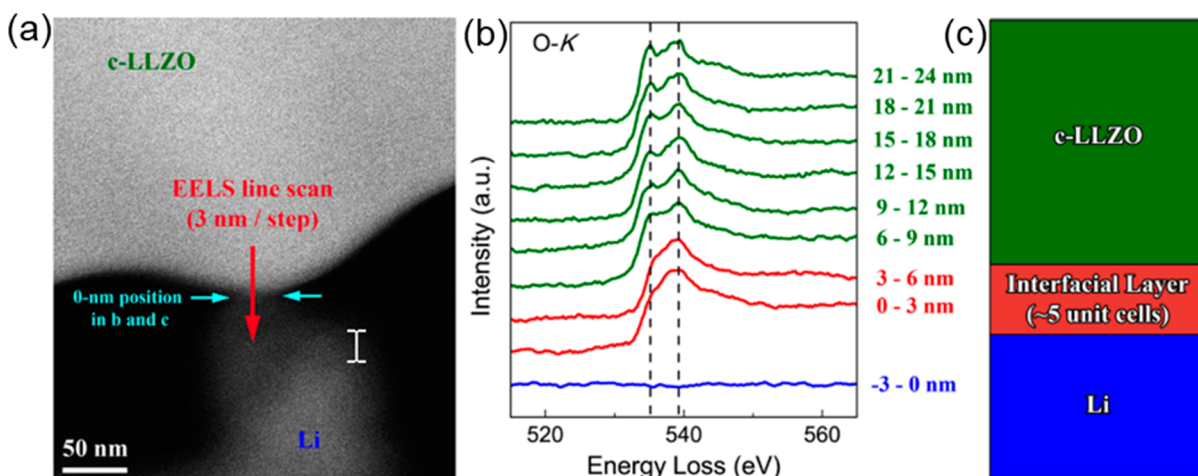


Figure 20. Formation of the c-LLZO–Li interfacial layer. (a) HAADF-STEM image of c-LLZO in situ contacted with Li. The variation of the O K-edge across the c-LLZO–Li interface was examined using an EELS line scan with a 3 nm step size. (b) O K-edges obtained in the EELS line scan described in panel a. The two-peak characteristic of c-LLZO is indicated with dashed lines. (c) Schematic illustration of the interfacial behavior suggested by the EELS line scan. Reproduced with permission from ref 162. Copyright 2016 American Chemical Society.

exchange more readily than the mobile Li ions (Figure 19a).⁸⁰ A similar NMR technique has been reported by Thangadurai and co-workers to study Li-ion occupancy sites and proton exchange reaction in garnet SSEs.^{189,217} Recently, Bachman et al. studied Li dendrite growth in LLZO using Li NMR,⁷ which can detect early stages of Li dendrite growth before short-circuits.⁹ Besides the Li transport mechanism in the crystal structures of garnet SSEs, NMR has also been used to study Li-ion transport in garnet based composite electrolytes. Hu et al. successfully used NMR to probe Li-ion transport in PEO-LLZO composite electrolytes and determined that Li ions prefer to transport through the ceramic phase instead of the PEO-LLZO interface or the PEO (Figure 19b, c).²¹⁸

4.2.4. In Situ Characterizations. *In situ* characterization methods are always needed to study real-time changes of material properties. In solid-state batteries, interfaces are the one of the main factors that affect the battery performance and attract the most concern. However, solid-state makes *in situ* characterization more challenging, especially for interface characterizations. Chi and co-workers applied *in situ* electron

microscopy to study the interfacial layer between Li metal and garnet SSEs. The electron energy loss spectroscopy (EELS) analysis indicates that Li metal contact with garnet SSEs (Figure 20a) caused variation of the EELS O K-edge across the interface. Since the O K-edge can be directly related to local atomic and electronic structures, the variation of EELS O K-edge indicates the formation of an interfacial layer (Figure 20b). The thickness of this interfacial layer was estimated to about 6 nm, less than five unit cells of cubic garnet (Figure 20c).¹⁶² This *in situ* observation explains the origin of the interfacial resistance between Li metal and garnet SSEs and also reveals the excellent chemical stability of garnet SSEs against Li metal anode.

Another powerful *in situ* characterization technique for solid-state Li batteries is neutron depth profiling (NDP), which can directly and quantitatively measure the Li element. Hu et al. successfully used NDP to monitor Li transport and study Li stripping-plating behavior of garnet-based cells in real time (Figure 21a,b).²¹⁹ Since NDP is a quantitative characterization technique, it demonstrated great capability in diagnosing short-circuits in symmetric solid-state cells. As mentioned previously,

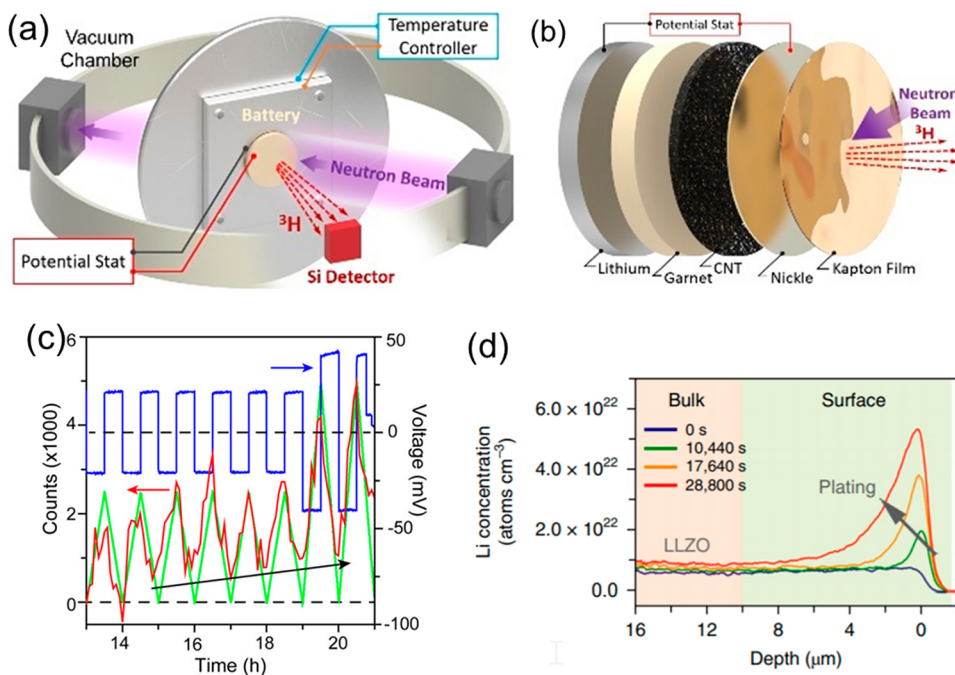


Figure 21. (a) Schematic of the NDP system. (b) Cell configuration of the asymmetric cell for NDP measurement. (c) Prediction capability of NDP for short-circuit diagnosis. Reproduced with permission from ref 219. Copyright 2016 American Chemical Society. (d) Time-resolved lithium concentration profiles for Li/LLZO/Cu cell. Reproduced with permission from ref 173. Copyright 2019 Springer Nature.

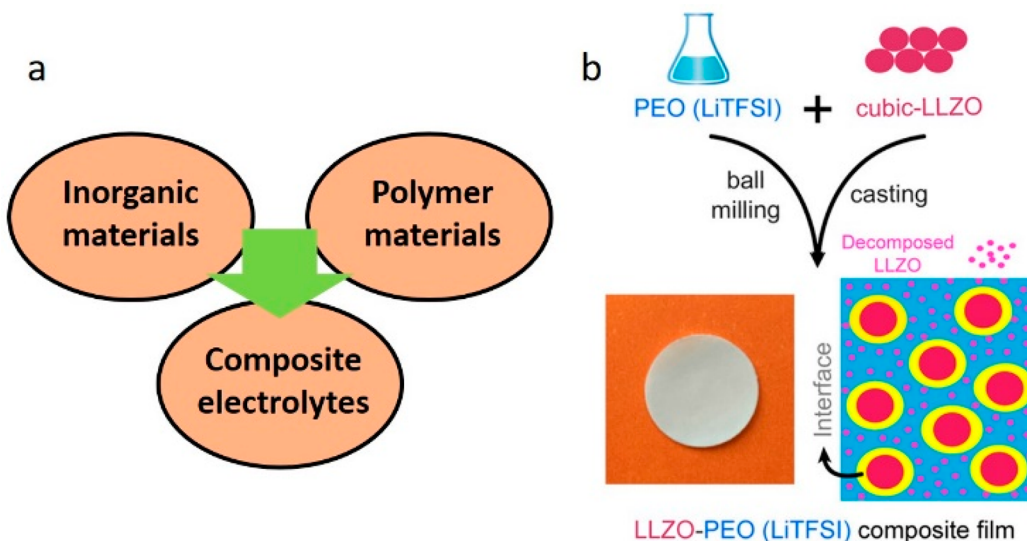


Figure 22. (a) Composite electrolytes consisting of inorganic and polymer materials. (b) Schematic of the preparation process of a typical solid composite electrolyte. Reproduced with permission from ref 224. Copyright 2018 American Chemical Society.

the short-circuit diagnosis of symmetric cells is challenging with electrochemical or other techniques. In NDP measurements, once the short-circuit causes low Coulombic efficiency, the NDP count curve will start to deviate from the charge curve. Even a soft short in a symmetric cell can be quantitatively identified with the NDP technique (Figure 21c), which is not achievable for EIS or other methods. The depth dependence enables NDP to provide more Li distribution information at the surfaces or interfaces of solid-state batteries. On the basis of this capability, Wang and his co-workers used NDP technique to demonstrate that the dendrite formation in LLZO and Li_3PS_4 SSEs is mainly due to the high electronic conductivities, since Li was directly deposited in the bulk of SSEs during cycling (Figure 21d).¹⁷³

5. EMERGING NANOSTRUCTURED SOLID ELECTROLYTE DESIGN

5.1. Nanogarnet Solid Electrolyte Synthesis

Designing solid electrolytes into nanostructures has been widely considered as an effective and promising way to improve the electrochemical and mechanical properties of solid electrolytes. Nanostructured solid electrolytes in the form of nanoparticles, nanorods, or nanofibers exhibit high surface area and highly active surface sites, and compared to the bulk structure of solid electrolytes, these nanostructured solid electrolytes provide different ion transport mechanisms when they are hybridized with polymers and Li salts.^{218,220–223} With the rapid develop-

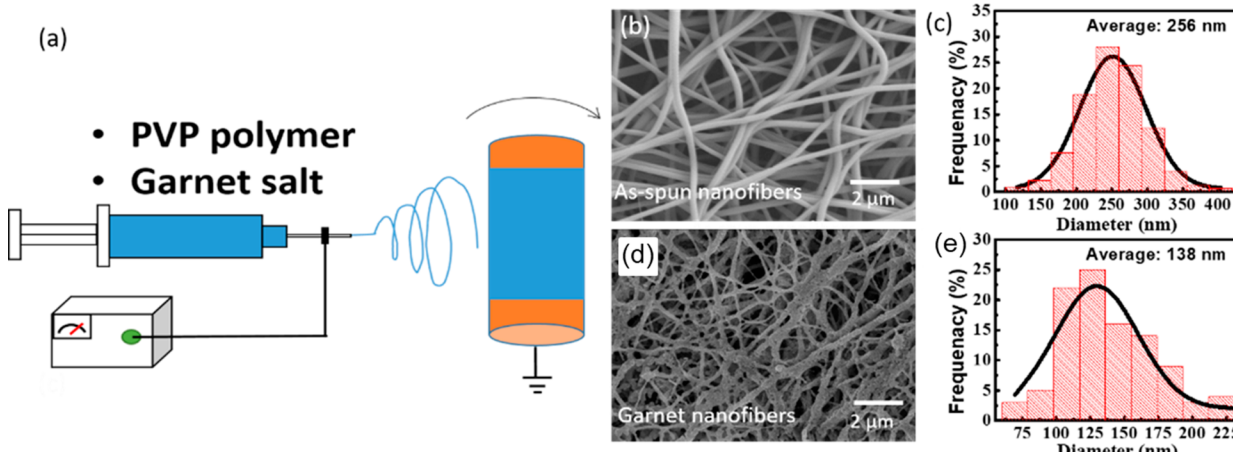


Figure 23. (a) Schematic of electrospinning setup for LLZO precursor nanofibers. PVP is used as carrier polymer to load garnet LLZO salt. (b, c) SEM images and diameter distribution of as-spun nanofibers before sintering. (d, e) SEM images and diameter distribution of sintered LLZO nanofibers. Reproduced with permission from ref 225. Copyright 2016 National Academy of Sciences.

ment of solid-state electrolytes and batteries, recently extensive work has been reported about the synthesis of solid electrolytes in nanostructures and the exploration of ion transport mechanisms in hybrid solid electrolytes. A typical composite electrolyte consists of inorganic solid electrolytes and Li-salt containing polymer electrolytes (Figure 22a). Integration of solid components into polymers has been demonstrated across a range of material sets including 0D nanoparticles, 1D nanofibers, 2D thin films, 3D networks. In the composite system, nanoparticles are incorporated to influence the recrystallization kinetics of the PEO polymer chains to promote local amorphous regions, thereby increasing the Li salt/polymer system's ionic conductivity. Figure 22b shows a typical preparation and structure of a composite electrolyte using polymer electrolyte (e.g., PEO and LiTFSI salt) and inorganic ion conducting nanoparticles such as garnet-type $\text{Li}_{6.4}\text{La}_3\text{Zr}_2\text{Al}_{0.2}\text{O}_{12}$ (LLZO) particles.²²⁴ In this composite system, Li ions may transport via the polymer matrix, inorganic fillers, the organic–inorganic interfaces, or a combination of the three. Li-ion transport pathways, together with active Li-ion concentration and Li-ion mobility, will determine the ionic conductivity of solid composite electrolytes.

Recently, Al-doped c-LLZO nanofibers (average diameter of 138 nm) were prepared by electrospinning, and these LLZO nanofibers were used as continuous nanostructured ceramic fillers for PEO-based composite electrolytes.²²⁵ The nanofiber mat directly obtained after electrospinning (Figure 23) was calcined, and then a PEO/LiTFSI solution was infiltrated into the empty space within the three-dimensional LLZO network to create a “fiber-reinforced” composite polymer electrolyte with extended interfaces between the LLZO and PEO. With an approximate LLZO filler loading of 20 wt %, the resulting CPEs displayed excellent thermal stability, room temperature ionic conductivity of $2.5 \times 10^{-4} \text{ S cm}^{-1}$. This work shows a promising strategy to apply solid electrolyte nanostructures to reinforce polymer electrolytes in the aspect of mechanical property and ionic conductivity. Beside electrospinning, cellulosic materials can be also used as templates to sinter LLZO nanowires by soaking LLZO salt precursors into cellulose nanofibrils or bacterial cellulose, followed by sintering at high temperature to decompose cellulose and subsequently form crystal LLZO nanowires.^{223,226} It is anticipated that if long-range fiber templates could be produced, it is possible to produce

continuous LLZO single fibers, which can be potentially used as solid electrolytes for wearable solid-state batteries.

5.2. Transport Mechanism in Garnet-Based Composite Electrolytes

Establishing a better understanding of the ion transport mechanism and the corresponding control parameters in composite electrolytes is very important to guide future solid composite electrolyte development. Currently, it is widely accepted that adding nanoscale filler can largely reduce the crystallinity of polymer electrolytes to become amorphous, thus allowing ions to move and transport more freely in the surrounding environment. However, it remains unclear if it is cations (e.g., Li^+) or anions (e.g., TFSI^-) that get free movement in the electrolyte system. Very often, the transference number is neglected. Since PEO is mostly used in solid polymer composite electrolyte systems, its ion transport mechanism has been known to involve cations (Li^+) coordinating with oxygen atoms along the PEO polymer chains and diffusing in a mechanism of interchain or intrachain hopping. On the basis of this understanding, the amorphous region created by the nanoscale fillers in PEO electrolyte is actually providing free space for anions (e.g., TFSI^-) to move, therefore, the PEO-based electrolyte composite system normally shows a low transfer number.²²⁷ Recently, ionic transference numbers in PEO/LLZO composites with different concentrations of nanoparticles have been studied (Table 2). The highest ionic transference number of the highest ionically conductive composites (16% LLZO in PEO) is only 0.39. Determining how to improve the

Table 2. Ionic Transference Number (T_{Li^+}) for Composites with Different Volume Fractions of LLZO Nanoparticles²²⁷

sample	I_0 (μA)	I_s (μA)	R_0 (Ω)	R_s (Ω)	T_{Li^+}
PEO:4%Ga-LLZO	0.27	0.08	823	935	0.29
PEO:6%Ga-LLZO	1.29	0.42	322	643	0.31
PEO:8%Ga-LLZO	2.47	0.82	289	424	0.33
PEO:10%Ga-LLZO	6.33	2.37	123	176	0.36
PEO:12%Ga-LLZO	5.50	1.98	121	162	0.35
PEO:14%Ga-LLZO	15.45	6.07	43	48	0.37
PEO:16%Ga-LLZO	18.68	8.22	35	38	0.39
PEO:18%Ga-LLZO	15.71	6.22	56	62	0.36
PEO:20%Ga-LLZO	7.90	2.69	101	122	0.32

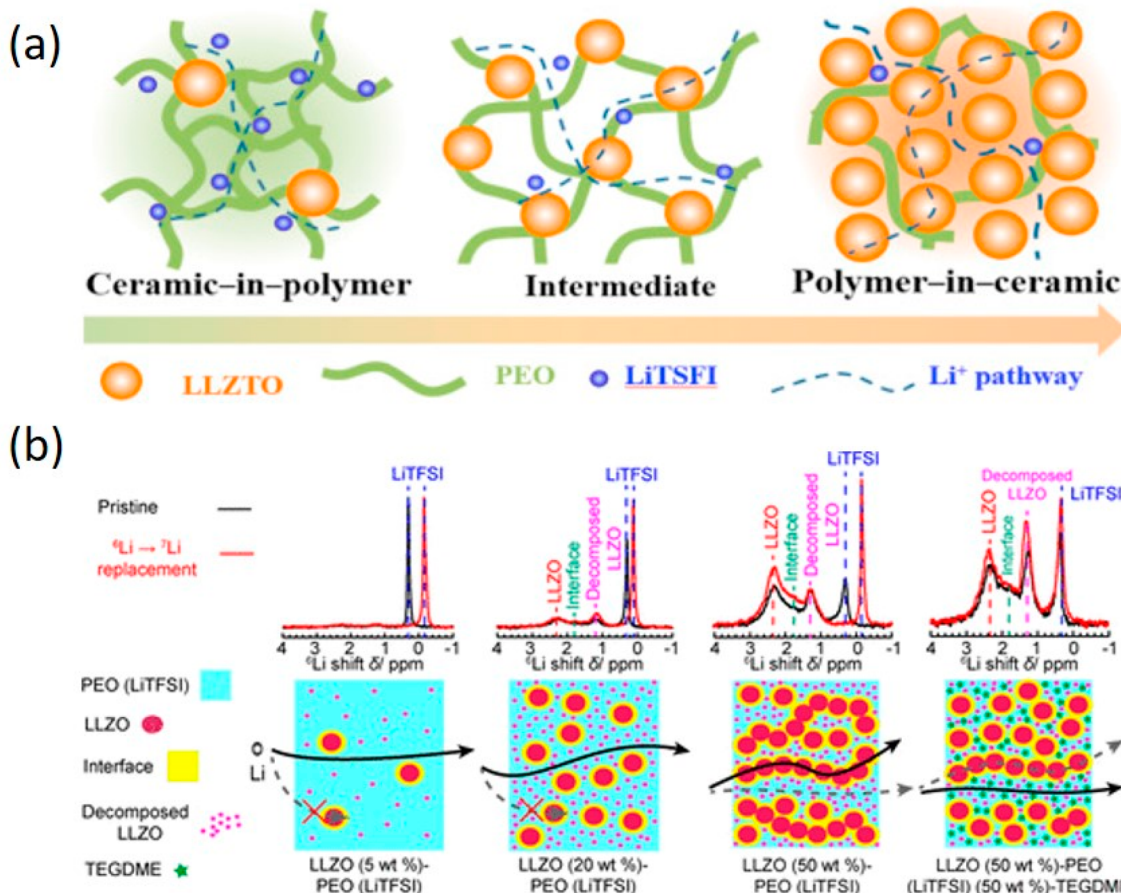


Figure 24. (a) Schematic of possible ion transport mechanism in “ceramic-in-polymer” and “polymer-in-ceramic” electrolyte system. Reproduced with permission from ref 228. Copyright 2017 Elsevier. (b) Schematic of Li-ion pathways within LLZO-PEO electrolyte system with different LLZO concentrations and the ^{6}Li NMR comparison for each type. Reproduced with permission from ref 224. Copyright 2018 American Chemical Society.

ionic transference number in composite electrolytes is one of the key directions for the future.

Although the amorphous region mechanism for fast ion transport is widely accepted in PEO-based composites, extensive studies and research groups put much effort into the development of nanofillers to study their effects on the electrochemical and chemical performance of solid electrolytes. Recently, a study to compare the “ceramic-in-polymer” and “polymer-in-ceramic” electrolytes was reported (Figure 24a²²⁸). It claims that Li⁺ transport channels provided by the LLZO could contribute to an enhancement of the Li⁺ conduction capability as well as the mechanical properties due to the presence of rigid LLZO particles that forms a robust and stable framework. It is still not clear whether LLZO contributes to the ion conduction pathway or not. The work has shown that the highest ion conductivity comes from 10 wt % LLZO fillers in PEO electrolytes with the ionic conductivity of 1.17×10^{-4} S/cm at 30 °C. More and more research groups believe that adding nanofillers, especially active inorganic solid electrolyte nanostructured fillers could significantly increase the ionic conductivity of their hybrid electrolytes.

To characterize the interface between inorganic LLZO fillers and polymers and identify the possible Li⁺-ion transport pathways is very important. Recently, Hu and co-workers employed solid-state NMR to determine the ion mobility, ion transport pathways, and active concentration in the LLZO-PEO composite electrolytes (Figure 24b²²⁴). Their work shows that

the ion mobility decreases with the increase of LLZO in PEO, and the ion transport pathways gradually transform from PEO to the loosely connected LLZO particles. This work can be considered to be the first time evidence provided to confirm the inorganic LLZO solid electrolyte indeed contributes and dominates the Li⁺-ion transport in LLZO-PEO hybrid electrolyte composites. However, the concentration of LLZO fillers in PEO electrolyte varies in different works. It suggests that content of LLZO fillers in PEO electrolyte may vary in terms of ionic conductivity, and thus ionic performance would be dominated either by the LLZO network or the bulk polymer electrolyte. A new question arises, which is associated with the percolated network of LLZO. If this is the case, is it possible prepare a loosely sintered LLZO pellet and infiltrate PEO electrolyte to the porous structure to achieve high ionic conductivity as well? The ion transport mechanism should be completely different from the vacancy disorder within the Li sublattice leading to enhanced hopping paths for Li⁺ ions and an increase in conductivity over well sintered and densified LLZO.

Recently, experimental results have shown that the enhancement of ionic conductivity is closely related to the space charge region, with a thickness of ~3 nm formed at the interface between the polymer matrix and LLZO nanoparticles.²²⁷ The space charge is caused by the redistribution of lithium vacancies and ions. In this region, some of the Li⁺ ions at regular LLZO lattice sites tend to move to surface sites, resulting in negatively charged vacancies in the lattice and positively charged Li⁺ ions

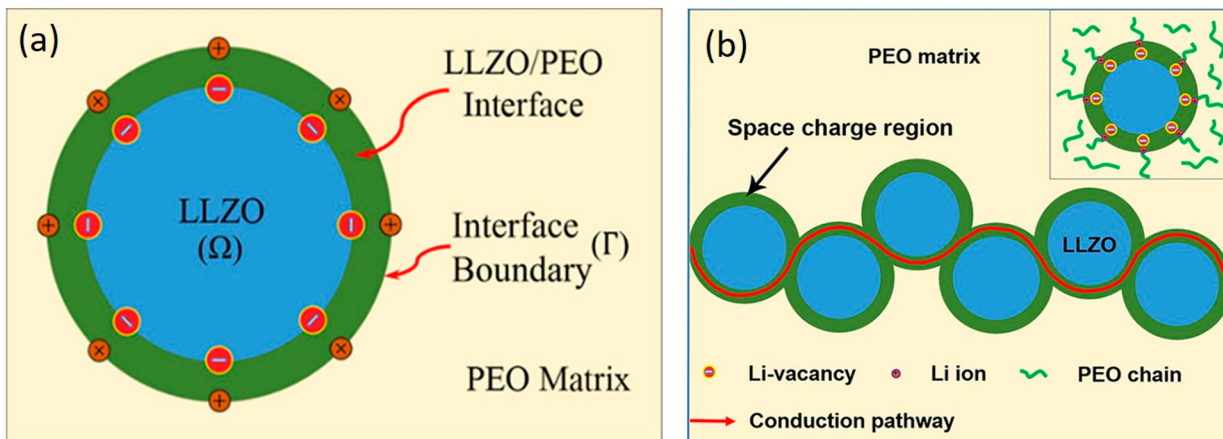


Figure 25. (a) Schematic of LLZO nanoparticles in PEO/LLZO composite. The surface is the space charge region. (b) Schematic of the fast ionic conduction pathway along the space charge regions. Reproduced with permission from ref 227. Copyright 2018 American Chemical Society.

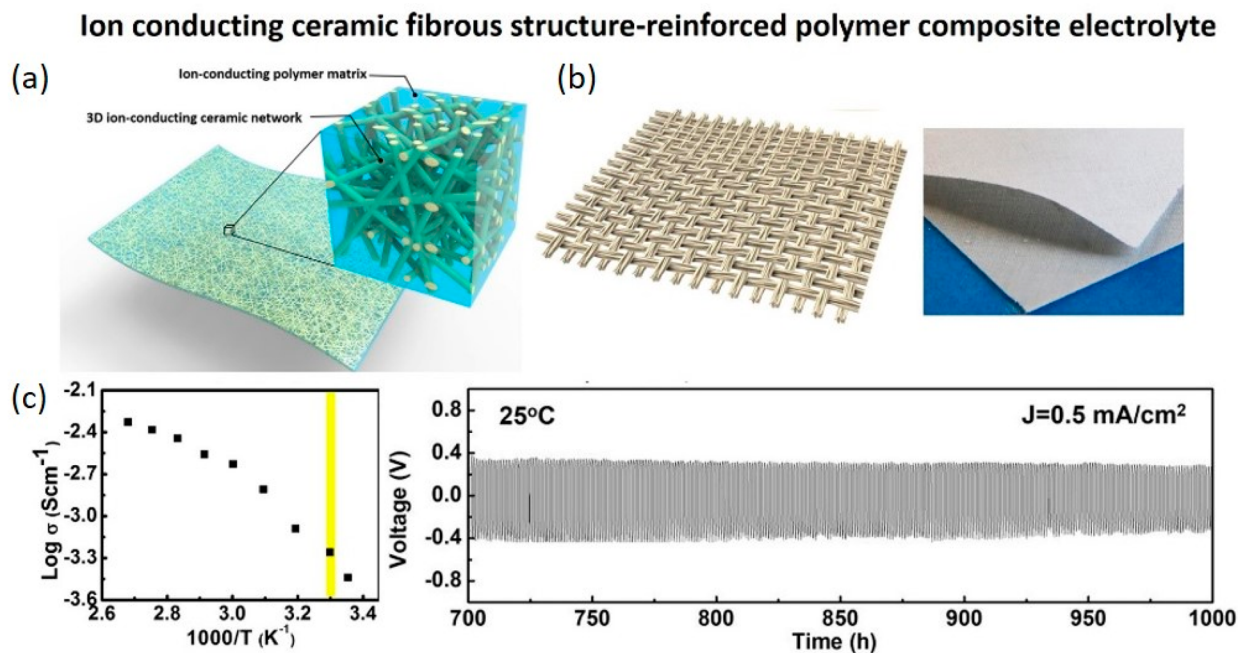


Figure 26. Ion-conducting ceramic-based fibrous networks (a, nanofibers; b, textile woven structure) for electrochemical enhancement of solid composite electrolyte. (c) Fiber-based composite electrolyte shows a high room-temperature ionic conductivity and stable long-term Li stripping/plating cycles with no sign of Li dendrite-induced short circuit. Reproduced with permission from refs 225 and 229. Copyright 2016 National Academy of Sciences. Copyright 2018 Elsevier.

on the surface, as shown in Figure 25a. The ion transfer mechanism is suggested in Figure 25b. When the generated space regions in individual nanoparticles are connected to each other, a continuous pathway for the space charge regions is formed. Even though the LLZO content exceeds the percolation threshold value, the continuous pathway of the space charge region can be still treated as a fast channel for lithium-ion transportation.

5.3. Nanostructure Design toward Flexibility and High Conductivity

Developing nanostructures is an essential approach to increase the ionic conductivity of composite electrolytes due to the increased surface area of the amorphous region and improved interface between fillers and polymers. How to increase the rate of Li $^{+}$ -ion transport is thus a question of immense practical

interest; it is also fundamentally challenging due to the intrinsic coupling between property-structure-process that governs ion transport and mechanical behavior. To further increase the ionic conductivity and mechanical strength, the inorganic nanoparticles must be connected into a continuous network thus facilitating fast ion transport and mechanical interlock. Recently, Hu and co-workers have pioneered solid composite electrolytes using inorganic garnet-type solid-state electrolytes in the form of continuous and interconnected fibrous structures, such as nanofibers, textiles, and cellulose nanofibrils, to reinforce PEO-based ion conducting polymer electrolytes and good electrochemical and mechanical properties have been achieved.^{225,226,229} A fibrous structure with a high surface area/volume ratio would be the ideal architecture for the ionic conduction and electrochemical reactions that occur in batteries. The electrospinning method was used to co-

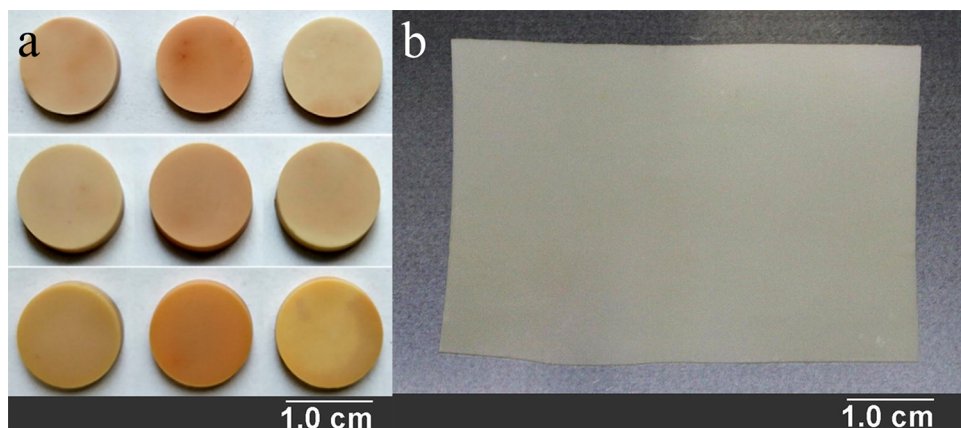


Figure 27. Thickness of garnet solid-state electrolyte with different processing technique: pressing versus tape casting. Reproduced with permission from refs 230 and 231. Copyright 2018 Elsevier. Copyright 2018 Elsevier.

electrospin ceramic salt and carrier polymer for making nanofibers. Similarly, a textile fabric was also used as sacrificial template instead of the polymer nanofibers to generate the necessary nano- and microstructures, wherein the template contained ceramic precursors. The fibers and template could then be pyrolyzed under high temperature to remove the organic components and the template, leaving ion conducting fibrous structures derived from the nanofibers or template (Figure 26a). The flexible solid-state electrolyte composite membrane developed in our previous work exhibited an ionic conductivity of 2.5×10^{-4} S/cm at room temperature. The membrane can effectively block dendrites in a symmetric Li/electrolyte/Li cell during repeated lithium stripping/plating at room temperature, with a current density of 0.2 mA/cm² for around 500 h and a current density of 0.5 mA/cm² for over 300 h (Figure 26c). Therefore, we believe that fibrous-reinforced composite electrolytes are emerging as a promising strategy to deliver high ionic conductivity and electrochemical performance, better thermal stability, and improved mechanical robustness for high-performance solid-state batteries.

Recently, Hu and co-workers also employed a textile-template process to create the proof-of-concept Li⁺-ion conductive fibrous ceramic fabrics (Figure 26b), which generates a unique structure with fine 3D scale distribution of continuous Li⁺-ion conductive phase, high surface area/volume ratio, low gravimetric density, multilevel porosity, certain strength and flexibility, for solid-state safe, high energy Li-metal batteries.²²⁹ The architectural advantages may allow the fibrous ceramic fabrics to be integrated to build components of batteries such as flexible composite polymer electrolytes with a rigid electrode skeleton. The fibrous garnet textile shows pronounced new characteristic features to tolerate certain flexural strain, geometrical tailoring, and organic solvent erosion, which are distinct from the rigid appearance of typical sintered ceramic bodies. The chemical analysis confirmed cubic phase of the fibrous garnet fabrics and homogeneous distribution of the constituent elements. Because of the simplicity, rapidity, and cost saving characteristics of the template method, applicable transition from laboratory scale fabrication procedure to industry scale manufacturing is potentially achievable.

6. BATTERIES USING SOLID-STATE ELECTROLYTES

6.1. Architectures

In addition to optimizing the electrochemical properties of Li garnet electrolyte materials, cell level rational design is essential to attaining practical solid-state Li-ion batteries (SSLiBs). The design considerations include electrolyte thickness, anode structure, cathode structure, interface modifications, current collectors, and packaging. Stack level design is not discussed here.

6.1.1. Thin Film Planar Structure. To achieve maximum energy and powder density, the electrolyte layer needs to be as thin as possible. At the current early development stage of SSLiBs, most of the lab scale research uses thick dense pellets, usually 500 μ m or larger.²³⁰ For high energy density SSLiBs, thin electrolyte layers of less than 30 μ m are required to be competitive with conventional Li-ion batteries. The tape casting process has been used to achieve a thickness as low as 15 μ m.²³¹

Figure 27 provides a visual comparison between thick dense pellets and garnet thin film. Further reducing electrolyte thickness to hundred nanometers can be achieved by using thin film deposition techniques. Conventional SSLiBs have been targeted for embedded devices, where longevity and stability are paramount, rather than capacity, power density, and cost. To meet these needs, thin film structures have been extensively adopted. There are many good reviews on this topic, and we refer interested readers elsewhere to learn more.²³²

6.1.2. Ordered LLZO Scaffold Structure. Unlike sulfide solid electrolytes, which are ductile, Li garnet electrolytes are hard and brittle. When the thickness of the thin Li garnet electrolyte is less than 100 μ m, they are vulnerable to electrode volume change and external vibrations. The Li metal anode has infinite volume change during charging and discharging. Assuming there's 10% excess Li at the anode side, the anode volume will expand 11 times from fully discharged state to fully charged state. Such a high strain, could lead to cracks in the garnet electrolyte, especially with thinner electrolytes. Supporting structures are needed to accommodate the volume change. One possible solution is to use a scaffold structure, such as metal foam, carbon foam, or porous garnet. Since metal foam and carbon foam are only electronic conductors, Li metal is expected to plate at the contacting point between the scaffold and electrolyte during charging. Further plating is expected to push the scaffold away from the electrolyte unless a large pressure is applied, in which case mechanical stability is a concern. As a

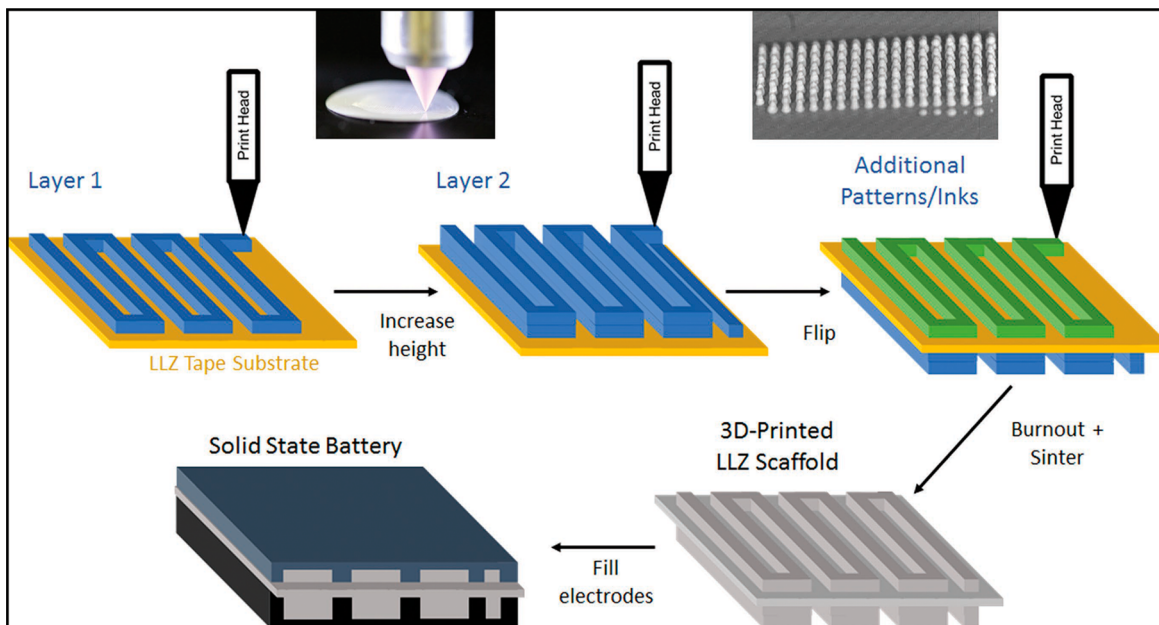


Figure 28. Ordered garnet scaffold fabricated by 3D printing. Reproduced with permission from ref 234. Copyright 2018 Wiley-VCH.

result, such scaffolds are not reported in literature. On the other hand, LLZO scaffolds can be sintered on one or both sides of the thin garnet electrolyte to enhance mechanical strength and tolerate electrode volume change.

Li^+ -ion transport in porous garnet scaffolds for both anode and cathode greatly depends on the tortuosity of the ionic transport path. In the ideal case, tortuosity is as low as unity, which means the transport path is straight. Such structure can be achieved by freeze tape casting. Freeze tape casting has been widely used for fuel cells and solid-state Li-ion batteries. A LATP flexible composite electrolyte was demonstrated,²³³ where the vertically aligned LATP ceramic phase provided fast ion transport. However, there's no such report for garnet type solid electrolytes. Ordered porous LLZO scaffolds have well-defined structures, which can provide good ion transport. There are several ways to achieve such ordered structures, such as 3D printing, templating and phase inversion.

In a report by Wachsman and co-workers, ordered LLZO scaffold was fabricated using a textile as a template.²²⁹ The garnet scaffold can be sintered onto a garnet dense pellet to form an order bilayer structure. The same group demonstrated 3D-printed LLZO column arrays and grids on top of dense LLZO electrolyte (Figure 28).²³⁴ A self-supporting ink slurry containing garnet particles was 3D printed onto green garnet tape. The printed ordered scaffold was then sintered together with substrate tape. The two ordered garnet scaffolds have large openings which is useful for infiltration of cathode active materials. However, the spacing between the printed LLZO features can be as large as $100\ \mu\text{m}$, which could lead to slow mass transport.

Phase inversion is a promising method to achieve ordered vertical-oriented scaffold structures with pore size of less than $10\ \mu\text{m}$.^{233,235,236} Buannic and co-workers demonstrated the freeze casting process,²³⁶ in which a ceramic slurry is first thoroughly mixed as in the conventional casting method. Immediately after casting, the thin film is transferred to a cool surface. Solidification occurs from the bottom due to the temperature gradient. The decreased solubility of the solute in the freezing solvent leads to phase separation. As cooling propagates up, the

liquid solvent prefers to solidify at the existing frozen solvent surface, which leads to vertical growth. Once the whole film is frozen, it is placed under vacuum to sublimate the solvent. The end product is a ceramic scaffold with a vertically aligned porous structure (Figure 29).

6.1.3. Random LLZO Scaffold Structure. Because of the ease of fabrication, porous garnet scaffolds have been demonstrated in several reports.^{231,237–241} It can be cosintered onto a thin garnet electrolyte layer, hence there is no need for external pressure. Because of its ionic conductivity, Li metal can

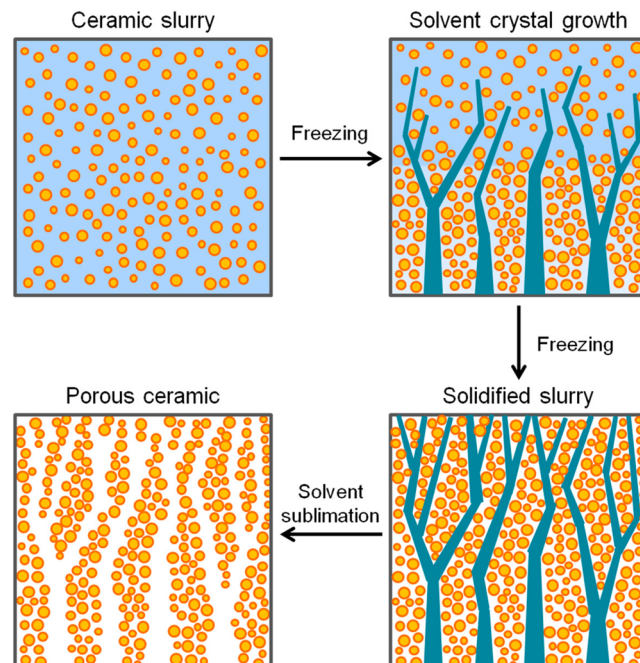


Figure 29. Schematic illustration of freeze casting processing to fabricate vertically aligned porous structure. Reproduced with permission from ref 236. Copyright 2018 The American Ceramic Society.

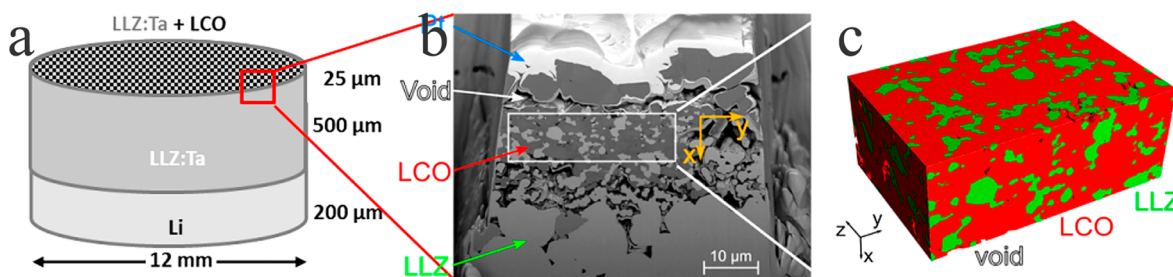


Figure 30. Microstructure of porous garnet scaffold. (a, b) Schematics and FIB-SEM of garnet scaffold on thick dense garnet pellet. (c) Reconstructed cathode structure in panel b. Reproduced with permission from ref 243. Copyright 2018 American Chemical Society.

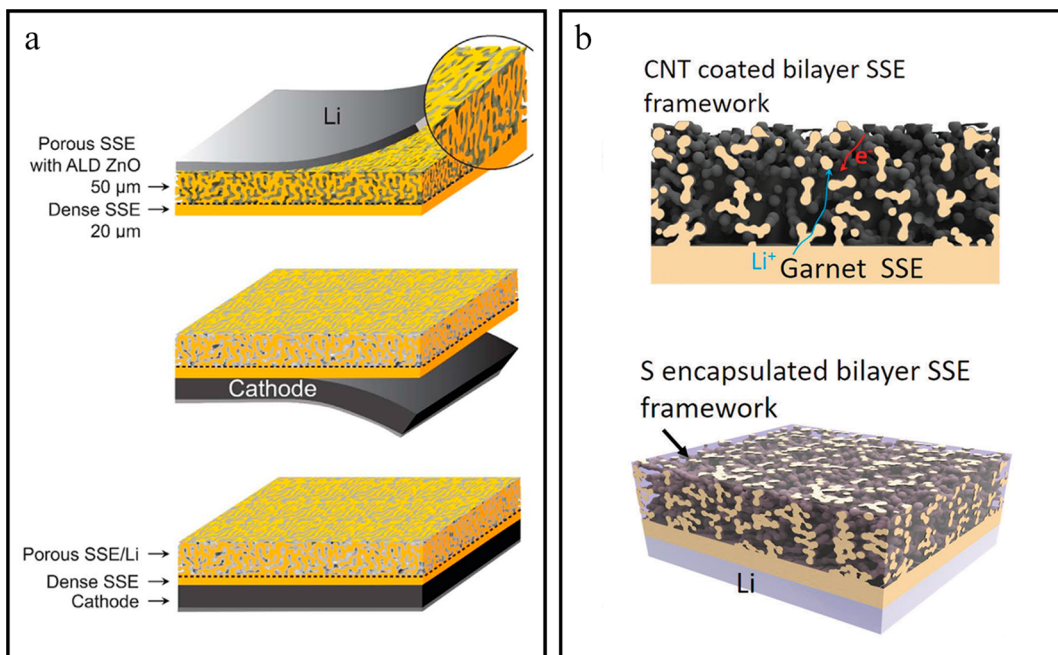


Figure 31. Bilayer garnet where a garnet scaffold is sintered onto thin, dense garnet. (a) Garnet scaffold provides ionic paths and support for Li anode. Commercial cathode tape can be laminated onto the dense side to form a full cell. (b) Garnet scaffold provides ionic path for cathode materials. Reproduced with permission from refs 237 and 240. Copyright 2017 The Royal Society of Chemistry. Copyright 2018 Elsevier B.V.

be plated all over the surface of the scaffold structure and stored in the void space. As a result, there's no mechanical stress on the thin electrolyte. The porous garnet scaffold also adds mechanical support to thin electrolyte so that the structure can withstand more external pressure and vibration.

Li^+ -ion conductivity in most cathode active materials is too low to be used without additional ionic transport paths. Therefore, cathode layers should be a composite containing active materials, electrolyte, binder, and conducting agents. In conventional Li-ion batteries, a slurry of active materials, binder and conducting agents is casted onto metal foil and pressed to increase density and then soaked with liquid electrolyte. In SSLIBs, the solid electrolyte should be mixed in the slurry prior to casting. Then the cathode layer is either pressed onto the garnet electrolyte or stuck by binder or thermal treatment. Again, external pressure is not preferred due to the brittle nature of garnet electrolyte. A gel polymer layer between composite cathode and bilayer garnet electrolyte was demonstrated by Hu and co-workers.²⁴⁰ Thermal treatment to anchor composite cathode onto thick garnet dense pellet has also been demonstrated.^{242,243} The thick garnet pellet hinders high energy density. A promising solution was demonstrated,²³¹ in which a porous garnet scaffold was cosintered onto garnet electrolyte, so

that it can replace the solid electrolyte in the composite cathode. Active materials and conducting agents need to be infiltrated into the garnet scaffold structure. This solution was ideal for Li–S chemistry, because molten sulfur can be easily infiltrated.²³⁷ However, the infiltration process of oxide cathodes still needs development.

As shown in Figure 30a–c, Finsterbusch and co-workers demonstrated the advantage of composite cathode over a pure cathode.²⁴³ Because of the lack of highly conductive Li^+ -ion pathways, pure LCO cathode can only achieve 3% utilization at a thickness of 25 μm . Screen printing was used to apply a LCO/garnet composite cathode onto a thick garnet dense pellet. Garnet in the composite cathode greatly improves ionic transport and reduces mass diffusion resistance. As a result, LCO utilization was improved to 81%. Nearly 1 mAh/cm^2 areal capacity was achieved by adding a 25 μm thick LCO/LLZO cathode onto a 500 μm thick LLZO dense pellet. According to their simulations, a 500 μm thick LLZO dense pellet contributes to an ohmic overpotential of 0.1 V. If a thin dense LLZO dense pellet of a few tens of microns thick was used, ohmic loss will be significantly reduced. The thin electrolyte layer is a more demanding request to achieve high specific energy. However, free-standing LLZO dense pellets less than 50 μm thick is hard

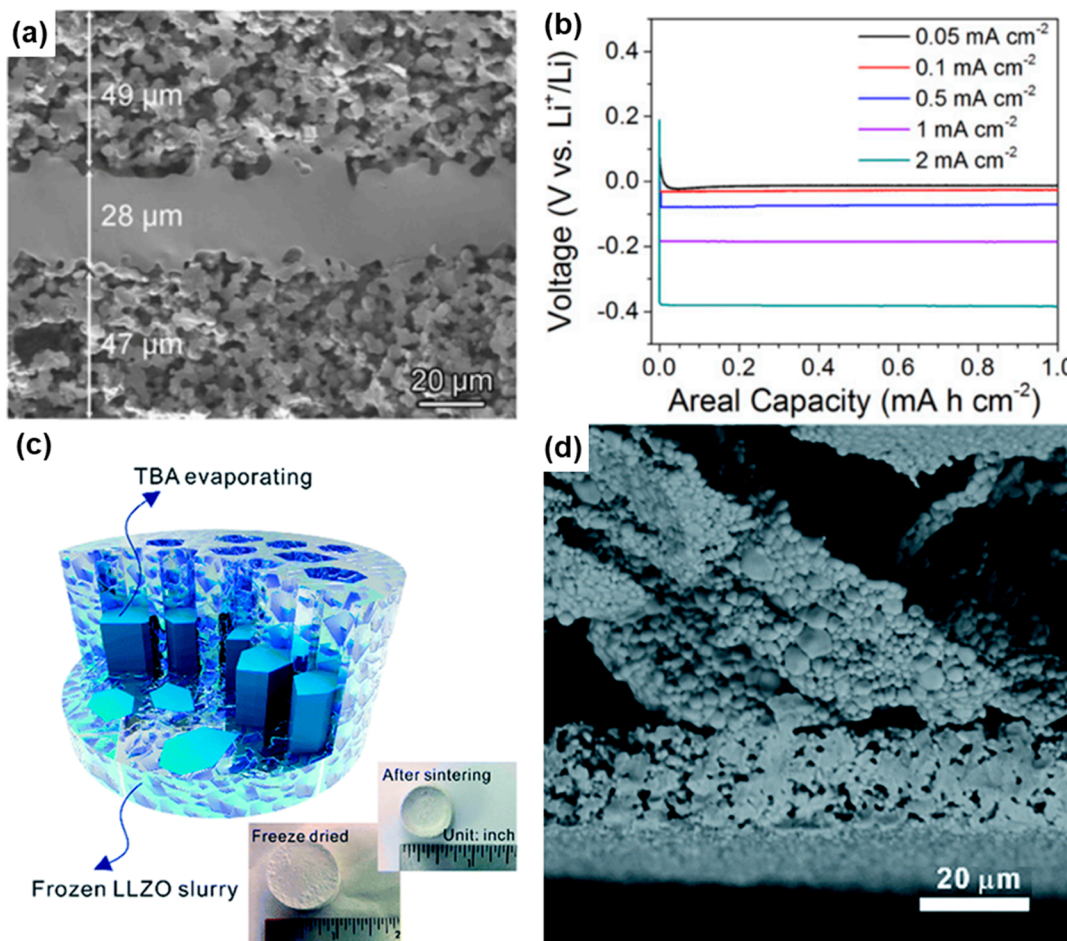


Figure 32. (a) Microstructure of a trilayer garnet scaffold. (b) High current density cycling. (c) Coin size LLZO garnet scaffold made by freeze casting. (d) Microstructure of the aligned porous structure. Reproduced with permission from refs 235 and 238. Copyright 2018 National Academy of Sciences. Copyright 2019 Royal Society of Chemistry.

to fabricate and process. Reinforcement of the thin electrolyte is required.

Nan and co-workers demonstrated the infiltration of LCO into a garnet scaffold,²⁴² in which case the bilayer has a thick dense electrolyte layer. The empty space in the porous layer was made by using pore former such as starch. Porous structures made in this way are random with pore sizes ranging from 1 to 10 μm , depending on the pore former. The porous phase is highly tortuous, which makes infiltration of cathode powders difficult. Instead, they infiltrated a LCO precursor solution and then fired at 700 $^{\circ}\text{C}$ to form the LCO active material. This process is likely difficult to scale due to the low loading and slow processing.

The ion conducting phase within a composite cathode is usually the same material as Li garnet electrolyte. Instead of firing a composite cathode onto a densified LLZO dense pellet, a garnet scaffold can be sintered with the dense garnet electrolyte in one step to form a “bilayer” or “trilayer” structure.^{235,237–240} Then active electrode materials can be infiltrated into the porous layer(s) to form a composite anode or cathode.

To accelerate its wide application, LLZO solid-state electrolyte should be compatible with conventional Li-ion battery production procedure. The organic liquid electrolyte in conventional Li-ion battery is the main cause for its various drawbacks. The replacement of liquid electrolyte by LLZO solid electrolyte can eliminate fire hazards and prevent lithium dendrite growth. While conventional composite cathodes can be

integrated into solid-state lithium metal battery. This provides many options for cell chemistry and materials selection. Hu and co-workers demonstrated the integration of bilayer LLZO scaffold with commercial lithium-manganese-cobalt-oxide (NMC) cathode tapes (Figure 31a).²⁴⁰ The porous LLZO structure hosted Li metal to mitigate anode volume change. Commercial NMC cathode tapes were laminated to the dense side of the bilayer scaffold. A gel polymer layer was used to provide a good interface between LLZO dense electrolyte and commercial cathode tape.

The same group demonstrated the infiltration of a sulfur cathode into a LLZO bilayer as well (Figure 31b).²³⁷ The low melting temperature of sulfur makes the infiltration process relatively simple and scalable. Sulfur reduction involves several steps. Lithium polysulfide is soluble in liquid electrolyte, which promotes reaction kinetics. To take advantage of this mechanism, a liquid electrolyte was added in the composite S/LLZO cathode. Although the cell is not all solid-state, its performance is reasonably stable.

Lithium metal anode has infinite volume expansion from fully the discharged state to fully charged state. Such large expansion can form cracks in the LLZO solid electrolyte due to its brittleness. If porous LLZO scaffold is introduced to the anode side, lithium stripping/plating will be confined in the empty space and there is no external volume change. Together with the porous LLZO scaffold on the cathode side, such a porous/

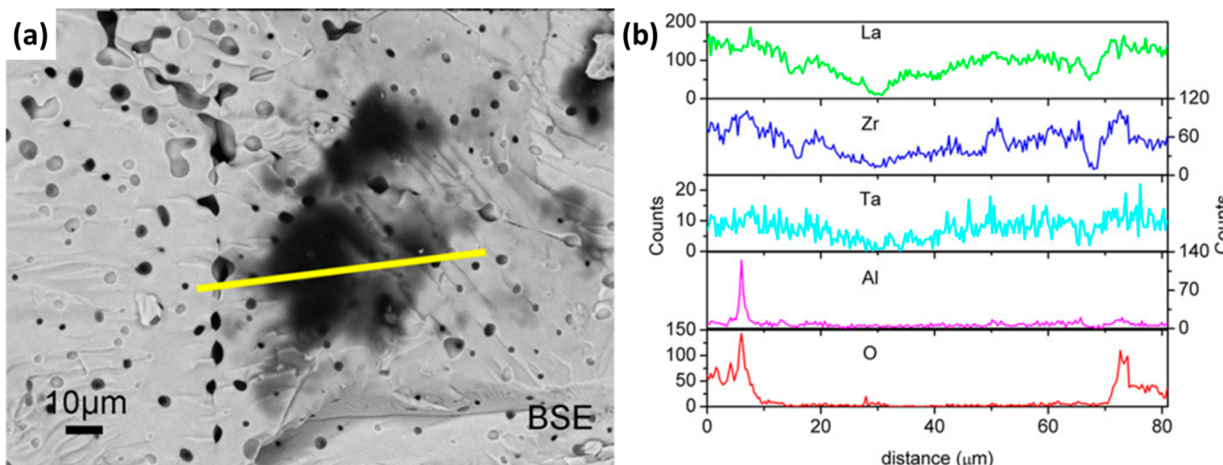


Figure 33. (a) SEM image of lithium plated through pores in lithium garnet electrolyte and (b) EDS line scan along marked yellow line. Reproduced with permission from ref 147. Copyright 2015 Elsevier.

dense/porous LLZO sandwich structure is called a “trilayer” structure (Figure 32a).²³⁸ Besides its volume change buffering effect, the anode side porous structure vastly increases the interface area between lithium metal and LLZO electrolyte, which significantly reduces interface resistance. Meanwhile, the effective area specific current density is reduced. Wolfenstine and co-worker demonstrated the relationship between critical current density (CCD) and lithium dendrite growth.¹⁶⁵ As effective area specific current density is reduced, higher CCD can be achieved. Hu and co-workers presented a detailed study on how lithium metal strips/plates at the anode side during cycling (Figure 32b).²³⁸ It was observed that lithium metal was confined in the empty space. Although random porous structure can accommodate molten lithium or dissolved sulfur, metal oxide intercalation cathode particles cannot be infiltrated into the structure. Doeuff and co-workers used freeze casting to fabricate vertically aligned porous channels as shown in Figure 32c and d. They demonstrated the ability to infiltrate NMC particles in the pores.²³⁵

6.2. Degradation and Failure: Mechanisms, *In Situ/Ex Situ* Characterizations, and Mitigations

Lithium metal anodes have been long been sought for their high energy density. The drive to create lower cost, higher specific energy batteries has led to significant work to develop a compatible electrolyte for a lithium metal anode. The 2007 invention of LLZO lithium garnet¹³⁵ has created a solid electrolyte that meets all the necessary requirements: high conductivity, high thermal stability, high voltage stability, stability to lithium metal and good fabricability.²⁴⁴ Even still, lithium metal anodes are not widely considered ready for deployment in real world secondary batteries.²⁴⁵ This is due to the potential for formation of lithium dendrites and other electronic conduction pathways that could form between the lithium metal and the positive electrode.

To understand the formation of lithium dendrites and other failures of the electrolytes, this paper reviews the examples in literature in which lithium has been cycled across an LLZO electrolyte. General failure modes and conditions which encourage dendrite formation will be discussed and a summary table of all literature.

6.2.1. Failure Modes and Causes. The most likely failure modes of a ceramic lithium electrolyte which can lead to a short circuit are the following. Discussion will consider the causes of

these failures, present evidence from literature, and discuss potential solutions:

1. Plating through pre-existing pores/pinholes
2. Plating through grains
3. Plating through grain boundaries
4. Electronic conduction through grains due to material breakdown
5. Electronic conduction through grain boundaries due to material breakdown
6. Cracking of ceramic separator

6.2.2. Plating through Existing Pores (Pinholes or Other Physical Flaws).

A common failure mode of a solid-state electrolyte is lithium plating through pinholes in the ceramic separator membrane that were created during fabrication of the membrane. Lithium ions will travel the least resistance path from electrode to electrode, which in most cases will result in plating at the closest location between electrodes. Fabrication of a pinhole-free ceramic membranes is a well-established field outside of batteries, with heavy research into minimizing,²⁴⁶ detecting,²⁴⁷ and repairing²⁴⁸ pinholes due to the necessity of an intact membrane for device function. However, in early stage or laboratory scale manufacturing, such defects are common.

Figure 33a shows an SEM image of a pressed and sintered $\text{Li}_{0.75}\text{La}_3\text{Zr}_{1.75}\text{Ta}_{0.25}\text{O}_{12}$ lithium garnet pellet after DC cycling with lithium metal electrodes. Membranes of this porosity are unable to prevent lithium from plating through the pores. This cell short circuited due to lithium plated through pores, as confirmed by an EDS line scan in Figure 33b.

It has been suggested that high density sintering (~96% relative density) will prevent such dendrites,^{146,193,249} but such experiments continue to see dendritic growth. It is possible that even such high densities may have minuscule pores between grains, which continue to allow lithium plating and dendrite formation.

Fabricating ceramic membranes with consistent, perfect integrity is difficult to do at the lab scale without the dust mitigation and closed systems available at the industrial level. Some publications which see the formation of dendrites formed may simply be due to the inevitable result of plating and stripping across a membrane with microscopic pinholes. To limit misinterpretation of results, researchers should test for membrane integrity before cycling.

6.2.3. Plating through Grains (Decomposition or Mechanical Failure of Material). Various theories have suggested that due to the strength and stability of lithium garnet, lithium metal dendrites should not form,¹⁴³ though dendrites do clearly form in many cases. Some models allow for dendrite formation at high currents and low fracture toughness¹⁶⁵ or when there are localized high current densities at the lithium–garnet interface.²⁰⁷ Recently, Chiang et al. conducted Li cycling across a single crystal garnet sample and confirmed that Li dendrites can grow into single crystal garnet SSEs and cause cracks at high localized current densities,^{167,250} which can help test the different models of dendrite propagation that have been proposed.

6.2.4. Plating through Grain Boundaries (Decomposition or Mechanical Failure of Grain Boundary). Models for stability of the garnet material generally do not account for the amorphous character and high impurity/secondary phase content of grain boundaries,²⁵¹ as this is difficult to quantify and varies based on exact composition, synthesis conditions of the garnet material, and fabrication conditions of the garnet body. Intergranular plating is supported by experimental evidence, such as the report in which Cheng et al. cycled lithium across a lithium garnet pellet until short circuit then disassembled for SEM analysis (Figure 34).²⁵² It can be seen in this image, and was otherwise demonstrated in the publication, that the grains themselves are intact but have been separated by lithium metal growth.

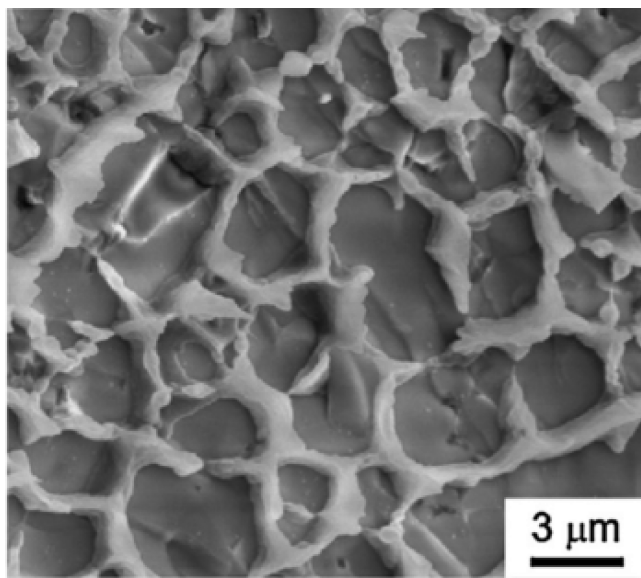


Figure 34. SEM image of lithium metal plated through the grain boundaries of a lithium garnet electrolyte. Reproduced with permission from ref 252. Copyright 2016 Elsevier.

It should be noted that grain boundary chemistry is both an intrinsic and extrinsic property of the material. For example, LLZO is susceptible to Li_2CO_3 segregation in the grain boundaries, whereas lithium beta-alumina is not. However, grain boundary chemistry can be controlled through green body recipe and processing method as well as sintering time, temperature, and environment. For example, a paper by Xia et al. demonstrated that small changes in processing can affect the composition of the grain boundaries.²⁵³ Specifically, they showed that sintering in a Pt crucible leaves less Li_2CO_3

between the grains after sintering (Figure 35). While their claim was an increase in conductivity, decreasing Li_2CO_3 content in grain boundaries also likely slows dendrite propagation, as Li_2CO_3 is not as stable to reduction²⁵⁴ and not as mechanically strong as garnet.

6.2.5. Electronic Conduction through Material (Breakdown of Material). Cyclic voltammetry and Hebb-Wagner polarization studies have demonstrated the stability of garnet between 0 and at least 6 V, even in contact with lithium metal.^{156,255–257} However, modeling has predicted that garnet is only thermodynamically stable between 0.05 and 2.91 V.^{12,258} Outside of this range, irreversible decomposition theoretically takes place, which produces $\text{Li}_6\text{Zr}_2\text{O}_7$, Li_2O_2 , La_2O_3 , $\text{La}_2\text{Zr}_2\text{O}_7$, or O_2 at high voltage and Zr_3O , Li_2O , and La_2O_3 at low voltage as shown in Figure 9. This reaction does not propagate through the garnet due to the low electronic conductivity of the breakdown products, but the Zr_3O can be reduced to Zr at 0.004 V, which is electronically conductive. If this reaction does carry through from the anode to the cathode, this produces a short circuit due to electronic conductivity without true dendrite formation.

Ma et al. demonstrated through high-resolution transmission electron microscopy (HRTEM) that when cubic LLZO contacts lithium, a 5 nm layer of tetragonal LLZO forms.¹⁶² While this is a less conductive phase, it is not electronically conductive and is still ionically conductive. Dr. Ma has communicated that his future studies may investigate this same interface with an applied voltage to determine if breakdown products are formed.

The possibility of reduction of component species is increased with the common practice of transition metal doping, such as $\text{Nb}^{4+/\text{5}+}$ and $\text{Ta}^{4+/\text{5}+}$. However, beyond theoretical effects, experimental evidence suggests that breakdown leading to significant electronic conductivity in the garnet is not occurring. The electronic conductivity in lithium garnet has been shown to be on the order of 10^{-10} S/cm or lower at room temperature.^{253,259} Moreover, Samson et al. demonstrated that even when doping with iron, manganese, cobalt or nickel, the room temperature electronic conductivity never surpassed 6.1×10^{-8} S/cm (Figure 36) and actually decreased to 4.7×10^{-10} S/cm upon exposure to a reducing 7% hydrogen atmosphere.²⁶⁰

In a Hebb-Wagner polarization experiment reported by Cheng et al., LLZO pellets processed under argon showed an order of magnitude higher (though still small, 2.2×10^{-9} S/cm) electronic leakage than similar pellets processed under oxygen.²⁶¹ Their analysis suggested that more reducing conditions lead to more oxygen vacancies and, through them, a higher electronic conductivity. However, this also was a small effect.

Overall, there are multiple factors which can increase electronic conductivity by orders of magnitude, but none of these factors has shown electronic conductivity within four orders of magnitude of the ionic conductivity (i.e., $\tau_i > 0.9999$), which is well within the limit ($\tau_i > 0.99$) to be considered a pure ionic conductor.

6.2.6. Electronic Conduction through Grain Boundaries (Breakdown of Grain Boundary). It is also possible for grain boundaries to break down into electronically conductive states, which leads to a short circuit without necessitating a full lithium metal connection from one electrode to the other. Recent computational study performed by Tian et al. shows that excess electrons can be trapped at the pore/crack surfaces and possibly grain boundaries, which can cause Li metal formation (Figure 37 a).²⁶² Aguesse et al. also proposed that isolated Li metal can form by gaining electrons from the oxygen backbone

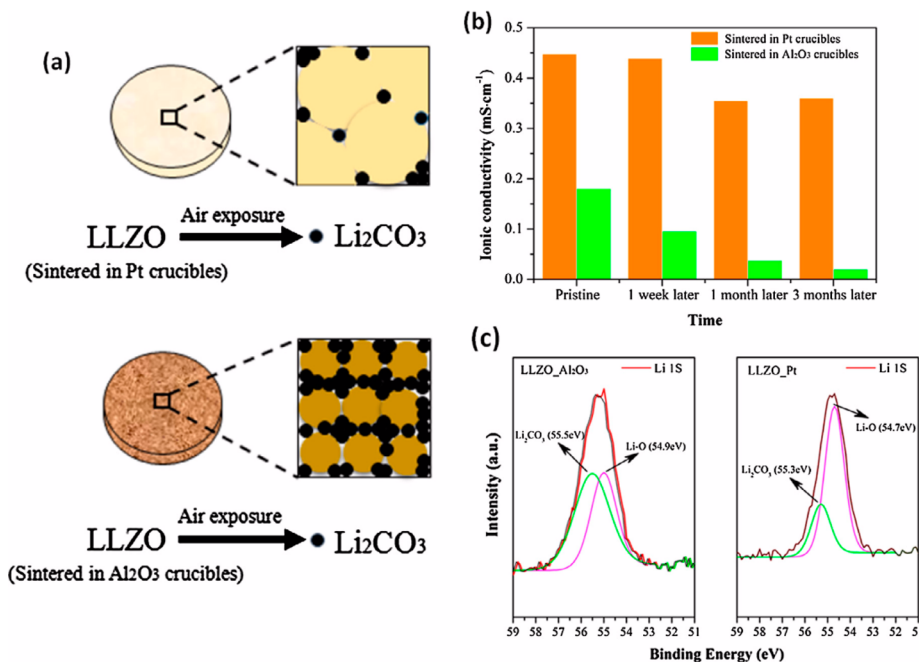


Figure 35. (a) Diagram comparing sintering of LLZO in a Pt crucible and Al₂O₃ crucible. (b) Conductivity of both samples initially and after sitting in air for 1, 4, and 12 weeks. (c) XPS measurements of both samples showing significantly more Li₂CO₃ in the sample sintered in an Al₂O₃ crucible. Reproduced with permission from ref 253. Copyright 2016 American Chemical Society.

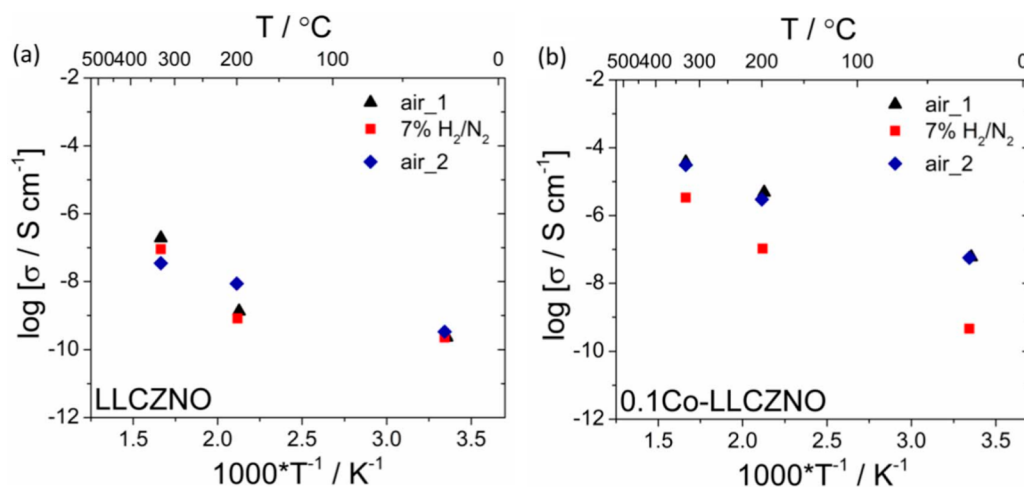


Figure 36. Electronic conductivity of (a) LLCZN and (b) Li₇La_{2.75}Ca_{0.25}Zr_{1.55}Co_{0.2}Nb_{0.25}O₁₂ as measured by Hebb-Wagner polarization. Reproduced with permission from ref 260. Copyright 2018 The Electrochemical Society.

of garnet or residual conductivity (Figure 35 b).²⁶³ No direct evidence has been presented that this occurs in lithium garnet due to lithium contact, however the presence of transition metals in many common compositions,^{193,204} lithium carbonate at grain boundaries,²⁵³ and aluminum contamination from crucibles^{265,266} all introduce defects which could increase electronic conductivity on their own or through the introduction of oxygen vacancies. While all of these effects can affect the grain or grain boundary, these impurities are likely to concentrate in grain boundaries.^{265,267} As discussed in the previous section, if grain boundaries are considered to be lithium garnet with high impurity and defect concentrations, the conductivity is likely to be purely ionic. However, other species such as lithium carbonate and lithium aluminates are also present in the grain boundaries and may contribute significantly. Direct measure-

ment of grain boundary electronic conductivity has not been published.

6.2.7. Cracking of Ceramic Separator (Mechanical Failure of Material or Grain Boundary). Another failure mode for a ceramic separator is cracking due to mechanical stresses or vibrations. There are some more obvious causes of separator cracking such as damage during assembly, mechanical shocks, bending, and vibration of the packaged cell. There is also some evidence for cracking due to electrochemical pressure. Any such physical failure of the ceramic separator will allow lithium to plate through the crack and cause a short circuit.

Schmidt et al. galvanostatically cycled symmetric cells and measured their response to a nondestructive acoustic signal.²⁶⁸ In every case, a short circuit was preceded by a decrease in wave speed, suggesting that a crack formed and lithium metal quickly plated through the crack (Figure 38). As no external forces were

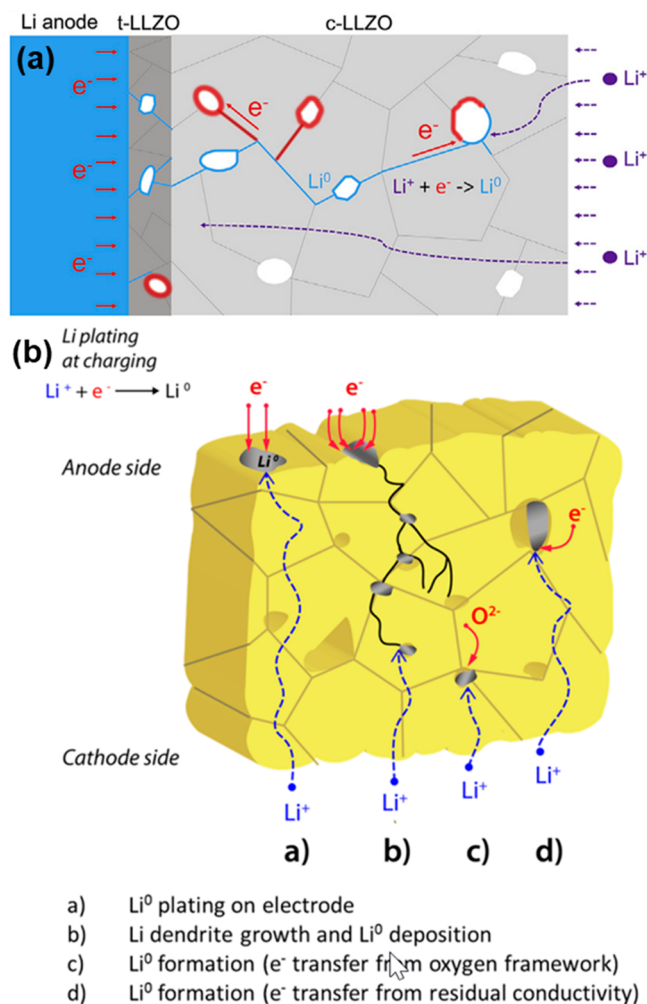


Figure 37. (a) Schematic of metallic Li⁰ (blue color) formation on the pore surfaces inside of c-LLZO due to the electron pathway provided by the pore surfaces and possibly grain boundaries. Reproduced with permission from ref 262. Copyright 2018 Elsevier. (b) Schematic of the proposed potential Li-ion reduction mechanisms in garnet electrolyte. Reproduced with permission from ref 263. Copyright 2017 American Chemical Society.

being applied, the conclusion is that electrochemical pressure from the lithium ions under the applied field were sufficient to crack the garnet membrane.

While the mechanical properties of lithium garnet are not thoroughly documented, significant work has begun in recent years as this technology approaches real world deployment.^{150,269,270} The outcome of these studies will set realistic bounds on device design as well as packaging requirements and application readiness. For cells to be truly ready for commercial acceptance, the mechanical properties of the garnet, the effect of cell structure on robustness, and forces generated by lithium cycling must be fully understood.

6.3. Proof-of-Concept Batteries with Garnet Electrolyte

Lithium garnets have been successfully demonstrated in batteries with a variety of chemistries. In general, most of the reported batteries use lithium metal due to the intrinsically high energy density, although a variety of different interfaces have been employed. On the cathode side, a wide range of materials have successfully been cycled with LLZO garnet electrolyte, including oxide (LiCoO₂, LiNi_xMn_yCo_zO₄, LiFePO₄), sulfur,

and oxygen/air cathodes. Often, the cathode–electrolyte interface is a primary limiting factor in the cell performance. At this interface, it has proven challenging to achieve good contact and low interfacial impedance while also maintaining chemical and electrochemical stability between the materials.

6.3.1. Oxide Cathodes. After the development of LLZO, many researchers initially focused on demonstrating the solid electrolyte with most commonly used Li-ion battery electrode at the time, LiCoO₂.^{175,178,179,214,271–274} The compositional simplicity of LiCoO₂ was also attractive for fundamental studies of cycling stability with LLZO. It became clear that despite the high electrochemical stability of LLZO demonstrated on passive Au or Pt electrodes, a side reaction with the LiCoO₂ cathode was causing severe capacity decay in cases where LiCoO₂ cathode was used directly on LLZO electrolyte with no interface modification. This was triggered by interdiffusion of the Co shown in Figure 11, causing a nonconductive La₂CoO₄ interface to form.¹⁷⁵ A research group from Toyota focused on developing a LLZO-based battery with LiCoO₂ (Figure 39, and cell data are summarized in Table 3). They achieved 100 cycles with little capacity decay using PLD-deposited LiCoO₂.²¹⁴ There was no evidence of a La₂CoO₄ interface forming, perhaps due to differences in garnet composition compared to previous studies. Because of the nature of the cathode; however, the cell had low cathode loading and cycled at a low current density of 3.5 μ A/cm² (0.1C).

To achieve more practical levels of cathode loading, the Toyota group cosintered a paste of LiCoO₂ and Li₃BO₃ on a LLZO pellet.¹⁷⁸ At 700 °C, the Li₃BO₃ melts to become a glass, establishing improved interfacial contact with the LiCoO₂ and LLZO. The result was a relatively low 230 Ω cm² interfacial impedance at room temperature, and the full cell had little capacity decay after a reported five cycles and 74% theoretical capacity (115 mAh/g).

Han et al. recently improved on this approach by cosintering a mixture of Li₂CO₃-coated LLZO, Li₂CO₃-coated LiCoO₂, and Li_{2.3}C_{0.7}B_{0.3}O₃ glass on a Li₂CO₃-coated LLZO pellet (Figure 15b–d).¹⁸² The Li₂CO₃ coating on the LLZO and LiCoO₂ ensured the materials remained out of contact to prevent any deleterious side reactions during cosintering and cycling. At room temperature, the capacity started at 94 mAh/g and stabilized to 83 mAh/g after 100 cycles, representing remarkable performance for the all-solid-state system. In this work the authors found that cycling at 100 °C improved capacity to 106 mAh/g, but faster capacity decay was observed due to electrode volume change and mechanical degradation. In contrast, Tsai et al. cosintered crystallized layered structure LiCoO₂ with Ta-doped LLZO to prevent Al diffusion into LiCoO₂ and improve stability between the electrolyte and cathode materials.²⁷⁶ This composite electrode without additional additives to prevent interfacial reactions initially cycled with higher capacity (117 mAh/g) at 0.05 mA/cm² and slightly elevated temperature of 50 °C and Li-In anode. However, the capacity decayed consistently down to 36 mAh/g after 100 cycles as the full cell ASR increased from 1138 to 5804 Ω cm², perhaps due to mechanical forces of the electrode expansion/contraction creating fractures in the composite electrode over many cycles.

Hao et al. used LiBr as a low melting dopant (along with Al₂O₃) to LLZO to improve the density and conductivity of the LLZO.²⁷¹ Interestingly, the LiBr addition, which introduces Br⁻ anion doping to the LLZO, did improve cycling performance and stability with LiCoO₂ when compared to an identical cell without LiBr. In this study, full cells were fabricated with Li

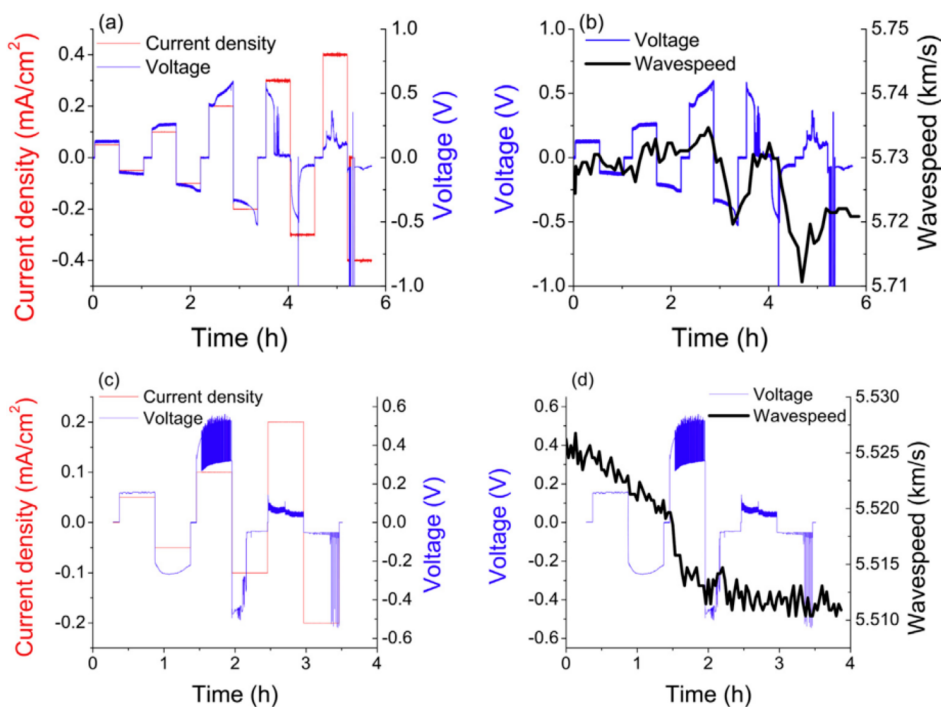


Figure 38. Cycling of two samples showing (a) current–voltage behavior of sample 1, (b) acoustic measurement of sample 1, (c) current–voltage behavior of sample 2, (d) acoustic measurement of sample 2. Reproduced with permission from ref 268. Copyright 2016 Elsevier.

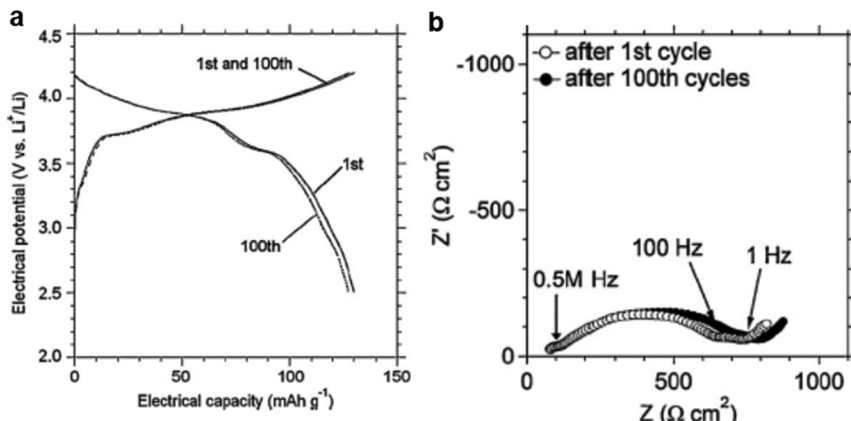


Figure 39. (a) Voltage profile of LLZO/PLD-LiCoO₂ during cycling and (b) EIS of the cell before and after 100 cycles. Reproduced with permission from ref 214. Copyright 2011 Elsevier.

metal, LLZO pellets with and without LiBr doping, LiCoO₂ slurry-based cathodes, and LiPF₆-based liquid electrolyte on the cathode side. With standard LLZO (no LiBr), the capacity started at 91.3 mAh/g and decreased to 77.9 mAh/g after just 20 cycles. The LiBr dopant improved the initial capacity to 121.5 mAh/g, which dropped slightly to 111.6 mAh/g after 70 cycles. The introduction of LiBr may change the composition of the LLZO grain boundaries and improve the stability toward the LiCoO₂ cathode. The presence of liquid electrolyte serves to improve interfacial contact at the cost of losing the inherent nonflammability of an all-solid-state system.

Because of the difficulty of cosintering cathode materials with LLZO without side reactions, it has become common to use a liquid or gel electrolyte at the cathode-electrolyte interface to ensure there is ionic contact between the materials. This is particularly true of oxide cathodes with multiple transitional metals, such as NMC. Although the incorporation of liquid

electrolyte means the battery is no longer all-solid-state, it enables the use already available commercial cathode foils, simplifying manufacturing. Using commercial NMC foil and a small amount (2–4 μL/cm²) of LiPF₆-based liquid electrolyte, Liu et al. reported a full cell employing bilayer garnet, which cycled with little capacity decay for 28 cycles at 175 mAh/g.²⁴⁰ The inclusion of liquid electrolyte does not necessarily sacrifice the inherent nonflammability of all-solid-state systems if an ionic liquid electrolyte is used. Using *N*-methyl-*N*-butyl pyrrolidinium bis(trifluoromethylsulfonyl)imide ionic liquid with 0.3 M LiTFSI as the liquid electrolyte, Shao et al. created a composite “toothpaste-like” cathode with NMC and carbon black (Figure 40).²⁸⁶ The cathode paste was applied to W-doped LLZO and the full cell demonstrated remarkable performance: the full cell had a starting capacity of 175 mAh/g at 0.5C rate and 80% capacity retention after 500 cycles. In addition, this cell

Table 3. Summary of Reported Batteries with LLZO Electrolyte^a

	garnet type	cathode type	cycles	efficiency	cathode discharge capacity (mAh/g)	current (mA/cm ²)	C-rate	ASR (Ω cm ²)	ref
oxide cathode	LLZN + Li ₃ BO ₃	LCO	5	85% (first), up to >99%	85	0.01	0.05 C	300	178
	LLCZN	LCO	1	80%	78		0.01C		179
	LLZN	LCO (PLD)	100	99.2 (first), 97.7 (100th)	127–129	0.0035	0.1C	820	275
	LLZN	LCO (PLD)	1	>99%	125	0.0035			272
	LLZA+LiBr	LCO	70	87.4 (first), 99.3 (50th)	112	0.0034	0.02C	1500	271
	LLZO + Li _{2.3} C _{0.7} B _{0.3} O ₃	LCO	100		94–83	0.007	0.05C		182
	LLZT	LCO (crystalline, 50 °C)	100	81.5 (1st) 99% (15th)	117–36	0.050	0.033C	1138	276
					7.4	0.50	0.33C		
	LLZA	LCO	70	>99%	120–89		0.05C		273
	LLZAW	NCM532	500	>99%	175–140		0.5C		277
				>99%	141		3.0C		
	LLCZN bilayer	NCM532	28	97	175	0.20	0.1C		240
sulfur cathode	LLZW	NCM111	20		142		0.09C		278
	LLZO	NCM111 (100 °C)	90		135	0.05	0.1C		279
					17	1.0	2C		
	LLCZN	LFP	70	93	140	0.05	1.0C	800	280
	LLZT+LiF	LFP (65 °C)	200	99.8	142	0.16	0.18C	385	198
	LLGZR	LFP (60 °C)	20		152–110	0.005	0.05C		14
	LLZT+LiF	Li–S	100		1074–988	0.20	0.13C	1000	198
	LLZTO	Li–S	30	>99%	1100–706			1405	281
	LLCZN trilayer	Li-polysulfide	50	N/A	3.0 mAh/cm ²	1.0	N/A		282
	LLCZN bilayer textile	Li–S	40		1250–1000	0.15	0.1C		229
air/O ₂ cathode	LLCZN	Li–S	100		1200	0.0625	0.03C		283
					400	1.0	0.5C		
	LLCZN trilayer	Li–S	50	>99%	1200–1100	0.27	0.04C	800	239
					400	1.62	0.25C		
air/O ₂ cathode	LLCZN	O ₂	10	N/A	0.015 mAh/cm ²	0.015	N/A		284
	LLZT	real air (80 °C)	50	N/A	316 (0.316 mAh/cm ²)	0.020	N/A		285

^aResults are at room temperature unless otherwise specified.

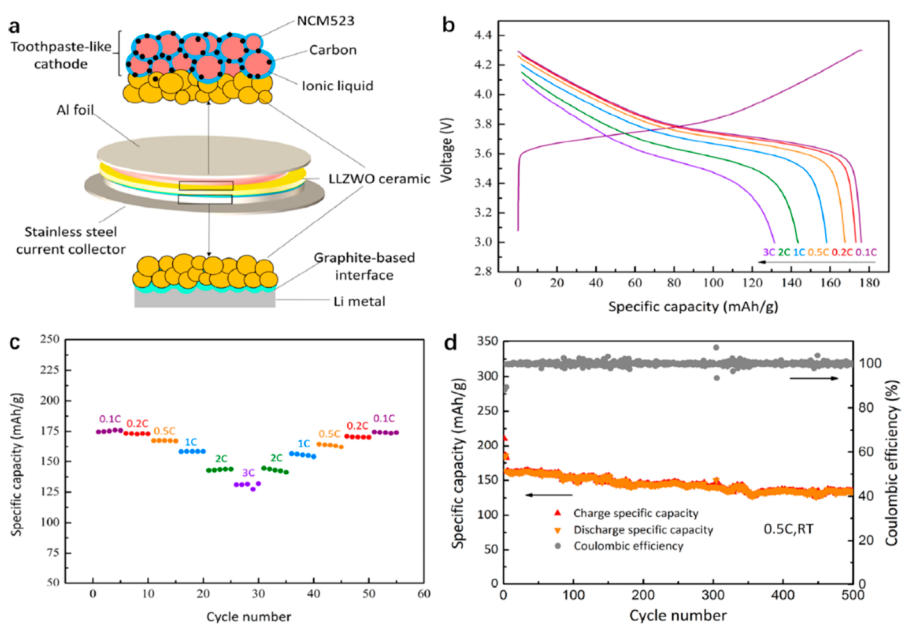


Figure 40. (a) Schematic of a W-doped LLZO battery with NMC532, ionic liquid electrolyte, carbon black composite cathode, and Li metal anode with graphite interface to improve Li wetting. (b) Voltage profile and (c) discharge capacity of the cell during high rate cycling up to 3C. (d) Long-term cycling at 0.5C. Reproduced with permission from ref 286. Copyright 2018 American Chemical Society.

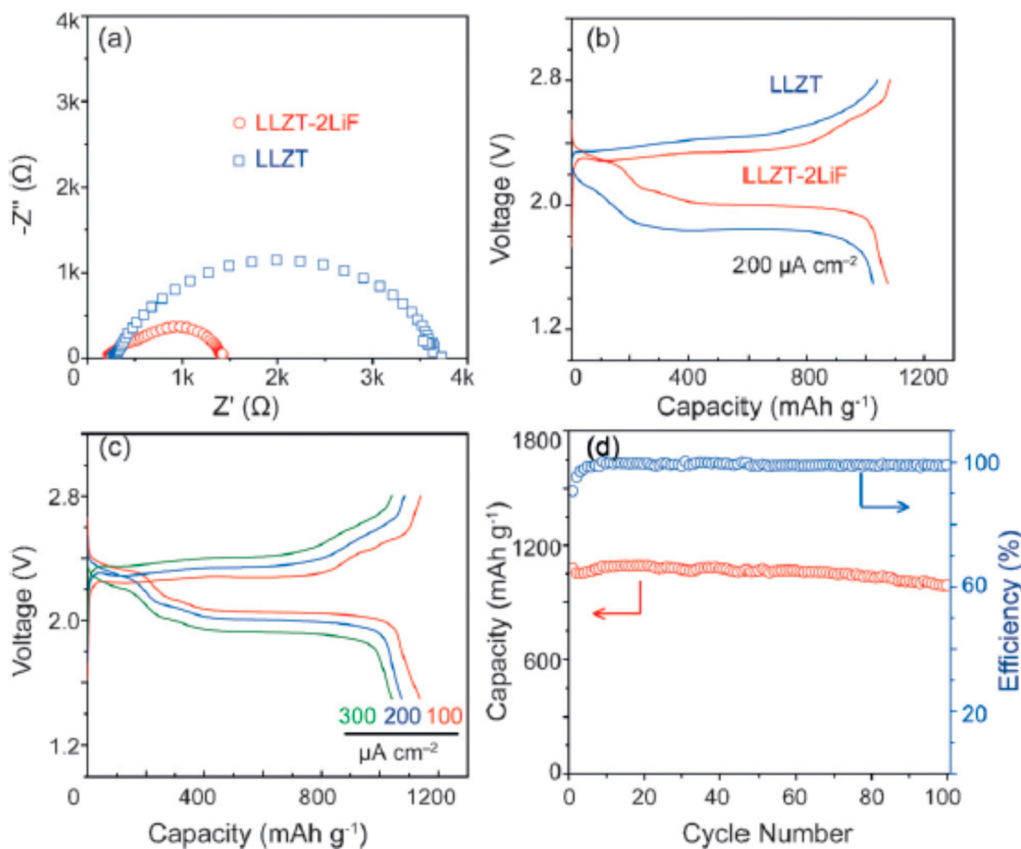


Figure 41. Li–S batteries using a Ta-doped LLZO electrolyte, with and without LiF (2 wt %) addition in the LLZO to inhibit the formation of high-impedance Li_2CO_3 on the LLZO surface in ambient air. (a) EIS and (b) voltage profile of Li–S full cells with and without LiF in the LLZO electrolyte. (c) Voltage profile of the full cell with LiF addition, up to $0.3 \text{ mA}/\text{cm}^2$ (0.13C) and (d) cycle life up to 100 cycles at $0.2 \text{ mA}/\text{cm}^2$. Reproduced with permission from ref 200. Copyright 2017 Wiley-VCH.

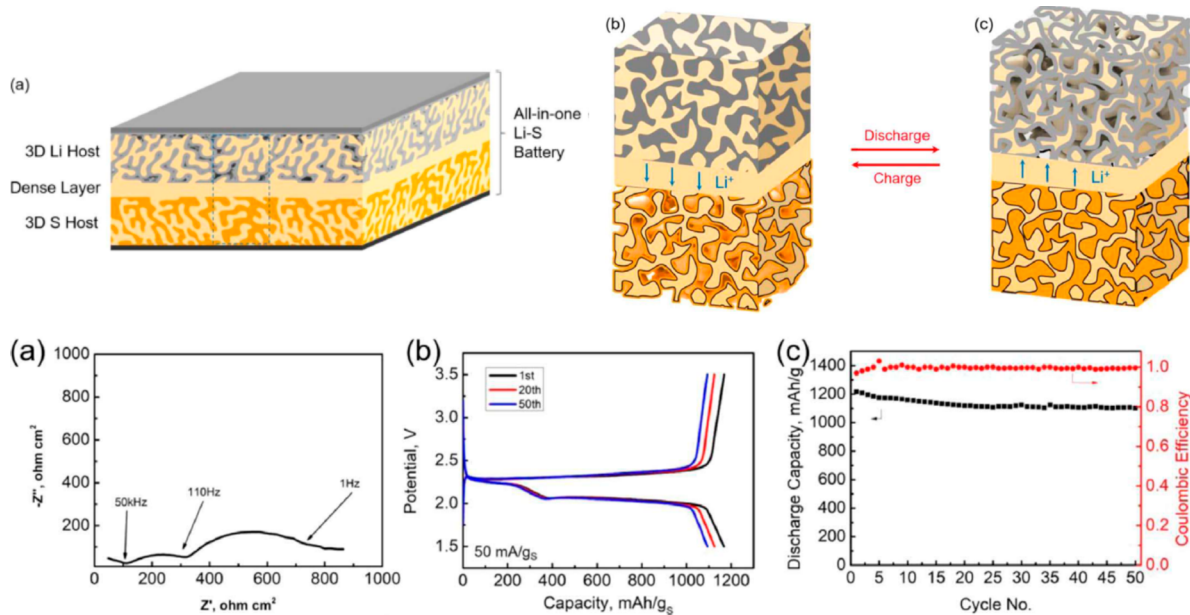


Figure 42. (a) Schematic of a trilayer LLZO electrolyte-based Li–S battery with Li metal and S within the opposing CNT-coated porous layers of LLZO. Diagrams of the trilayer cell during (b) discharge and (c) charge. (d) EIS, (e) voltage profiles, and (f) cycle life of a Li–S cell with trilayer LLZO electrolyte. Reproduced with permission from ref 239. Copyright 2018 Elsevier.

configuration had excellent rate performance, with 125 mAh/g capacity at 3C rate.

6.3.2. Sulfur Cathode. Another intrinsic advantage of solid electrolytes is the ability to block transport of otherwise soluble transition products between the cathode and anode. In the case

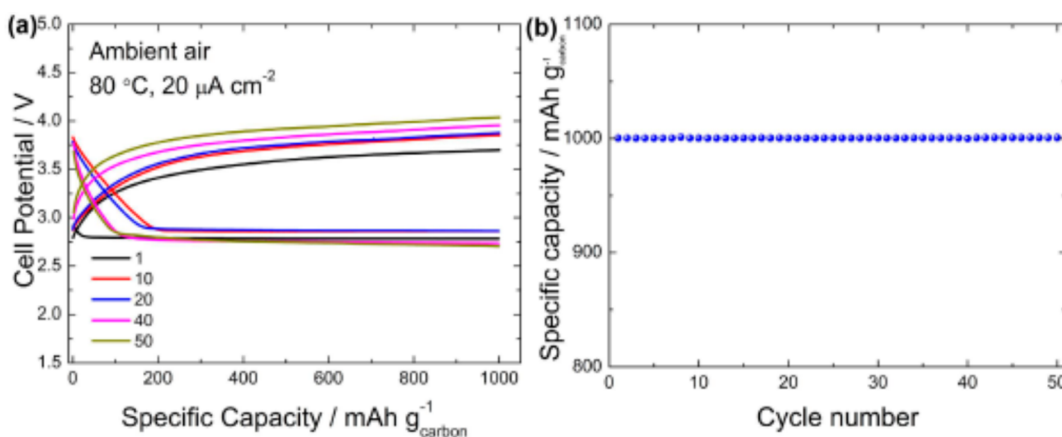


Figure 43. Cycling results at 80 °C of Li–air battery with LLZT garnet solid electrolyte and PPC:LiTFSI-based air cathode. The cell was cycled at 0.020 mA/cm² and a controlled discharge capacity of 1000 mAh/g_{carbon} (316 mAh/g_{cathode}). (a) Voltage profile and (b) capacity per gram carbon in the cathode over 50 cycles. Reproduced with permission from ref 285. Copyright 2017, Springer Nature.

of sulfur cathodes, the well-known polysulfide shuttle mechanism, which causes severe capacity fade, is effectively blocked when using a solid electrolyte. On the other hand, the poor conduction properties of both sulfur and its lithiated form (Li₂S) generally necessitate the use of liquid electrolyte (usually LiTFSI in DME/DOL solvent mixture) within the cathode to achieve practical cycling rates.

Li–S batteries with LLZO electrolyte have been demonstrated in several reports.^{168,198,229,239,281,287} Din et al. used a LLZO separator to block the polysulfide shuttle in a conventional Li–S battery design with polypropylene (PP) separators to create the configuration of Li|PP|LLZO|S.²⁸¹ A liquid electrolyte was used on the anode and cathode sides, which resulted in a full cell ASR over 1400 Ω cm². The cell cycled with high Coulombic efficiency after the initial 10 cycles and stabilized to 706 mAh/g capacity after 30 cycles (1100 mAh/g initially).

Li et al. reported a Li–S cell using LLZO separator. LiF was added to the LLZO prior to sintering, which had the interesting property of preventing surface carbonates from forming when exposed to air, which can cause high interfacial impedance.¹⁹⁸ The assembled full cell used an activated carbon nanofiber template impregnated with polysulfide and LiCF₃SO₃ DME/DOL liquid electrolyte as the cathode layer. The full cell ASR was 1000 Ω cm², and the cycling stabilized at near 1000 mAh/g after 100 cycles at 0.2 mA/cm² (Figure 41). Throughout cycling, the Coulombic efficiency remains near 100%, demonstrating the lack of any polysulfide shuttle effect.

Xu et al. demonstrated a quasi-flow type cell where a LLZO trilayer with Li metal anode was coupled with a liquid polysulfide catholyte, further exploiting the blocking nature of the LLZO solid electrolyte.²⁸⁷ With the Li metal side sealed, the cell was submerged in the catholyte solution. This cell showed stable performance at 1.0 mA/cm² at a controlled capacity of 3 mAh/cm² for 50 cycles.

A recently published study demonstrated a trilayer garnet-based Li–S battery where no liquid electrolyte was added (Figure 42).²³⁹ The porous structures of the trilayer were coated with CNTs, providing high surface for ionic/electronic charge transfer. To fill the pores with the electrodes, lithium metal was melted in one side and sulfur was melted into the other. In this case, the porous structure also serves to minimize the Li⁺-ion conduction path length, avoiding the need for a liquid electrolyte. With this configuration, the full cell ASR was 800

Ω cm², lower than most full cells that incorporate a liquid electrolyte. At 0.27 mA/cm² (0.04C), the cell capacity started at 1200 mAh/g and stabilized to 1100 mAh/g after 50 cycles. At a higher current density of 1.67 mA/cm² (0.25C), the capacity reduced to 400 mAh/g, which is quite notable for an all-solid-state system.

6.3.3. Oxygen/Air Cathode. A solid-state battery using a Li metal and an O₂ or air cathode is highly attractive due to the potential for exceptionally high energy density and the blocking nature of the solid electrolyte can prevent any reactions of the Li anode with oxygen or any redox mediators. This area of study is currently in its infancy, but two reports recently demonstrated its feasibility with the LLZO electrolyte.^{168,285} Using a LLZO pellet with lithium metal wetted to one side, Fu et al. applied conductive carbon with 1 M LiTFSI TEGDME electrolyte on the O₂ cathode side.¹⁶⁸ At 20 °C, the cell was cycled at 0.015 mA/cm² for 10 cycles at a controlled capacity of 0.015 mAh/cm². Although the cell experienced high overpotential and cycled at low current density, it serves as a proof of concept for a Li–O₂ battery based on the LLZO electrolyte.

Sun et al. demonstrated a similar LLZO-based cell with Li metal, but developed an air cathode using LiTFSI dissolved in polypropylene carbonate (PPC) and mixed with Ketjen black and LLZT powder, which together significantly reduced interfacial resistance.²⁸⁵ The cell was cycled in real air at 80 °C and partially reversible reaction with CO₂ to form Li₂CO₃ was demonstrated, which is a key to practical applications of Li–air batteries. The higher temperature was used to reduce reaction with ambient moisture. At first discharge, 6430 mAh/g_{cathode} (6.43 mAh/cm²) was achieved. However, the capacity decayed significantly after only a few cycles, likely due to buildup of Li₂CO₃. With support from *in situ* XPS measurements, the report suggested that during the initial stages of discharge, Li₂O₂ is formed which then reacts with ambient CO₂ to form Li₂CO₃. By limiting the discharge capacity to 316 mAh/g_{cathode} (0.316 mAh/cm²) to reduce Li₂CO₃ buildup, the cell could cycle for 50 cycles without decay (Figure 43). These results show that while there are clear barriers to practical application, solid-state Li–air batteries based on garnet electrolytes are likely to become prominently explored going forward.

7. CONCLUSIONS AND FUTURE PERSPECTIVE

In this Review, we introduced the history of solid-state electrolytes development, and mainly discussed the garnet-type LLZO solid-state electrolyte including its discovery and recent development. Garnet solid-state electrolyte is considered as the most promising candidate for solid-state batteries with potential benefits in energy density, electrochemical stability, temperature stability, and safety. We discussed the design principles of garnet-type solid-state electrolyte and introduced experimental and computational results to explain the Li-ion conduction mechanism in LLZO solid electrolytes. The chemical composition–structure relationship of LLZO electrolyte and its relevant mechanical properties were discussed. The relevant interfaces as the most challenging issue in solid-state battery were particularly discussed. We also discussed the most recent work on the study of LLZO electrolyte interface chemical and electrochemical stability against various types of anodes (e.g., Li metal and alloy-type anodes) and cathodes (e.g., conversion cathodes and intercalation cathodes). We also talked about LLZO electrolyte's chemical stability with liquid electrolytes for a semisolid battery concept. We explored the origins of the interface and showed strategies to address the interface challenges. We discussed the opportunities of LLZO nanostructures in promoting a high-performance solid-state electrolyte. Using nanoscale LLZO with different types of structures (e.g., nanopowders, nanoribbons, and nanofibers) can effectively enhance the mechanical property and ionic conductivity in polymer-based electrolytes. We reviewed nano-LLZO synthesis methods and discussed the possible ion transport mechanism in composite electrolytes. Additionally, we examined how to design solid and rigid ceramic electrolytes into soft and flexible electrolytes. We surveyed how garnet-type LLZO solid electrolyte functions in a full battery and how to design and develop a bilayer or trilayer structural electrolyte framework for high energy and high power battery applications. The degradation and failure mechanisms and analysis, as well as potential solid-state battery designs for Li–S and Li–O₂ applications, are discussed.

For the future perspective of solid-state electrolyte development, we have a few thoughts:

1. The thickness and weight of electrolytes should be considered in electrolyte design. To achieve a high energy density, it is necessary to apply a thin and lightweight electrolyte while maintaining sufficient mechanical properties.
2. Is it possible to design a composite electrolyte based on two or more inorganic electrolytes to show the merits of each? Some solid electrolytes have high ionic conductivity but poor contact and interfaces with a cathode or anode, but some others are opposite. Therefore, a composite structure may help to mitigate the adverse parts of each and promote the advantages.
3. The electrolyte–cathode interface needs more attention. The interface challenge involves not only the assembled contact interface but also the newly developed interface during cycling. Determining how to address the physical or chemical interface contact in the cathode will help to better understand and optimized the solid-state electrolyte function at a full cell level.
4. The transference number should not be selectively neglected in inorganic/organic composite electrolytes. High transference number is a challenge for composite

electrolytes. Polymer chemists are anticipated to develop novel polymer material for electrolyte applications.

5. Full cell level analysis is highly needed to evaluate solid-state electrolyte properties. Additionally, thermal analysis of solid-state batteries is needed.

AUTHOR INFORMATION

Corresponding Authors

Liangbing Hu — Department of Materials Science and Engineering, University of Maryland, College Park, Maryland 20742, United States;  orcid.org/0000-0002-9456-9315; Email: binghu@umd.edu

Venkataraman Thangadurai — Department of Chemistry, University of Calgary, Calgary T2N 1N4, Canada;  orcid.org/0000-0001-6256-6307; Email: vthangad@ucalgary.ca

Authors

Chengwei Wang — Department of Materials Science and Engineering, University of Maryland, College Park, Maryland 20742, United States

Kun Fu — Department of Materials Science and Engineering, University of Maryland, College Park, Maryland 20742, United States; Department of Mechanical Engineering, University of Delaware, Newark, Delaware 19716, United States;  orcid.org/0000-0003-4963-615X

Sanoop Palakkathodi Kammampata — Department of Chemistry, University of Calgary, Calgary T2N 1N4, Canada

Dennis W. McOwen — Department of Materials Science and Engineering and Maryland Energy Innovation Institute, University of Maryland, College Park, Maryland 20742, United States

Alfred Junio Samson — Department of Chemistry, University of Calgary, Calgary T2N 1N4, Canada

Lei Zhang — Department of Materials Science and Engineering and Maryland Energy Innovation Institute, University of Maryland, College Park, Maryland 20742, United States

Gregory T. Hitz — Department of Materials Science and Engineering and Maryland Energy Innovation Institute, University of Maryland, College Park, Maryland 20742, United States

Adelaide M. Nolan — Department of Materials Science and Engineering, University of Maryland, College Park, Maryland 20742, United States

Eric D. Wachsman — Department of Materials Science and Engineering and Maryland Energy Innovation Institute, University of Maryland, College Park, Maryland 20742, United States;  orcid.org/0000-0002-0667-1927

Yifei Mo — Department of Materials Science and Engineering, University of Maryland, College Park, Maryland 20742, United States;  orcid.org/0000-0002-8162-4629

Complete contact information is available at:

<https://pubs.acs.org/10.1021/acs.chemrev.9b00427>

Author Contributions

[¶]These authors contributed equally to this work.

Notes

The authors declare no competing financial interest.

Biographies

Chengwei Wang received his B.S. (2011) from University of Science and Technology of China (USTC) and PhD (2015) from Arizona State

University in Materials Science and Engineering. He is currently an Assistant Research Scientist at University of Maryland, College Park. His research focuses on solid state batteries and nanomaterials for ionic devices.

Kun (Kelvin) Fu is currently an assistant professor in Mechanical Engineering at the University of Delaware (UD), and he is also affiliated to the Center for Composite Materials at UD. Fu received his PhD in Fiber and Polymer Science from North Carolina State University in 2014; after that he worked as postdoctoral research associate and then assistant research scientist at the University of Maryland and Maryland Energy Innovation Institute. Fu's current research is focusing on additive manufacturing and processing of materials, structures, and devices across multiple length scales for applications in energy, environment, and health.

Sanoop Palakkathodi Kammampata is pursuing his PhD degree under the guidance of Dr. Thangadurai at the Department of Chemistry, University of Calgary, Canada. His current research is focused on developing garnet-type solid Li-ion electrolytes for all-solid-state Li batteries.

Dennis McOwen obtained his PhD in chemical engineering at North Carolina State University in 2014. His doctoral research focused on the study and development of new liquid electrolytes for lithium batteries. As a postdoctoral researcher at the University of Maryland Energy Research Center, Dennis worked towards the advancement of microstructured solid electrolytes for solid state batteries. In 2017, he transitioned to a research scientist position and became group leader for solid state battery research. With a unique background in both liquid and solid electrolytes, and a driven interest in chemistry and energy technology, Dennis's current work centers on improving lithium battery electrolytes and their electrode interfaces for next generation lithium batteries.

Alfred Junio Samson is a research associate in Prof. Venkataraman Thangadurai's laboratory at the Department of Chemistry, University of Calgary, Canada. He earned his double M.Sc. in materials science and engineering from Luleå University of Technology in Sweden and Saarland University in Germany, and PhD in energy conversion from Technical University of Denmark. His current research is geared towards the development of solid-state lithium batteries using ceramic electrolytes.

Lei Zhang received his B.S. (2007) from Zhejiang University, P.R. China, M.S. (2010) from Institute of Physics, Chinese Academy of Sciences, and PhD (2015) from University of Utah in Materials Science and Engineering. He is currently a Research Associate at University of Maryland, College Park. His research focuses on garnet type solid state electrolyte for Li-metal battery applications.

Gregory Hitz earned his PhD in materials science at the University of Maryland in 2016. In his doctoral research, he codeveloped the process for fabricating garnet trilayers with Dr. McOwen. His work explored garnet stability during fabrication and mapped the conditions required for sintering trilayers, achieving phase pure garnet trilayers with densified center layers and porous outer layers. He is a cofounder and Chief Technology Officer of Ion Storage Systems, a startup commercializing lithium garnet battery based on the trilayer and bilayer designs. He is leading the development of this technology into commercial products.

Adelaide M. Nolan is a doctoral candidate at the University of Maryland in the Department of Materials Science and Engineering, under the supervision of Dr. Yifei Mo. Her research focuses on the computational modeling of solid electrolytes and energy dense electrodes for energy

storage. She received her B.S. in Materials Science and Engineering from Cornell University in 2017.

Eric D. Wachsman is Director of the Maryland Energy Innovation Institute, and Crentz Centennial Chair in Energy Research at the University of Maryland. He is a Fellow of The Electrochemical Society (ECS) and the American Ceramic Society, Vice President of ECS, Editor-in-Chief of Ionics, and on the Editorial Board of Scientific Reports, Energy Systems, and Energy Technology. His research is focused on solid ion-conducting materials and the development of solid-state fuel cells, batteries, ion-transport membrane reactors, and gas sensors.

Yifei Mo is an Associate Professor of Materials Science and Engineering at the University of Maryland, College Park, MD, USA. He received his Ph.D. from the University of Wisconsin-Madison, and conducted his postdoctoral research at Massachusetts Institute of Technology. His research aims to advance the understanding, design, and discovery of engineering materials through computational techniques, with current emphases on critical materials problems in solid-state electrochemical devices for energy storage and conversion including solid-state batteries.

Venkataraman Thangadurai is full professor of chemistry at the University of Calgary, Canada. He is a Fellow of the Royal Society of Chemistry, United Kingdom. He is a co-founder and scientific advisor of Ion Storage Systems. He received his PhD from the Indian Institute of Science, Bangalore, India in 1999 and did his PDF at the University of Kiel, Germany. He received a prestigious PDF fellowship from the Alexander von Humboldt Foundation, Bonn, Germany. In 2004, Dr. Thangadurai received his Habilitation degree from the University of Kiel. His current research activities include discovery of novel ceramic membranes and mixed ion and electron conductors for all-solid-state-Li batteries, solid oxide fuel cells, solid oxide electrolysis cells, and electrochemical gas sensors. He has published over 200 scientific papers in international refereed journals. Dr. Thangadurai received the Keith Laidler award from the Chemical Institute of Canada in 2016 for his outstanding contribution to physical chemistry.

Liangbing Hu received his B.S. in applied physics from the University of Science and Technology of China (USTC) in 2002. He received his PhD at UCLA, focusing on carbon nanotube based nanoelectronics. In 2006, he joined Unidym Inc. as a cofounding scientist. He worked at Stanford University from 2009 to 2011, where he worked on various energy devices based on nanomaterials and nanostructures. Currently, he is a Minta Martin professor at University of Maryland College Park. His research interests include nanomaterials and nanostructures, flexible and printed electronics, energy storage and conversion, and roll-to-roll nanomanufacturing.

ACKNOWLEDGMENTS

We acknowledge the support of the U.S. Department of Energy, Office of Energy Efficiency, and Renewable Energy (Award Nos. DE-EE0006860 and DE-EE0007807). We also acknowledge the support of the ARPA-E Robust Affordable Next Generation Energy Storage Systems program (Contract Nos. AR-DE0000384 and AR-DE0000787). The Natural Sciences and Engineering Research Council of Canada (NSERC) has also supported this work through discovery grants to one of us (V. T.) (Award number: RGPIN-2016-03853).

REFERENCES

- (1) Manthiram, A.; Yu, X.; Wang, S. Lithium Battery Chemistries Enabled by Solid-State Electrolytes. *Nat. Rev. Mater.* **2017**, 2, 1–16.

- (2) Bachman, J. C.; Muy, S.; Grimaud, A.; Chang, H. H.; Pour, N.; Lux, S. F.; Paschos, O.; Maglia, F.; Lupart, S.; Lamp, P. Inorganic Solid-State Electrolytes for Lithium Batteries: Mechanisms and Properties Governing Ion Conduction. *Chem. Rev.* **2016**, *116*, 140.
- (3) Goodenough, J. B.; Singh, P. Review-Solid Electrolytes in Rechargeable Electrochemical Cells. *J. Electrochem. Soc.* **2015**, *162*, A2387–A2392.
- (4) Sun, C.; Liu, J.; Gong, Y.; Wilkinson, D. P.; Zhang, J. Recent Advances in All-Solid-State Rechargeable Lithium Batteries. *Nano Energy* **2017**, *33*, 363.
- (5) Fan, L.; Wei, S.; Li, S.; Li, Q.; Lu, Y. Recent Progress of the Solid-State Electrolytes for High-Energy Metal-Based Batteries. *Adv. Energy Mater.* **2018**, *8*, 1–31.
- (6) Kerman, K.; Luntz, A.; Viswanathan, V.; Chiang, Y.-M.; Chen, Z. Review—Practical Challenges Hindering the Development of Solid State Li Ion Batteries. *J. Electrochem. Soc.* **2017**, A1731.
- (7) Bachman, J. C.; Muy, S.; Grimaud, A.; Chang, H. H.; Pour, N.; Lux, S. F.; Paschos, O.; Maglia, F.; Lupart, S.; Lamp, P.; et al. Inorganic Solid-State Electrolytes for Lithium Batteries: Mechanisms and Properties Governing Ion Conduction. *Chem. Rev.* **2016**, *116*, 140–162.
- (8) Zhang, Z.; Shao, Y.; Lotsch, B.; Hu, Y. S.; Li, H.; Janek, J.; Nazar, L. F.; Nan, C. W.; Maier, J.; Armand, M.; et al. New Horizons for Inorganic Solid State Ion Conductors. *Energy Environ. Sci.* **2018**, *11*, 1945–1976.
- (9) Marbella, L. E.; Zekoll, S.; Kasemchainan, J.; Emge, S. P.; Bruce, P. G.; Grey, C. P. ^{7}Li NMR Chemical Shift Imaging to Detect Microstructural Growth of Lithium in All-Solid-State Batteries. *Chem. Mater.* **2019**, *31*, 2762–2769.
- (10) Wu, J. F.; Guo, X. Origin of the Low Grain Boundary Conductivity in Lithium Ion Conducting Perovskites: $\text{Li}_{3x}\text{La}_{0.67}\text{XTiO}_3$. *Phys. Chem. Chem. Phys.* **2017**, *19*, 5880–5887.
- (11) Wu, J. F.; Guo, X. Size Effect in Nanocrystalline Lithium-Ion Conducting Perovskite: $\text{Li}_{0.30}\text{La}_{0.57}\text{TiO}_3$. *Solid State Ionics* **2017**, *310*, 38–43.
- (12) Zhu, Y.; He, X.; Mo, Y. Origin of Outstanding Stability in the Lithium Solid Electrolyte Materials: Insights from Thermodynamic Analyses Based on First-Principles Calculations. *ACS Appl. Mater. Interfaces* **2015**, *7*, 23685–23693.
- (13) Deiseroth, H. J.; Kong, S. T.; Eckert, H.; Vannahme, J.; Reiner, C.; Zaif, T.; Schlosser, M. Li_{6}PSSX : A Class of Crystalline Li-Rich Solids with an Unusually High Li^{+} Mobility. *Angew. Chem., Int. Ed.* **2008**, *47*, 755–758.
- (14) Wu, J. F.; Pang, W. K.; Peterson, V. K.; Wei, L.; Guo, X. Garnet-Type Fast Li-Ion Conductors with High Ionic Conductivities for All-Solid-State Batteries. *ACS Appl. Mater. Interfaces* **2017**, *9*, 12461–12468.
- (15) Murugan, R.; Thangadurai, V.; Weppner, W. Fast Lithium Ion Conduction in Garnet-Type $\text{Li}_7\text{La}_3\text{Zr}_2\text{O}_{12}$. *Angew. Chem., Int. Ed.* **2007**, *46*, 7778–7781.
- (16) Teng, S.; Tan, J.; Tiwari, A. Recent Developments in Garnet Based Solid State Electrolytes for Thin Film Batteries. *Curr. Opin. Solid State Mater. Sci.* **2014**, *18*, 29.
- (17) Thangadurai, V.; Narayanan, S.; Pinzaru, D. Garnet-Type Solid-State Fast Li Ion Conductors for Li Batteries: Critical Review. *Chem. Soc. Rev.* **2014**, *43*, 4714–4727.
- (18) Ramakumar, S.; Deviannapoorani, C.; Dhivya, L.; Shankar, L. S.; Murugan, R. Lithium Garnets: Synthesis, Structure, Li^{+} Conductivity, Li^{+} Dynamics and Applications. *Prog. Mater. Sci.* **2017**, *88*, 325–411.
- (19) Thangadurai, V.; Narayanan, S.; Pinzaru, D. Garnet-Type Solid-State Fast Li Ion Conductors for Li Batteries: Critical Review. *Chem. Soc. Rev.* **2014**, *43*, 4714–4727.
- (20) Zhao, N.; Khokhar, W.; Bi, Z.; Shi, C.; Guo, X.; Fan, L. Z.; Nan, C. W. Solid Garnet Batteries. *Joule* **2019**, *3*, 1190–1199.
- (21) Liu, Q.; Geng, Z.; Han, C.; Fu, Y.; Li, S.; He, Y.-B.; Kang, F.; Li, B. Challenges and Perspectives of Garnet Solid Electrolytes for All Solid-State Lithium Batteries. *J. Power Sources* **2018**, *389*, 120–134.
- (22) He, X.; Zhu, Y.; Mo, Y. Origin of Fast Ion Diffusion in Super-Ionic Conductors. *Nat. Commun.* **2017**, *8*, 15893.
- (23) Han, X.; Gong, Y.; Fu, K.; He, X.; Hitz, G. T.; Dai, J.; Pearse, A.; Liu, B.; Wang, H.; Rubloff, G.; et al. Negating Interfacial Impedance in Garnet-Based Solid-State Li Metal Batteries. *Nat. Mater.* **2017**, *16*, 572–579.
- (24) Fu, K.; Gong, Y.; Hitz, G. T.; McOwen, D. W.; Li, Y.; Xu, S.; Wen, Y.; Zhang, L.; Wang, C.; Pastel, G.; et al. Three-Dimensional Bilayer Garnet Solid Electrolyte Based High Energy Density Lithium Metal-Sulfur Batteries. *Energy Environ. Sci.* **2017**, *10*, 1568–1575.
- (25) Yamamoto, O. Solid State Ionics: A Japan Perspective. *Sci. Technol. Adv. Mater.* **2017**, *18*, 504–527.
- (26) Faraday, M. *Experimental Researches in Electricity*; Taylor and Francis: London, 2012; Vol. 2.
- (27) Funke, K. Solid State Ionics: From Michael Faraday to Green Energy - The European Dimension. *Sci. Technol. Adv. Mater.* **2013**, *14*, 43502.
- (28) Faraday, M. Experimental Researches in Electricity. *Exp. Res. Electr.* **2012**, *2*, 1–307.
- (29) Warburg, E. *Ann. Phys. Chem. N. F.* **1994**, *21*, 662.
- (30) Warburg, E.; Tegetmeier, F. Ueber Die ElectroZytisc7w Leitmzg Des Bergkrystrlls. *Ann. Phys.* **1888**, *32*, 455.
- (31) Nernst, W.; Wild, W. Some Points on the Behaviors of Electrolytic Mantles. *Z. Elektrochem. Angew. Phys. Chem.* **1900**, *7*, 373–376.
- (32) Wagner, C. Über Den Mechanismus Der Elektrischen Stromleitung Im Nernststift. *Naturwissenschaften* **1943**, *31*, 265–268.
- (33) Tubandt, C.; Lorenz, E. Molekularzustand Und Elektrisches Leitvermogen Ktistallisiener Salze. *Z. Phys. Chem.* **1914**, *87*, 513–542.
- (34) Frenkel, J. Über Die Warmebewegung in Festen Und Flüssigen Körpern. *Eur. Phys. J. A* **1926**, *35*, 652–660.
- (35) Wagner, C.; Schottky, W. *Z. Phys. Chem. B-Chem.* **1930**, *E11*, 163.
- (36) Wagner, C. *Z. Phys. Chem. B-Chem.* **1933**, *E22*, 181.
- (37) Hebb, M. H. Electrical Conductivity of Silver Sulfide. *J. Chem. Phys.* **1952**, *20*, 185–190.
- (38) Wagner, J. B.; Wagner, C. Electrical Conductivity Measurements on Cuprous Halides. *J. Chem. Phys.* **1957**, *26*, 1597–1601.
- (39) Wagner, C. Investigations on Silver Sulfide. *J. Chem. Phys.* **1953**, *21*, 1819–1827.
- (40) Thangadurai, V.; Weppner, W. $\text{Li}_6\text{Al}_2\text{Ta}_2\text{O}_{12}$ (A = Sr, Ba): Novel Garnet-like Oxides for Fast Lithium Ion Conduction. *Adv. Funct. Mater.* **2005**, *15*, 107–112.
- (41) Hartmann, P.; Leichtweiss, T.; Busche, M. R.; Schneider, M.; Reich, M.; Sann, J.; Adelhelm, P.; Janek, J. Degradation of NASICON-Type Materials in Contact with Lithium Metal: Formation of Mixed Conducting Interphases (MCI) on Solid Electrolytes. *J. Phys. Chem. C* **2013**, *117*, 21064–21074.
- (42) Rupp, G. M.; Glowacki, M.; Fleig, J. Electronic and Ionic Conductivity of $\text{La}_{0.95}\text{Sr}_{0.05}\text{Ga}_{0.95}\text{Mg}_{0.05}\text{O}_{3-\delta}$ (LSGM) Single Crystals. *J. Electrochem. Soc.* **2016**, *163*, F1189–F1197.
- (43) Kiukkola, K.; Wagner, C. Measurements on Galvanic Cells Involving Solid Electrolytes. *J. Electrochem. Soc.* **1957**, *104*, 379–387.
- (44) Takahashi, T.; Yamamoto, O. The $\text{Ag}/\text{Ag}_3\text{Si}/\text{I}_2$ Solid-Electrolyte Cell. *Electrochim. Acta* **1966**, *11*, 779–789.
- (45) Owens, B. B.; Argue, G. R. High-Conductivity Solid Electrolytes: MAg_4S . *Science (Washington, DC, U. S.)* **1967**, *157*, 308–310.
- (46) Bradley, J. N.; Greene, P. D. Solids with High Ionic Conductivity in Group 1 Halide Systems. *Trans. Faraday Soc.* **1967**, *63*, 424–430.
- (47) Takahashi, T.; Yamamoto, O.; Yamada, S.; Hayashi, S. Solid-State Ionics: High Copper Ion Conductivity of the System $\text{CuCl}-\text{CuCl}_2-\text{RbCl}$. *J. Electrochem. Soc.* **1979**, *126*, 1654–1658.
- (48) Yu Yao, Y.-F.; Kummer, J. T. Ion Exchange Properties of and Rates of Ionic Diffusion in Beta-Alumina. *J. Inorg. Nucl. Chem.* **1967**, *29*, 2453–2475.
- (49) Kummer, J. T.; Weber, N. Sodium-Sulfur Secondary Battery. *SAE Tech. Pap. Ser.* **1967**, *76*, 88–89.
- (50) Kuwabara, K.; Takahashi, T. Formation of β -Alumina Type Potassium Gallate and Its Ionic Conductivity. *J. Solid State Chem.* **1976**, *19*, 147–153.

- (51) Boilot, J. P.; Théry, J.; Collongues, R. Phases de Type Alumine β et B" Dans Le Système Na₂O–Ga₂O₃. *Mater. Res. Bull.* **1973**, *8*, 1143–1151.
- (52) Goodenough, J. B.; Hong, H. Y.-P.; Kafalas, J. A. Fast Na⁺ Ion Transport in Skeleton Structures. *Mater. Res. Bull.* **1976**, *11*, 203–220. <https://ja.scribd.com/document/88168641/1976-Fast-Na-Ion-Transport-in-Skeleton-Structures>.
- (53) Hong, H. Y. P. Crystal Structures and Crystal Chemistry in the System Na_{1+x}Zr₂Si_xP₃–XO₁₂. *Mater. Res. Bull.* **1976**, *11*, 173–182.
- (54) Boukamp, B. A.; Huggins, R. A. Fast Ionic Conductivity in Lithium Nitride. *Mater. Res. Bull.* **1978**, *13*, 23–32.
- (55) Liang, C. C. Conduction Characteristics of the Lithium Iodide–Aluminum Oxide Solid Electrolytes. *J. Electrochem. Soc.* **1973**, *120*, 1289–1292.
- (56) Schneider, A. A.; Harney, D. E.; Harney, M. J. The Lithium–Iodine Cell for Medical and Commercial Applications. *J. Power Sources* **1980**, *5*, 15–23.
- (57) Hong, H. Y. P. Crystal Structure and Ionic Conductivity of Li₁₄Zn(GeO₄)₄ and Other New Li⁺ Superionic Conductors. *Mater. Res. Bull.* **1978**, *13*, 117–124.
- (58) Kanno, R.; Hata, T.; Kawamoto, Y.; Irie, M. Synthesis of a New Lithium Ionic Conductor, Thio-LISICON-Lithium Germanium Sulfide System. *Solid State Ionics* **2000**, *130*, 97–104.
- (59) Thangadurai, V.; Kaack, H.; Wepner, W. J. F. Novel Fast Lithium Ion Conduction in Garnet-Type Li₅La₃M₂O₁₂ (M = Nb, Ta). *J. Am. Ceram. Soc.* **2003**, *86*, 437–440.
- (60) Zhao, Y.; Daemen, L. L. Superionic Conductivity in Lithium-Rich Anti-Perovskites. *J. Am. Chem. Soc.* **2012**, *134*, 15042–15047.
- (61) Murugan, R.; Thangadurai, V.; Wepner, W. Fast Lithium Ion Conduction in Garnet-Type Li₇La₃Zr₂O₁₂. *Angew. Chem., Int. Ed.* **2007**, *46*, 7778–7781.
- (62) Kim, Y.; Yoo, A.; Schmidt, R.; Sharifi, A.; Lee, H.; Wolfenstein, J.; Sakamoto, J. Electrochemical Stability of Li_{6.5}La₃Zr_{1.5}M_{0.5}O₁₂ (M = Nb or Ta) against Metallic Lithium. *Front. Energy Res.* **2016**, *4*, 20.
- (63) Cox, E. G. *Structural Inorganic Chemistry*, 4th ed.; Clarendon Press: Oxford, 1951; Vol. 168.
- (64) Cussen, E. J.; O'Callaghan, M. P.; Powell, A. S.; Titman, J. J.; Chen, G. Z. Switching on Fast Lithium Ion Conductivity in Garnets: The Structure and Transport Properties of Li_{3+x}Nd₃Te₂–Xs_xO₁₂. *Chem. Mater.* **2008**, *20*, 2360–2369.
- (65) O'Callaghan, M. P.; Lynham, D. R.; Cussen, E. J.; Chen, G. Z. Structure and Ionic-Transport Properties of Lithium-Containing Garnets Li₃Ln₃Te₂O₁₂ (Ln = Y, Pr, Nd, Sm–Lu). *Chem. Mater.* **2006**, *18*, 4681–4689.
- (66) Cussen, E. J. Structure and Ionic Conductivity in Lithium Garnets. *J. Mater. Chem.* **2010**, *20*, 5167–5173.
- (67) Xie, H.; Alonso, J. A.; Li, Y.; Fernández-Díaz, M. T.; Goodenough, J. B. Lithium Distribution in Aluminum-Free Cubic Li₇La₃Zr₂O₁₂. *Chem. Mater.* **2011**, *23*, 3587–3589.
- (68) Li, Y.; Han, J. T.; Wang, C. A.; Xie, H.; Goodenough, J. B. Optimizing Li⁺ Conductivity in a Garnet Framework. *J. Mater. Chem.* **2012**, *22*, 15357–15361.
- (69) Awaka, J.; Kijima, N.; Hayakawa, H.; Akimoto, J. Synthesis and Structure Analysis of Tetragonal Li₇La₃Zr₂O₁₂ with the Garnet-Related Type Structure. *J. Solid State Chem.* **2009**, *182*, 2046–2052.
- (70) Adams, S.; Rao, R. P. Ion Transport and Phase Transition in Li₇–xLa₃(Zr₂–xM_x)O₁₂ (M = Ta⁵⁺, Nb⁵⁺, x = 0, 0.25). *J. Mater. Chem.* **2012**, *22*, 1426–1434.
- (71) Xu, M.; Park, M. S.; Lee, J. M.; Kim, T. Y.; Park, Y. S.; Ma, E. Mechanisms of Li⁺ Transport in Garnet-Type Cubic Li_{3+x}La₃M₂O₁₂ (M = Te, Nb, Zr). *Phys. Rev. B: Condens. Matter Mater. Phys.* **2012**, *85*, 052301.
- (72) Bernstein, N.; Johannes, M. D.; Hoang, K. Origin of the Structural Phase Transition in Li₇La₃Zr₂O₁₂. *Phys. Rev. Lett.* **2012**, *109*, 205702.
- (73) Jalem, R.; Yamamoto, Y.; Shiiba, H.; Nakayama, M.; Munakata, H.; Kasuga, T.; Kanamura, K. Concerted Migration Mechanism in the Li Ion Dynamics of Garnet-Type Li₇La₃Zr₂O₁₂. *Chem. Mater.* **2013**, *25*, 425–430.
- (74) Meier, K.; Laino, T.; Curioni, A. Solid-State Electrolytes: Revealing the Mechanisms of Li-Ion Conduction in Tetragonal and Cubic LLZO by First-Principles Calculations. *J. Phys. Chem. C* **2014**, *118*, 6668–6679.
- (75) Klenk, M.; Lai, W. Local Structure and Dynamics of Lithium Garnet Ionic Conductors: Tetragonal and Cubic Li₇La₃Zr₂O₇. *Phys. Chem. Chem. Phys.* **2015**, *17*, 8758–8768.
- (76) Kuhn, A.; Narayanan, S.; Spencer, L.; Goward, G.; Thangadurai, V.; Wilkening, M. Li Self-Diffusion in Garnet-Type Li₇La₃Zr₂O₁₂ as Probed Directly by Diffusion-Induced ⁷Li Spin-Lattice Relaxation NMR Spectroscopy. *Phys. Rev. B: Condens. Matter Mater. Phys.* **2011**, *83*, 94302.
- (77) Larraz, G.; Orera, A.; Sanz, J.; Sobrados, I.; Diez-Gómez, V.; Sanjuán, M. L. NMR Study of Li Distribution in Li₇–XHxLa₃Zr₂O₁₂ Garnets. *J. Mater. Chem. A* **2015**, *3*, 5683–5691.
- (78) Hayamizu, K.; Terada, Y.; Kataoka, K.; Akimoto, J. Toward Understanding the Anomalous Li Diffusion in Inorganic Solid Electrolytes by Studying a Single-Crystal Garnet of LLZO-Ta by Pulsed-Gradient Spin-Echo Nuclear Magnetic Resonance Spectroscopy. *J. Chem. Phys.* **2019**, *150*, 194502.
- (79) Geiger, C. A.; Alekseev, E.; Lazic, B.; Fisch, M.; Armbruster, T.; Langner, R.; Fechtelkord, M.; Kim, N.; Pettke, T.; Wepner, W. Crystal Chemistry and Stability of "Li₇La₃Zr₂O₁₂" Garnet: A Fast Lithium-Ion Conductor. *Inorg. Chem.* **2011**, *50*, 1089–1097.
- (80) Nyman, M.; Alam, T. M.; McIntyre, S. K.; Bleier, G. C.; Ingersoll, D. Alternative Approach to Increasing Li Mobility in Li–La–Nb/Ta Garnet Electrolytes. *Chem. Mater.* **2010**, *22*, 5401–5410.
- (81) Wang, Y.; Huq, A.; Lai, W. Insight into Lithium Distribution in Lithium-Stuffed Garnet Oxides through Neutron Diffraction and Atomistic Simulation: Li₇–XLa₃Zr₂–XTaxO₁₂ (X = 0–2) Series. *Solid State Ionics* **2014**, *255*, 39–49.
- (82) Narayanan, S.; Hitz, G. T.; Wachsman, E. D.; Thangadurai, V. Effect of Excess Li on the Structural and Electrical Properties of Garnet-Type Li₆La₃Ta_{1.5}YO_{0.5}O₁₂. *J. Electrochem. Soc.* **2015**, *162*, A1772–A1777.
- (83) Narayanan, S.; Ramezanipour, F.; Thangadurai, V. Dopant Concentration–Porosity–Li-Ion Conductivity Relationship in Garnet-Type Li₅ + 2xLa₃Ta₂–XYxO₁₂ (0.05 ≤ x ≤ 0.75) and Their Stability in Water and 1 M LiCl. *Inorg. Chem.* **2015**, *54*, 6968–6977.
- (84) Peng, H.; Li, L.; Feng, L.; Zhang, Y.; Zou, Y. Effect of Na Substitution for La on Li Ion Conductivity of Li₅La₃Nb₂O₁₂ Garnets by Sol–Gel Process. *Mater. Res. Bull.* **2018**, *99*, 414–418.
- (85) Abdel-Basset, D. M.; Mulmi, S.; El-Bana, M. S.; Fouad, S. S.; Thangadurai, V. Structure, Ionic Conductivity, and Dielectric Properties of Li-Rich Garnet-Type Li₅ + 2xLa₃Ta₂–XSm_xO₁₂ (0 ≤ x ≤ 0.55) and Their Chemical Stability. *Inorg. Chem.* **2017**, *56*, 8865–8877.
- (86) Narayanan, S.; Baral, A. K.; Thangadurai, V. Dielectric Characteristics of Fast Li Ion Conducting Garnet-Type Li₅ + 2XLa₃Nb₂–XYxO₁₂ (x = 0.25, 0.5 and 0.75). *Phys. Chem. Chem. Phys.* **2016**, *18*, 15418–15426.
- (87) Peng, H.; Feng, L.; Li, L.; Zhang, Y.; Zou, Y. Synthesis of Li₅+xLa₃HfxNb₂–XO₁₂ (x = 0.2–1) Ceramics with Cubic Garnet-Type Structure. *Mater. Lett.* **2017**, *194*, 138–141.
- (88) Awaka, J.; Kijima, N.; Takahashi, Y.; Hayakawa, H.; Akimoto, J. Synthesis and Crystallographic Studies of Garnet-Related Lithium-Ion Conductors Li₆CaLa₂Ta₂O₁₂ and Li₆BaLa₂Ta₂O₁₂. *Solid State Ionics* **2009**, *180*, 602–606.
- (89) Xie, H.; Li, Y.; Han, J.; Wang, L.; Xu, M.; Gupta, A.; Goodenough, J. B.; Dong, Y.; Paranthaman, M. P.; Bi, Z.; et al. Li₆La₃SnMO₁₂ (M = Sb, Nb, Ta), a Family of Lithium Garnets with High Li-Ion Conductivity. *J. Electrochem. Soc.* **2012**, *159*, A1148–A1151.
- (90) Zeier, W. G.; Zhou, S.; Lopez-Bermudez, B.; Page, K.; Melot, B. C. Dependence of the Li-Ion Conductivity and Activation Energies on the Crystal Structure and Ionic Radii in Li₆MLa₂Ta₂O₁₂. *ACS Appl. Mater. Interfaces* **2014**, *6*, 10900–10907.
- (91) Ahmad, M. M.; Al-Jaafari, A. Concentration and Mobility of Mobile Li⁺ Ions in Li₆BaLa₂Ta₂O₁₂ and Li₅La₃Ta₂O₁₂ Garnet

- Lithium Ion Conductors. *J. Mater. Sci.: Mater. Electron.* **2015**, *26*, 8136–8142.
- (92) Wang, W. G.; Wang, X. P.; Gao, Y. X.; Fang, Q. F. Lithium-Ionic Diffusion and Electrical Conduction in the $\text{Li}_7\text{La}_3\text{Ta}_2\text{O}_{13}$ Compounds. *Solid State Ionics* **2009**, *180*, 1252–1256.
- (93) Zaiß, T.; Ortner, M.; Murugan, R.; Weppner, W. Fast Ionic Conduction in Cubic Hafnium Garnet $\text{Li}_7\text{La}_3\text{Hf}_2\text{O}_{12}$. *Ionics* **2010**, *16*, 855–858.
- (94) Ramzy, A.; Thangadurai, V. Tailor-Made Development of Fast Li Ion Conducting Garnet-like Solid Electrolytes. *ACS Appl. Mater. Interfaces* **2010**, *2*, 385–390.
- (95) Jin, Y.; McGinn, P. J. Al-Doped $\text{Li}_7\text{La}_3\text{Zr}_2\text{O}_{12}$ Synthesized by a Polymerized Complex Method. *J. Power Sources* **2011**, *196*, 8683–8687.
- (96) Wang, Y.; Lai, W. High Ionic Conductivity Lithium Garnet Oxides of $\text{Li}_7\text{XLa}_3\text{Zr}_2\text{XTa}_x\text{O}_{12}$ Compositions. *Electrochem. Solid-State Lett.* **2012**, *15*, A68.
- (97) Buschmann, H.; Berendts, S.; Mogwitz, B.; Janek, J. Lithium Metal Electrode Kinetics and Ionic Conductivity of the Solid Lithium Ion Conductors " $\text{Li}_7\text{La}_3\text{Zr}_2\text{O}_{12}$ " and $\text{Li}_7\text{xLa}_3\text{Zr}_2\text{xTa}_x\text{O}_{12}$ with Garnet-Type Structure. *J. Power Sources* **2012**, *206*, 236–244.
- (98) Allen, J. L.; Wolfenstine, J.; Rangasamy, E.; Sakamoto, J. Effect of Substitution (Ta, Al, Ga) on the Conductivity of $\text{Li}_7\text{La}_3\text{Zr}_2\text{O}_{12}$. *J. Power Sources* **2012**, *206*, 315–319.
- (99) Deviannapoorni, C.; Dhivya, L.; Ramakumar, S.; Murugan, R. Lithium Ion Transport Properties of High Conductive Tellurium Substituted $\text{Li}_7\text{La}_3\text{Zr}_2\text{O}_{12}$ Cubic Lithium Garnets. *J. Power Sources* **2013**, *240*, 18–25.
- (100) Dhivya, L.; Janani, N.; Palanivel, B.; Murugan, R. Li⁺ Transport Properties of W Substituted $\text{Li}_7\text{La}_3\text{Zr}_2\text{O}_{12}$ Cubic Lithium Garnets. *AIP Adv.* **2013**, *3*, 82115.
- (101) Bernuy-Lopez, C.; Manalastas, W.; Lopez Del Amo, J. M.; Aguadero, A.; Aguesse, F.; Kilner, J. A. Atmosphere Controlled Processing of Ga-Substituted Garnets for High Li-Ion Conductivity Ceramics. *Chem. Mater.* **2014**, *26*, 3610–3617.
- (102) Cao, Y.; Li, Y. Q.; Guo, X. X. Densification and Lithium Ion Conductivity of Garnet-Type $\text{Li}_7\text{XLa}_3\text{Zr}_2\text{XTa}_x\text{O}_{12}$ ($x = 0.25$) Solid Electrolytes. *Chin. Phys. B* **2013**, *22*, 78201.
- (103) Du, F.; Zhao, N.; Li, Y.; Chen, C.; Liu, Z.; Guo, X. All Solid State Lithium Batteries Based on Lamellar Garnet-Type Ceramic Electrolytes. *J. Power Sources* **2015**, *300*, 24–28.
- (104) Tong, X.; Thangadurai, V.; Wachsman, E. D. Highly Conductive Li Garnets by a Multielement Doping Strategy. *Inorg. Chem.* **2015**, *54*, 3600–3607.
- (105) Rettenwander, D.; Redhammer, G.; Preishuber-Pflügl, F.; Cheng, L.; Miara, L.; Wagner, R.; Welzl, A.; Suard, E.; Doeuff, M. M.; Wilkening, M.; et al. Structural and Electrochemical Consequences of Al and Ga Cosubstitution in $\text{Li}_7\text{La}_3\text{Zr}_2\text{O}_{12}$ Solid Electrolytes. *Chem. Mater.* **2016**, *28*, 2384–2392.
- (106) Wu, J. F.; Chen, E. Y.; Yu, Y.; Liu, L.; Wu, Y.; Pang, W. K.; Peterson, V. K.; Guo, X. Gallium-Doped $\text{Li}_7\text{La}_3\text{Zr}_2\text{O}_{12}$ Garnet-Type Electrolytes with High Lithium-Ion Conductivity. *ACS Appl. Mater. Interfaces* **2017**, *9*, 1542–1552.
- (107) He, M.; Cui, Z.; Chen, C.; Li, Y.; Guo, X. Formation of Self-Limited, Stable and Conductive Interfaces between Garnet Electrolytes and Lithium Anodes for Reversible Lithium Cycling in Solid-State Batteries. *J. Mater. Chem. A* **2018**, *6*, 11463–11470.
- (108) Murugan, R.; Weppner, W.; Schmid-Beurmann, P.; Thangadurai, V. Structure and Lithium Ion Conductivity of Bismuth Containing Lithium Garnets $\text{Li}_5\text{La}_3\text{Bi}_2\text{O}_{12}$ and $\text{Li}_6\text{Sr}_2\text{Bi}_2\text{O}_{12}$. *Mater. Sci. Eng., B* **2007**, *143*, 14–20.
- (109) Murugan, R.; Weppner, W.; Schmid-Beurmann, P.; Thangadurai, V. Structure and Lithium Ion Conductivity of Garnet-like $\text{Li}_5\text{La}_3\text{Sb}_2\text{O}_{12}$ and $\text{Li}_6\text{Sr}_2\text{Sb}_2\text{O}_{12}$. *Mater. Res. Bull.* **2008**, *43*, 2579–2591.
- (110) Gao, Y. X.; Wang, X. P.; Wang, W. G.; Zhuang, Z.; Zhang, D. M.; Fang, Q. F. Synthesis, Ionic Conductivity, and Chemical Compatibility of Garnet-like Lithium Ionic Conductor $\text{Li}_5\text{La}_3\text{Bi}_2\text{O}_{12}$. *Solid State Ionics* **2010**, *181*, 1415–1419.
- (111) Narayanan, S.; Thangadurai, V. Effect of y Substitution for Nb in $\text{Li}_5\text{La}_3\text{Nb}_2\text{O}_{12}$ on Li Ion Conductivity of Garnet-Type Solid Electrolytes. *J. Power Sources* **2011**, *196*, 8085–8090.
- (112) Kotobuki, M.; Kanamura, K. Fabrication of All-Solid-State Battery Using $\text{Li}_5\text{La}_3\text{Ta}_2\text{O}_{12}$ Ceramic Electrolyte. *Ceram. Int.* **2013**, *39*, 6481–6487.
- (113) Nemori, H.; Matsuda, Y.; Matsui, M.; Yamamoto, O.; Takeda, Y.; Imanishi, N. Relationship between Lithium Content and Ionic Conductivity in the $\text{Li}_5 + 2\text{xLa}_3\text{Nb}_2\text{XSc}_x\text{O}_{12}$ System. *Solid State Ionics* **2014**, *266*, 9–12.
- (114) Zeier, W. G. Structural Limitations for Optimizing Garnet-Type Solid Electrolytes: A Perspective. *Dalt. Trans.* **2014**, *43*, 16133–16138.
- (115) Qin, S.; Zhu, X.; Jiang, Y.; Ling, M.; Hu, Z.; Zhu, J. Growth of Self-Textured Ga³⁺-Substituted $\text{Li}_7\text{La}_3\text{Zr}_2\text{O}_{12}$ Ceramics by Solid State Reaction and Their Significant Enhancement in Ionic Conductivity. *Appl. Phys. Lett.* **2018**, *112*, 113901.
- (116) Miara, L. J.; Richards, W. D.; Wang, Y. E.; Ceder, G. First-Principles Studies on Cation Dopants and Electrolyte/Cathode Interphases for Lithium Garnets. *Chem. Mater.* **2015**, *27*, 4040–4047.
- (117) Chen, R. J.; Huang, M.; Huang, W. Z.; Shen, Y.; Lin, Y. H.; Nan, C. W. Sol-Gel Derived Li-La-Zr-O Thin Films as Solid Electrolytes for Lithium-Ion Batteries. *J. Mater. Chem. A* **2014**, *2*, 13277–13282.
- (118) Bitzer, M.; Van Gestel, T.; Uhlenbrück, S.; Hans-Peter-Buchkremer. Sol-Gel Synthesis of Thin Solid $\text{Li}_7\text{La}_3\text{Zr}_2\text{O}_{12}$ Electrolyte Films for Li-Ion Batteries. *Thin Solid Films* **2016**, *615*, 128–134.
- (119) Tadanaga, K.; Egawa, H.; Hayashi, A.; Tatsumisago, M.; Mosa, J.; Aparicio, M.; Duran, A. Preparation of Lithium Ion Conductive Al-Doped $\text{Li}_7\text{La}_3\text{Zr}_2\text{O}_{12}$ Thin Films by a Sol-Gel Process. *J. Power Sources* **2015**, *273*, 844–847.
- (120) Zarabian, M.; Bartolini, M.; Pereira-Almao, P.; Thangadurai, V. X-Ray Photoelectron Spectroscopy and AC Impedance Spectroscopy Studies of Li-La-Zr-O Solid Electrolyte Thin Film/LiCoO₂ Cathode Interface for All-Solid-State Li Batteries. *J. Electrochem. Soc.* **2017**, *164*, A1133–A1139.
- (121) Kazyak, E.; Chen, K.-H.; Wood, K. N.; Davis, A. L.; Thompson, T.; Bielinski, A. R.; Sanchez, A. J.; Wang, X.; Wang, C.; Sakamoto, J.; et al. Atomic Layer Deposition of the Solid Electrolyte Garnet $\text{Li}_7\text{La}_3\text{Zr}_2\text{O}_{12}$. *Chem. Mater.* **2017**, *29*, 3785–3792.
- (122) Kim, S.; Hirayama, M.; Taminato, S.; Kanno, R. Epitaxial Growth and Lithium Ion Conductivity of Lithium-Oxide Garnet for an All Solid-State Battery Electrolyte. *Dalt. Trans.* **2013**, *42*, 13112–13117.
- (123) Park, J. S.; Cheng, L.; Zorba, V.; Mehta, A.; Cabana, J.; Chen, G.; Doeuff, M. M.; Richardson, T. J.; Park, J. H.; Son, J. W.; et al. Effects of Crystallinity and Impurities on the Electrical Conductivity of Li-La-Zr-O Thin Films. *Thin Solid Films* **2015**, *576*, 55–60.
- (124) Tan, J.; Tiwari, A. Fabrication and Characterization of $\text{Li}_7\text{La}_3\text{Zr}_2\text{O}_{12}$ Thin Films for Lithium Ion Battery. *ECS Solid State Lett.* **2012**, *1*, Q57–Q60.
- (125) Rawlence, M.; Garbayo, I.; Buecheler, S.; Rupp, J. L. M. On the Chemical Stability of Post-Lithiated Garnet Al-Stabilized $\text{Li}_7\text{La}_3\text{Zr}_2\text{O}_{12}$ Solid State Electrolyte Thin Films. *Nanoscale* **2016**, *8*, 14746–14753.
- (126) Garbayo, I.; Struzik, M.; Bowman, W. J.; Pfenninger, R.; Stilp, E.; Rupp, J. L. M. Glass-Type Polyamorphism in Li-Garnet Thin Film Solid State Battery Conductors. *Adv. Energy Mater.* **2018**, *1702265*, 1–14.
- (127) Pfenninger, R.; Struzik, M.; Garbayo, I.; Stilp, E.; Rupp, J. L. M. A Low Ride on Processing Temperature for Fast Lithium Conduction in Garnet Solid-State Battery Films. *Nat. Energy* **2019**, *4*, 475–483.
- (128) Lohr, C.; Djenadic, R.; Bruns, M.; Clemens, O.; Hahn, H. Garnet-Type $\text{Li}_7\text{La}_3\text{Zr}_2\text{O}_{12}$ Solid Electrolyte Thin Films Grown by CO₂-Laser Assisted CVD for All-Solid-State Batteries. *J. Electrochem. Soc.* **2017**, *164*, A6131–A6139.
- (129) Kalita, D. J.; Lee, S. H.; Lee, K. S.; Ko, D. H.; Yoon, Y. S. Ionic Conductivity Properties of Amorphous Li-La-Zr-O Solid Electrolyte for Thin Film Batteries. *Solid State Ionics* **2012**, *229*, 14–19.
- (130) Lobe, S.; Dellen, C.; Finsterbusch, M.; Gehrke, H. G.; Sebold, D.; Tsai, C. L.; Uhlenbrück, S.; Guillou, O. Radio Frequency

- Magnetron Sputtering of Li₇La₃Zr₂O₁₂ Thin Films for Solid-State Batteries. *J. Power Sources* **2016**, *307*, 684–689.
- (131) Rawlence, M.; Filippin, A. N.; Wäckerlin, A.; Lin, T. Y.; Cuervo-Reyes, E.; Remhof, A.; Battaglia, C.; Rupp, J. L. M.; Buecheler, S. Effect of Gallium Substitution on Lithium-Ion Conductivity and Phase Evolution in Sputtered Li₇–₃XGa_xLa₃Zr₂O₁₂ Thin Films. *ACS Appl. Mater. Interfaces* **2018**, *10*, 13720–13728.
- (132) Nong, J.; Xu, H.; Yu, Z.; Zhu, G.; Yu, A. Properties and Preparation of Li-La-Ti-Zr-O Thin Film Electrolyte. *Mater. Lett.* **2015**, *154*, 167–169.
- (133) Yi, E.; Wang, W.; Kieffer, J.; Laine, R. M. Flame Made Nanoparticles Permit Processing of Dense, Flexible, Li⁺ Conducting Ceramic Electrolyte Thin Films of Cubic-Li₇La₃Zr₂O₁₂ (c-LLZO). *J. Mater. Chem. A* **2016**, *4*, 12947–12954.
- (134) Yi, E.; Wang, W.; Kieffer, J.; Laine, R. M. Key Parameters Governing the Densification of Cubic-Li₇La₃Zr₂O₁₂ Li⁺ Conductors. *J. Power Sources* **2017**, *352*, 156–164.
- (135) Murugan, R.; Thangadurai, V.; Weppner, W. Fast Lithium Ion Conduction in Garnet-Type Li₇La₃Zr₂O₁₂. *Angew. Chem., Int. Ed.* **2007**, *46*, 7778–7781.
- (136) Samson, A. J.; Hofstetter, K.; Bag, S.; Thangadurai, V. A Bird's-Eye View of Li-Stuffed Garnet-Type Li₇La₃Zr₂O₁₂ Ceramic Electrolytes for Advanced All-Solid-State Li Batteries. *Energy Environ. Sci.* **2019**, *12*, 2957–2975.
- (137) Janek, J.; Zeier, W. G. A Solid Future for Battery Development. *Nat. Energy* **2016**, *1*, 16141.
- (138) Koerver, R.; Zhang, W.; De Biasi, L.; Schweidler, S.; Kondrakov, A. O.; Kolling, S.; Brezesinski, T.; Hartmann, P.; Zeier, W. G.; Janek, J. Chemo-Mechanical Expansion of Lithium Electrode Materials on the Route to Mechanically Optimized All-Solid-State Batteries. *Energy Environ. Sci.* **2018**, *11*, 2142–2158.
- (139) Wang, A. N.; Nonemacher, J. F.; Yan, G.; Finsterbusch, M.; Malzbender, J.; Krüger, M. Mechanical Properties of the Solid Electrolyte Al-Substituted Li₇La₃Zr₂O₁₂ (LLZO) by Utilizing Micro-Pillar Indentation Splitting Test. *J. Eur. Ceram. Soc.* **2018**, *38*, 3201–3209.
- (140) Wolfenstine, J.; Allen, J. L.; Sakamoto, J.; Siegel, D. J.; Choe, H. Mechanical Behavior of Li-Ion-Conducting Crystalline Oxide-Based Solid Electrolytes: A Brief Review. *Ionics* **2018**, *24*, 1–6.
- (141) Ni, J. E.; Case, E. D.; Sakamoto, J. S.; Rangasamy, E.; Wolfenstine, J. B. Room Temperature Elastic Moduli and Vickers Hardness of Hot-Pressed LLZO Cubic Garnet. *J. Mater. Sci.* **2012**, *47*, 7978–7985.
- (142) Yu, S.; Schmidt, R. D.; Garcia-Mendez, R.; Herbert, E.; Dudney, N. J.; Wolfenstine, J. B.; Sakamoto, J.; Siegel, D. J. Elastic Properties of the Solid Electrolyte Li₇La₃Zr₂O₁₂ (LLZO). *Chem. Mater.* **2016**, *28*, 197–206.
- (143) Monroe, C.; Newman, J. The Impact of Elastic Deformation on Deposition Kinetics at Lithium/Polymer Interfaces. *J. Electrochem. Soc.* **2005**, *152*, A396.
- (144) Hofstetter, K.; Samson, A. J.; Narayanan, S.; Thangadurai, V. Present Understanding of the Stability of Li-Stuffed Garnets with Moisture, Carbon Dioxide, and Metallic Lithium. *J. Power Sources* **2018**, *390*, 297–312.
- (145) Xu, B.; Li, W.; Duan, H.; Wang, H.; Guo, Y.; Li, H.; Liu, H. Li₃PO₄-Added Garnet-Type Li_{6.5}La₃Zr_{1.5}Ta_{0.5}SO₁₂ for Li-Dendrite Suppression. *J. Power Sources* **2017**, *354*, 68–73.
- (146) Sudo, R.; Nakata, Y.; Ishiguro, K.; Matsui, M.; Hirano, A.; Takeda, Y.; Yamamoto, O.; Imanishi, N. Interface Behavior between Garnet-Type Lithium-Conducting Solid Electrolyte and Lithium Metal. *Solid State Ionics* **2014**, *262*, 151–154.
- (147) Ren, Y.; Shen, Y.; Lin, Y.; Nan, C. W. Direct Observation of Lithium Dendrites inside Garnet-Type Lithium-Ion Solid Electrolyte. *Electrochem. Commun.* **2015**, *57*, 27–30.
- (148) Wolfenstine, J.; Jo, H.; Cho, Y. H.; David, I. N.; Askeland, P.; Case, E. D.; Kim, H.; Choe, H.; Sakamoto, J. A Preliminary Investigation of Fracture Toughness of Li₇La₃Zr₂O₁₂ and Its Comparison to Other Solid Li-Ionconductors. *Mater. Lett.* **2013**, *96*, 117–120.
- (149) Fallis, A. *ASM Handbook: Mechanical Testing and Evaluation*, 2013; Vol. 8.
- (150) Kim, Y.; Jo, H.; Allen, J. L.; Choe, H.; Wolfenstine, J.; Sakamoto, J. The Effect of Relative Density on the Mechanical Properties of Hot-Pressed Cubic Li₇La₃Zr₂O₁₂. *J. Am. Ceram. Soc.* **2016**, *99*, 1367–1374.
- (151) Jackman, S. D.; Cutler, R. A. Effect of Microcracking on Ionic Conductivity in LATP. *J. Power Sources* **2012**, *218*, 65–72.
- (152) Cho, Y.-H.; Wolfenstine, J.; Rangasamy, E.; Kim, H.; Choe, H.; Sakamoto, J. Mechanical Properties of the Solid Li-Ion Conducting Electrolyte: Li_{0.33}La_{0.57}TiO₃. *J. Mater. Sci.* **2012**, *47*, 5970–5977.
- (153) Zhu, Y.; He, X.; Mo, Y. First Principles Study on Electrochemical and Chemical Stability of Solid Electrolyte-Electrode Interfaces in All-Solid-State Li-Ion Batteries. *J. Mater. Chem. A* **2016**, *4*, 3253.
- (154) Richards, W. D.; Miara, L. J.; Wang, Y.; Kim, J. C.; Ceder, G. Interface Stability in Solid-State Batteries. *Chem. Mater.* **2016**, *28*, 266–273.
- (155) Zhu, Y.; He, X.; Mo, Y. Origin of Outstanding Stability in the Lithium Solid Electrolyte Materials: Insights from Thermodynamic Analyses Based on First-Principles Calculations. *ACS Appl. Mater. Interfaces* **2015**, *7*, 23685–23693.
- (156) Thompson, T.; Yu, S.; Williams, L.; Schmidt, R. D.; Garcia-Mendez, R.; Wolfenstine, J.; Allen, J. L.; Kioupakis, E.; Siegel, D. J.; Sakamoto, J. Electrochemical Window of the Li-Ion Solid Electrolyte Li₇La₃Zr₂O₁₂. *ACS Energy Lett.* **2017**, *2*, 462–468.
- (157) Nolan, A. M.; Zhu, Y.; He, X.; Bai, Q.; Mo, Y. Computation-Accelerated Design of Materials and Interfaces for All-Solid-State Lithium-Ion Batteries. *Joule* **2018**, *2*, 2016–2046.
- (158) Han, F.; Zhu, Y.; He, X.; Mo, Y.; Wang, C. Electrochemical Stability of Li₁₀GeP₂S₁₂ and Li₇La₃Zr₂O₁₂ Solid Electrolytes. *Adv. Energy Mater.* **2016**, *6*, 1501590.
- (159) Urban, A.; Seo, D. H.; Ceder, G. Computational Understanding of Li-Ion Batteries. *npj Computational Materials* **2016**, *2*, 16010.
- (160) Hautier, G.; Ong, S. P.; Jain, A.; Moore, C. J.; Ceder, G. Accuracy of Density Functional Theory in Predicting Formation Energies of Ternary Oxides from Binary Oxides and Its Implication on Phase Stability. *Phys. Rev. B: Condens. Matter Mater. Phys.* **2012**, *85*, 155208.
- (161) Wolfenstine, J.; Allen, J. L.; Read, J.; Sakamoto, J. Chemical Stability of Cubic Li₇La₃Zr₂O₁₂ with Molten Lithium at Elevated Temperature. *J. Mater. Sci.* **2013**, *48*, 5846–5851.
- (162) Ma, C.; Cheng, Y.; Yin, K.; Luo, J.; Sharafi, A.; Sakamoto, J.; Li, J.; More, K. L.; Dudney, N. J.; Chi, M. Interfacial Stability of Li Metal-Solid Electrolyte Elucidated via in Situ Electron Microscopy. *Nano Lett.* **2016**, *16*, 7030–7036.
- (163) Zhu, Y.; Connell, J. G.; Tepavcevic, S.; Zapol, P.; Garcia-Mendez, R.; Taylor, N. J.; Sakamoto, J.; Ingram, B. J.; Curtiss, L. A.; Freeland, J. W.; et al. Dopant-Dependent Stability of Garnet Solid Electrolyte Interfaces with Lithium Metal. *Adv. Energy Mater.* **2019**, *9*, 1803440.
- (164) Nemori, H.; Matsuda, Y.; Mitsuoka, S.; Matsui, M.; Yamamoto, O.; Takeda, Y.; Imanishi, N. Stability of Garnet-Type Solid Electrolyte Li_xLa₃A₂-Y_{1-x}O₁₂ (A = Nb or Ta, B = Sc or Zr). *Solid State Ionics* **2015**, *282*, 7–12.
- (165) Raj, R.; Wolfenstine, J. Current Limit Diagrams for Dendrite Formation in Solid-State Electrolytes for Li-Ion Batteries. *J. Power Sources* **2017**, *343*, 119–126.
- (166) Deng, Z.; Wang, Z.; Chu, I. H.; Luo, J.; Ong, S. P. Elastic Properties of Alkali Superionic Conductor Electrolytes from First Principles Calculations. *J. Electrochem. Soc.* **2016**, *163*, A67–A74.
- (167) Porz, L.; Swamy, T.; Sheldon, B. W.; Rettenwander, D.; Frömling, T.; Thaman, H. L.; Berendts, S.; Uecker, R.; Carter, W. C.; Chiang, Y. M. Mechanism of Lithium Metal Penetration through Inorganic Solid Electrolytes. *Adv. Energy Mater.* **2017**, *7*, 1–12.
- (168) Fu, K. K.; Gong, Y.; Liu, B.; Zhu, Y.; Xu, S.; Yao, Y.; Luo, W.; Wang, C.; Lacey, S. D.; Dai, J.; et al. Toward Garnet Electrolyte-Based Li Metal Batteries: An Ultrathin, Highly Effective, Artificial Solid-State Electrolyte/Metallic Li Interface. *Sci. Adv.* **2017**, *3*, 1–11.

- (169) Yang, C.; Xie, H.; Ping, W.; Fu, K.; Liu, B.; Rao, J.; Dai, J.; Wang, C.; Pastel, G.; Hu, L. An Electron/Ion Dual-Conductive Alloy Framework for High-Rate and High-Capacity Solid-State Lithium-Metal Batteries. *Adv. Mater.* **2019**, *31*, 1804815.
- (170) Hiratani, M.; Miyauchi, K.; Kudo, T. Effect of a Lithium Alloy Layer Inserted between a Lithium Anode and a Solid Electrolyte. *Solid State Ionics* **1988**, *28–30*, 1406–1410.
- (171) Krauskopf, T.; Dippel, R.; Hartmann, H.; Peppler, K.; Mogwitz, B.; Richter, F. H.; Zeier, W. G.; Janek, J. Lithium-Metal Growth Kinetics on LLZO Garnet-Type Solid Electrolytes. *Joule* **2019**, *3*, 2030–2049.
- (172) Goodenough, J. B.; Kim, Y. Challenges for Rechargeable Li Batteries. *Chem. Mater.* **2010**, *22*, 587–603.
- (173) Han, F.; Westover, A. S.; Yue, J.; Fan, X.; Wang, F.; Chi, M.; Leonard, D. N.; Dudney, N. J.; Wang, H.; Wang, C. High Electronic Conductivity as the Origin of Lithium Dendrite Formation within Solid Electrolytes. *Nat. Energy* **2019**, *4*, 187–196.
- (174) Girishkumar, G.; McCloskey, B.; Luntz, A. C.; Swanson, S.; Wilcke, W. Lithium-Air Battery: Promise and Challenges. *J. Phys. Chem. Lett.* **2010**, *1*, 2193.
- (175) Kim, K. H.; Iriyama, Y.; Yamamoto, K.; Kumazaki, S.; Asaka, T.; Tanabe, K.; Fisher, C. A. J.; Hirayama, T.; Murugan, R.; Ogumi, Z. Characterization of the Interface between LiCoO₂ and Li₇La₃Zr₂O₁₂ in an All-Solid-State Rechargeable Lithium Battery. *J. Power Sources* **2011**, *196*, 764–767.
- (176) Vardar, G.; Bowman, W. J.; Lu, Q.; Wang, J.; Chater, R. J.; Aguadero, A.; Seibert, R.; Terry, J.; Hunt, A.; Waluyo, I.; et al. Structure, Chemistry, and Charge Transfer Resistance of the Interface between Li₇La₃Zr₂O₁₂ Electrolyte and LiCoO₂ Cathode. *Chem. Mater.* **2018**, *30*, 6259–6276.
- (177) Park, K.; Yu, B. C.; Jung, J. W.; Li, Y.; Zhou, W.; Gao, H.; Son, S.; Goodenough, J. B. Electrochemical Nature of the Cathode Interface for a Solid-State Lithium-Ion Battery: Interface between LiCoO₂ and Garnet-Li₇La₃Zr₂O₁₂. *Chem. Mater.* **2016**, *28*, 8051–8059.
- (178) Ohta, S.; Komagata, S.; Seki, J.; Saeki, T.; Morishita, S.; Asaoka, T. Short Communication All-Solid-State Lithium Ion Battery Using Garnet-Type Oxide and Li₃BO₃ Solid Electrolytes Fabricated by Screen-Printing. *J. Power Sources* **2013**, *238*, 53–56.
- (179) Ohta, S.; Seki, J.; Yagi, Y.; Kihira, Y.; Tani, T.; Asaoka, T. Co-Sinterable Lithium Garnet-Type Oxide Electrolyte with Cathode for All-Solid-State Lithium Ion Battery. *J. Power Sources* **2014**, *265*, 40–44.
- (180) Liu, T.; Ren, Y.; Shen, Y.; Zhao, S. X.; Lin, Y.; Nan, C. W. Achieving High Capacity in Bulk-Type Solid-State Lithium Ion Battery Based on Li_{6.75}La₃Zr_{1.75}Ta_{0.25}O₁₂ Electrolyte: Interfacial Resistance. *J. Power Sources* **2016**, *324*, 349–357.
- (181) Shoji, M.; Munakata, H.; Kanamura, K. Fabrication of All-Solid-State Lithium-Ion Cells Using Three-Dimensionally Structured Solid Electrolyte Li₇La₃Zr₂O₁₂ Pellets. *Front. Energy Res.* **2016**, *4*, 1–7.
- (182) Han, F.; Yue, J.; Chen, C.; Zhao, N.; Fan, X.; Ma, Z.; Gao, T.; Wang, F.; Guo, X.; Wang, C. Interphase Engineering Enabled All-Ceramic Lithium Battery. *Joule* **2018**, *2*, 497–508.
- (183) Kato, T.; Hamanaka, T.; Yamamoto, K.; Hirayama, T.; Sagane, F.; Motoyama, M.; Iriyama, Y. In-Situ Li₇La₃Zr₂O₁₂/LiCoO₂ Interface Modification for Advanced All-Solid-State Battery. *J. Power Sources* **2014**, *260*, 292–298.
- (184) Xu, B.; Duan, H.; Liu, H.; Wang, C. A.; Zhong, S. Stabilization of Garnet/Liquid Electrolyte Interface Using Superbase Additives for Hybrid Li Batteries. *ACS Appl. Mater. Interfaces* **2017**, *9*, 21077–21082.
- (185) Galven, C.; Dittmer, J.; Suard, E.; Le Berre, F.; Crosnier-Lopez, M. P. Instability of Lithium Garnets against Moisture. Structural Characterization and Dynamics of Li₇-XH_xLa₃Sn₂O₁₂ and Li₅-XH_xLa₃Nb₂O₁₂. *Chem. Mater.* **2012**, *24*, 3335–3345.
- (186) Shimonishi, Y.; Toda, A.; Zhang, T.; Hirano, A.; Imanishi, N.; Yamamoto, O.; Takeda, Y. Synthesis of Garnet-Type Li₇-XLa₃Zr₂O₁₂-1/2x and Its Stability in Aqueous Solutions. *Solid State Ionics* **2011**, *183*, 48–53.
- (187) Galven, C.; Fourquet, J. L.; Crosnier-Lopez, M. P.; Le Berre, F. Instability of the Lithium Garnet Li₇La₃Sn₂O₁₂: Li⁺/H⁺ Exchange and Structural Study. *Chem. Mater.* **2011**, *23*, 1892–1900.
- (188) Galven, C.; Suard, E.; Mounier, D.; Crosnier-Lopez, M. P.; Le Berre, F. Structural Characterization of a New Acentric Protonated Garnet: Li₆-XH_xCaLa₂Nb₂O₁₂. *J. Mater. Res.* **2013**, *28*, 2147–2153.
- (189) Truong, L.; Thangadurai, V. Soft-Chemistry of Garnet-Type Li₅+XBa_xLa₃-XNb₂O₁₂ (x = 0, 0.5, 1): Reversible H⁺ ↔ Li⁺ Ion-Exchange Reaction and Their X-Ray, ⁷Li MAS NMR, IR, and AC Impedance Spectroscopy Characterization. *Chem. Mater.* **2011**, *23*, 3970–3977.
- (190) Truong, L.; Colter, J.; Thangadurai, V. Chemical Stability of Li-Stuffed Garnet-Type Li₅+XBa_xLa₃-XTa₂O₁₂ (x = 0, 0.5, 1) in Water: A Comparative Analysis with the Nb Analogue. *Solid State Ionics* **2013**, *247*–248, 1–7.
- (191) Gam, F.; Galven, C.; Bulou, A.; Le Berre, F.; Crosnier-Lopez, M. P. Reinvestigation of the Total Li⁺/H⁺ Ion Exchange on the Garnet-Type Li₅La₃Nb₂O₁₂. *Inorg. Chem.* **2014**, *53*, 931–934.
- (192) Truong, L.; Thangadurai, V. First Total H⁺/Li⁺ Ion Exchange in Garnet-Type Li₅La₃Nb₂O₁₂ Using Organic Acids and Studies on the Effect of Li Stuffing. *Inorg. Chem.* **2012**, *51*, 1222–1224.
- (193) Ishiguro, K.; Nemori, H.; Sunahiro, S.; Nakata, Y.; Sudo, R.; Matsui, M.; Takeda, Y.; Yamamoto, O.; Imanishi, N. Ta-Doped Li₇La₃Zr₂O₁₂ Forwater-Stable Lithium Electrode of Lithium-Air Batteries. *J. Electrochem. Soc.* **2014**, *161*, A668–A674.
- (194) Ma, C.; Rangasamy, E.; Liang, C.; Sakamoto, J.; More, K. L.; Chi, M. Excellent Stability of a Lithium-Ion-Conducting Solid Electrolyte upon Reversible Li⁺/H⁺ Exchange in Aqueous Solutions. *Angew. Chem., Int. Ed.* **2015**, *54*, 129–133.
- (195) Liu, X.; Chen, Y.; Hood, Z. D.; Ma, C.; Yu, S.; Sharifi, A.; Wang, H.; An, K.; Sakamoto, J.; Siegel, D. J.; et al. Elucidating the Mobility of H⁺ and Li⁺ Ions in (Li_{6.25}-XH_xAl_{0.25})La₃Zr₂O₁₂ via Correlative Neutron and Electron Spectroscopy. *Energy Environ. Sci.* **2019**, *12*, 945–951.
- (196) Wang, M. J.; Choudhury, R.; Sakamoto, J. Characterizing the Li-Solid-Electrolyte Interface Dynamics as a Function of Stack Pressure and Current Density. *Joule* **2019**, *3*, 2165–2178.
- (197) Krauskopf, T.; Hartmann, H.; Zeier, W. G.; Janek, J. Toward a Fundamental Understanding of the Lithium Metal Anode in Solid-State Batteries - An Electrochemo-Mechanical Study on the Garnet-Type Solid Electrolyte Li_{6.25}Al_{0.25}La₃Zr₂O₁₂. *ACS Appl. Mater. Interfaces* **2019**, *11*, 14463–14477.
- (198) Li, Y.; Xu, B.; Xu, H.; Duan, H.; Lü, X.; Xin, S.; Zhou, W.; Xue, L.; Fu, G.; Manthiram, A.; et al. Hybrid Polymer/Garnet Electrolyte with a Small Interfacial Resistance for Lithium-Ion Batteries. *Angew. Chem., Int. Ed.* **2017**, *56*, 753–756.
- (199) Zhou, W.; Wang, S.; Li, Y.; Xin, S.; Manthiram, A.; Goodenough, J. B. Plating a Dendrite-Free Lithium Anode with a Polymer/Ceramic/Polymer Sandwich Electrolyte. *J. Am. Chem. Soc.* **2016**, *138*, 9385–9388.
- (200) Li, Y.; Xu, B.; Xu, H.; Duan, H.; Lü, X.; Xin, S.; Zhou, W.; Xue, L.; Fu, G.; Manthiram, A.; et al. Hybrid Polymer/Garnet Electrolyte with a Small Interfacial Resistance for Lithium-Ion Batteries. *Angew. Chem.* **2017**, *129*, 771–774.
- (201) Duan, H.; Yin, Y. X.; Shi, Y.; Wang, P. F.; Zhang, X. D.; Yang, C. P.; Shi, J. L.; Wen, R.; Guo, Y. G.; Wan, L. J. Dendrite-Free Li-Metal Battery Enabled by a Thin Asymmetric Solid Electrolyte with Engineered Layers. *J. Am. Chem. Soc.* **2018**, *140*, 82–85.
- (202) Zaghib, K.; Simoneau, M.; Armand, M.; Gauthier, M. Electrochemical Study of Li₄Ti₅O₁₂ as Negative Electrode for Li-Ion Polymer Rechargeable Batteries. *J. Power Sources* **1999**, *81*–82, 300–305.
- (203) Sharifi, A.; Kazyak, E.; Davis, A. L.; Yu, S.; Thompson, T.; Siegel, D. J.; Dasgupta, N. P.; Sakamoto, J. Surface Chemistry Mechanism of Ultra-Low Interfacial Resistance in the Solid-State Electrolyte Li₇La₃Zr₂O₁₂. *Chem. Mater.* **2017**, *29*, 7961–7968.
- (204) Wang, C.; Gong, Y.; Liu, B.; Fu, K.; Yao, Y.; Hitz, E.; Li, Y.; Dai, J.; Xu, S.; Luo, W.; et al. Conformal, Nanoscale ZnO Surface Modification of Garnet-Based Solid-State Electrolyte for Lithium Metal Anodes. *Nano Lett.* **2017**, *17*, 565–571.
- (205) Fu, K. K.; Gong, Y.; Liu, B.; Zhu, Y.; Xu, S.; Yao, Y.; Luo, W.; Wang, C.; Lacey, S. D.; Dai, J. Toward Garnet Electrolyte-Based Li

- Metal Batteries: An Ultrathin, Highly Effective, Artificial Solid-State Electrolyte/Metallic Li Interface. *Sci. Adv.* **2017**, *3*, e1601659.
- (206) Luo, W.; Gong, Y.; Zhu, Y.; Fu, K. K.; Dai, J.; Lacey, S. D.; Wang, C.; Liu, B.; Han, X.; Mo, Y.; et al. Transition from Superlithiophobicity to Superlithiophilicity of Garnet Solid-State Electrolyte. *J. Am. Chem. Soc.* **2016**, *138*, 12258–12262.
- (207) Tsai, C. L.; Roddatis, V.; Chandran, C. V.; Ma, Q.; Uhlenbruck, S.; Bram, M.; Heitjans, P.; Guillon, O. Li₇La₃Zr₂O₁₂ Interface Modification for Li Dendrite Prevention. *ACS Appl. Mater. Interfaces* **2016**, *8*, 10617–10626.
- (208) Wakasugi, J.; Munakata, H.; Kanamura, K. Effect of Gold Layer on Interface Resistance between Lithium Metal Anode and Li_{6.25}Al_{0.25}La₃Zr₂O₁₂ Solid Electrolyte. *J. Electrochem. Soc.* **2017**, *164*, A1022–A1025.
- (209) Li, Y.; Chen, X.; Dolocan, A.; Cui, Z.; Xin, S.; Xu, H.; Park, K.; Goodenough, J. B.; Li, Y.; Chen, X.; et al. Garnet Electrolyte with an Ultra-Low Interfacial Resistance for Li-Metal Batteries Garnet Electrolyte with an Ultra-Low Interfacial Resistance for Li-Metal Batteries. *J. Am. Chem. Soc.* **2018**, *140*, 6448–6455.
- (210) Wang, C.; Xie, H.; Ping, W.; Dai, J.; Feng, G.; Yao, Y.; He, S.; Weaver, J.; Wang, H.; Gaskell, K.; et al. A General, Highly Efficient, High Temperature Thermal Pulse toward High Performance Solid State Electrolyte. *Energy Storage Mater.* **2019**, *17*, 234–241.
- (211) Wu, J. F.; Pu, B. W.; Wang, D.; Shi, S. Q.; Zhao, N.; Guo, X.; Guo, X. In Situ Formed Shields Enabling Li₂CO₃-Free Solid Electrolytes: A New Route to Uncover the Intrinsic Lithiophilicity of Garnet Electrolytes for Dendrite-Free Li-Metal Batteries. *ACS Appl. Mater. Interfaces* **2019**, *11*, 898–905.
- (212) Wang, C.; Xie, H.; Zhang, L.; Gong, Y.; Pastel, G.; Dai, J.; Liu, B.; Wachsman, E. D.; Hu, L. Universal Soldering of Lithium and Sodium Alloys on Various Substrates for Batteries. *Adv. Energy Mater.* **2018**, *8*, 1701963.
- (213) Cheng, L.; Crumlin, E. J.; Chen, W.; Qiao, R.; Hou, H.; Franz Lux, S.; Zorba, V.; Russo, R.; Kostecki, R.; Liu, Z.; et al. The Origin of High Electrolyte-Electrode Interfacial Resistances in Lithium Cells Containing Garnet Type Solid Electrolytes. *Phys. Chem. Chem. Phys.* **2014**, *16*, 18294–18300.
- (214) Ohta, S.; Kobayashi, T.; Seki, J.; Asaoka, T. Electrochemical Performance of an All-Solid-State Lithium Ion Battery with Garnet-Type Oxide Electrolyte. *J. Power Sources* **2012**, *202*, 332–335.
- (215) Zhang, W.; Richter, F. H.; Culver, S. P.; Leichtweiss, T.; Lozano, J. G.; Dietrich, C.; Bruce, P. G.; Zeier, W. G.; Janek, J. Degradation Mechanisms at the Li₁₀GeP₂S₁₂/LiCoO₂ Cathode Interface in an All-Solid-State Lithium-Ion Battery. *ACS Appl. Mater. Interfaces* **2018**, *10*, 22226.
- (216) Albertus, P.; Babinec, S.; Litzelman, S.; Newman, A. Status and Challenges in Enabling the Lithium Metal Electrode for High-Energy and Low-Cost Rechargeable Batteries. *Nat. Energy* **2018**, *3*, 16–21.
- (217) Narayanan, S.; Epp, V.; Wilkening, M.; Thangadurai, V. Macroscopic and Microscopic Li⁺ Transport Parameters in Cubic Garnet-Type “Li_{6.5}La_{2.5}Ba_{0.5}Zr₂TaO₁₂” as Probed by Impedance Spectroscopy and NMR. *RSC Adv.* **2012**, *2*, 2553–2561.
- (218) Zheng, J.; Tang, M.; Hu, Y. Y. Lithium Ion Pathway within Li₇La₃Zr₂O₁₂-Polyethylene Oxide Composite Electrolytes. *Angew. Chem., Int. Ed.* **2016**, *55*, 12538–12542.
- (219) Wang, C.; Gong, Y.; Dai, J.; Zhang, L.; Xie, H.; Pastel, G.; Liu, B.; Wachsman, E.; Wang, H.; Hu, L. In Situ Neutron Depth Profiling of Lithium Metal-Garnet Interfaces for Solid State Batteries. *J. Am. Chem. Soc.* **2017**, *139*, 14257–14264.
- (220) Chan, C. K.; Yang, T.; Mark Weller, J. Nanostructured Garnet-Type Li₇La₃Zr₂O₁₂: Synthesis, Properties, and Opportunities as Electrolytes for Li-Ion Batteries. *Electrochim. Acta* **2017**, *253*, 268–280.
- (221) Yang, T.; Zheng, J.; Cheng, Q.; Hu, Y. Y.; Chan, C. K. Composite Polymer Electrolytes with Li₇La₃Zr₂O₁₂ Garnet-Type Nanowires as Ceramic Fillers: Mechanism of Conductivity Enhancement and Role of Doping and Morphology. *ACS Appl. Mater. Interfaces* **2017**, *9*, 21773–21780.
- (222) Yang, T.; Gordon, Z. D.; Li, Y.; Chan, C. K. Nanostructured Garnet-Type Solid Electrolytes for Lithium Batteries: Electrospinning Synthesis of Li₇La₃Zr₂O₁₂ Nanowires and Particle Size-Dependent Phase Transformation. *J. Phys. Chem. C* **2015**, *119*, 14947–14953.
- (223) Gordon, Z. D.; Yang, T.; Gomes Morgado, G. B.; Chan, C. K. Preparation of Nano- and Microstructured Garnet Li₇La₃Zr₂O₁₂ Solid Electrolytes for Li-Ion Batteries via Cellulose Templating. *ACS Sustainable Chem. Eng.* **2016**, *4*, 6391–6398.
- (224) Zheng, J.; Hu, Y. Y. New Insights into the Compositional Dependence of Li-Ion Transport in Polymer-Ceramic Composite Electrolytes. *ACS Appl. Mater. Interfaces* **2018**, *10*, 4113–4120.
- (225) Fu, K.; Gong, Y.; Dai, J.; Gong, A.; Han, X.; Yao, Y.; Wang, C.; Wang, Y.; Chen, Y.; Yan, C.; et al. Flexible, Solid-State, Ion-Conducting Membrane with 3D Garnet Nanofiber Networks for Lithium Batteries. *Proc. Natl. Acad. Sci. U. S. A.* **2016**, *113*, 7094–7099.
- (226) Xie, H.; Yang, C.; Fu, K. K.; Yao, Y.; Jiang, F.; Hitz, E.; Liu, B.; Wang, S.; Hu, L. Flexible, Scalable, and Highly Conductive Garnet-Polymer Solid Electrolyte Tempered by Bacterial Cellulose. *Adv. Energy Mater.* **2018**, *8*, 1703474.
- (227) Li, Z.; Huang, H. M.; Zhu, J. K.; Wu, J. F.; Yang, H.; Wei, L.; Guo, X. Ionic Conduction in Composite Polymer Electrolytes: Case of PEO:Ga-LLZO Composites. *ACS Appl. Mater. Interfaces* **2019**, *11*, 784–791.
- (228) Chen, L.; Li, Y.; Li, S. P.; Fan, L. Z.; Nan, C. W.; Goodenough, J. B. PEO/Garnet Composite Electrolytes for Solid-State Lithium Batteries: From “Ceramic-in-Polymer” to “Polymer-in-Ceramic”. *Nano Energy* **2018**, *46*, 176–184.
- (229) Gong, Y.; Fu, K.; Xu, S.; Dai, J.; Hamann, T. R.; Zhang, L.; Hitz, G. T.; Fu, Z.; Ma, Z.; McOwen, D. W.; et al. Lithium-Ion Conductive Ceramic Textile: A New Architecture for Flexible Solid-State Lithium Metal Batteries. *Mater. Today* **2018**, *21*, 594–601.
- (230) Huang, X.; Song, Z.; Xiu, T.; Badding, M. E.; Wen, Z. Sintering, Micro-Structure and Li⁺ Conductivity of Li_{7-x}La₃Zr_{2-x}Nb_xO₁₂/MgO (X = 0.2–0.7) Li-Garnet Composite Ceramics. *Ceram. Int.* **2019**, *45*, 56–63.
- (231) Hitz, G. T.; McOwen, D. W.; Zhang, L.; Ma, Z.; Fu, Z.; Wen, Y.; Gong, Y.; Dai, J.; Hamann, T. R.; Hu, L.; et al. High-Rate Lithium Cycling in a Scalable Trilayer Li-Garnet-Electrolyte Architecture. *Mater. Today* **2019**, *22*, 50–57.
- (232) Moitzheim, S.; Put, B.; Vereecken, P. M. Advances in 3D Thin-Film Li-Ion Batteries. *Adv. Mater. Interfaces* **2019**, *6*, 1–17.
- (233) Zhai, H.; Xu, P.; Ning, M.; Cheng, Q.; Mandal, J.; Yang, Y. A Flexible Solid Composite Electrolyte with Vertically Aligned and Connected Ion-Conducting Nanoparticles for Lithium Batteries. *Nano Lett.* **2017**, *17*, 3182–3187.
- (234) McOwen, D. W.; Xu, S.; Gong, Y.; Wen, Y.; Godbey, G. L.; Gritton, J. E.; Hamann, T. R.; Dai, J.; Hitz, G. T.; Hu, L.; et al. 3D-Printing Electrolytes for Solid-State Batteries. *Adv. Mater.* **2018**, *30*, 1707132.
- (235) Shen, H.; Yi, E.; Amores, M.; Cheng, L.; Tamura, N.; Parkinson, D. Y.; Chen, G.; Chen, K.; Doeff, M. Oriented Porous LLZO 3D Structures Obtained by Freeze Casting for Battery Applications. *J. Mater. Chem. A* **2019**, *7*, 20861–20870.
- (236) Buannic, L.; Naviroj, M.; Miller, S. M.; Zagorski, J.; Faber, K. T.; Llordés, A. Dense Freeze-Cast Li₇La₃Zr₂O₁₂ Solid Electrolytes with Oriented Open Porosity and Contiguous Ceramic Scaffold. *J. Am. Ceram. Soc.* **2019**, *102*, 1021–1029.
- (237) Fu, K.; Gong, Y.; Hitz, G. T.; McOwen, D. W.; Li, Y.; Xu, S.; Wen, Y.; Zhang, L.; Wang, C.; Pastel, G.; et al. Three-Dimensional Bilayer Garnet Solid Electrolyte Based High Energy Density Lithium Metal-Sulfur Batteries. *Energy Environ. Sci.* **2017**, *10*, 1568–1575.
- (238) Yang, C.; Zhang, L.; Liu, B.; Xu, S.; Hamann, T.; McOwen, D.; Dai, J.; Luo, W.; Gong, Y.; Wachsman, E. D.; et al. Continuous Plating/Stripping Behavior of Solid-State Lithium Metal Anode in a 3D Ion-Conductive Framework. *Proc. Natl. Acad. Sci. U. S. A.* **2018**, *115*, 3770–3775.
- (239) Xu, S.; McOwen, D. W.; Zhang, L.; Hitz, G. T.; Wang, C.; Ma, Z.; Chen, C.; Luo, W.; Dai, J.; Kuang, Y.; et al. All-in-One Lithium-Sulfur Battery Enabled by a Porous-Dense-Porous Garnet Architecture. *Energy Storage Mater.* **2018**, *15*, 458–464.

- (240) Liu, B.; Zhang, L.; Xu, S.; McOwen, D. W.; Gong, Y.; Yang, C.; Pastel, G. R.; Xie, H.; Fu, K.; Dai, J.; et al. 3D Lithium Metal Anodes Hosted in Asymmetric Garnet Frameworks toward High Energy Density Batteries. *Energy Storage Mater.* **2018**, *14*, 376–382.
- (241) Li, Y.; Chen, X.; Dolocan, A.; Cui, Z.; Xin, S.; Xue, L.; Xu, H.; Park, K.; Goodenough, J. B. Garnet Electrolyte with an Ultralow Interfacial Resistance for Li-Metal Batteries. *J. Am. Chem. Soc.* **2018**, *140*, 6448–6455.
- (242) Ren, Y.; Liu, T.; Shen, Y.; Lin, Y.; Nan, C. W. Garnet-Type Oxide Electrolyte with Novel Porous-Dense Bilayer Configuration for Rechargeable All-Solid-State Lithium Batteries. *Ionics* **2017**, *23*, 2521–2527.
- (243) Finsterbusch, M.; Danner, T.; Tsai, C. L.; Uhlenbruck, S.; Latz, A.; Guillou, O. High Capacity Garnet-Based All-Solid-State Lithium Batteries: Fabrication and 3D-Microstructure Resolved Modeling. *ACS Appl. Mater. Interfaces* **2018**, *10*, 22329–22339.
- (244) Wang, Y.; Richards, W. D.; Ong, S. P.; Miara, L. J.; Kim, J. C.; Mo, Y.; Ceder, G. Design Principles for Solid-State Lithium Superionic Conductors. *Nat. Mater.* **2015**, *14*, 1026–1031.
- (245) Lin, D.; Liu, Y.; Cui, Y. Reviving the Lithium Metal Anode for High-Energy Batteries. *Nat. Nanotechnol.* **2017**, *12*, 194–206.
- (246) Murphy, M. W.; Armstrong, T. R.; Smith, P. A. Tape Casting of Lanthanum Chromite. *J. Am. Ceram. Soc.* **1997**, *80*, 165–170.
- (247) Rahaman, G. M. A.; Hossain, M. M. Automatic Defect Detection and Classification Technique from Image: A Special Case Using Ceramic Tiles. *J. Comput. Sci.* **2009**, *1*, 9.
- (248) Zhu, J.; Fan, Y.; Xu, N. Modified Dip-Coating Method for Preparation of Pinhole-Free Ceramic Membranes. *J. Membr. Sci.* **2011**, *367*, 14–20.
- (249) Ishiguro, K.; Nakata, Y.; Matsui, M.; Uechi, I.; Takeda, Y.; Yamamoto, O.; Imanishi, N. Stability of Nb-Doped Cubic Li₇La₃Zr₂O₁₂ with Lithium Metal. *J. Electrochem. Soc.* **2013**, *160*, A1690–A1693.
- (250) Swamy, T.; Park, R.; Sheldon, B. W.; Rettenwander, D.; Porz, L.; Berendts, S.; Uecker, R.; Craig Carter, W.; Chiang, Y. M. Lithium Metal Penetration Induced by Electrodeposition through Solid Electrolytes: Example in Single-Crystal Li₆La₃ZrTaO₁₂ Garnet. *J. Electrochem. Soc.* **2018**, *165*, A3648–A3655.
- (251) Cahn, J. W. The Impurity-Drag Effect in Grain Boundary Motion. *Acta Metall.* **1962**, *10*, 789–798.
- (252) Cheng, E. J.; Sharafi, A.; Sakamoto, J. Intergranular Li Metal Propagation through Polycrystalline Li₆2.5Al0.25La₃Zr₂O₁₂ Ceramic Electrolyte. *Electrochim. Acta* **2017**, *223*, 85–91.
- (253) Xia, W.; Xu, B.; Duan, H.; Guo, Y.; Kang, H.; Li, H.; Liu, H. Ionic Conductivity and Air Stability of Al-Doped Li₇La₃Zr₂O₁₂ Sintered in Alumina and Pt Crucibles. *ACS Appl. Mater. Interfaces* **2016**, *8*, 5335–5342.
- (254) Yin, W.; Grimaud, A.; Lepoivre, F.; Yang, C.; Tarascon, J. M. Chemical vs Electrochemical Formation of Li₂CO₃ as a Discharge Product in Li-O₂/CO₂ Batteries by Controlling the Superoxide Intermediate. *J. Phys. Chem. Lett.* **2017**, *8*, 214–222.
- (255) Thangadurai, V.; Weppner, W. Li₆Al₂Ta₂O₁₂ (A = Sr, Ba): Novel Garnet-like Oxides for Fast Lithium Ion Conduction. *Adv. Funct. Mater.* **2005**, *15*, 107–112.
- (256) Rettenwander, D.; Welzl, A.; Cheng, L.; Fleig, J.; Musso, M.; Suard, E.; Doeff, M. M.; Redhammer, G. J.; Amthauer, G. Synthesis, Crystal Chemistry, and Electrochemical Properties of Li_{7-2x}La₃Zr₂-XMo₁₂ (x = 0.1–0.4): Stabilization of the Cubic Garnet Polymorph via Substitution of Zr⁴⁺ by Mo⁶⁺. *Inorg. Chem.* **2015**, *54*, 10440–10449.
- (257) Kumazaki, S.; Iriyama, Y.; Kim, K. H.; Murugan, R.; Tanabe, K.; Yamamoto, K.; Hirayama, T.; Ogumi, Z. High Lithium Ion Conductive Li₇La₃Zr₂O₁₂ by Inclusion of Both Al and Si. *Electrochim. Commun.* **2011**, *13*, 509–512.
- (258) Han, F.; Zhu, Y.; He, X.; Mo, Y.; Wang, C. Electrochemical Stability of Li₁₀GeP₂S₁₂ and Li₇La₃Zr₂O₁₂ Solid Electrolytes. *Adv. Energy Mater.* **2016**, *6*, 1–9.
- (259) Buschmann, H.; Dölle, J.; Berendts, S.; Kuhn, A.; Bottke, P.; Wilkening, M.; Heijmans, P.; Senyshyn, A.; Ehrenberg, H.; Lotnyk, A.; et al. Structure and Dynamics of the Fast Lithium Ion Conductor “Li₇La₃Zr₂O₁₂”. *Phys. Chem. Chem. Phys.* **2011**, *13*, 19378–19392.
- (260) Samson, A. J.; Hofstetter, K.; Wachsman, E.; Thangadurai, V. Towards Mixed Ionic and Electronic Conducting Li-Stuffed Garnets. *J. Electrochem. Soc.* **2018**, *165*, A2303–A2311.
- (261) Cheng, L.; Hou, H.; Lux, S.; Kostecki, R.; Davis, R.; Zorba, V.; Mehta, A.; Doeff, M. Enhanced Lithium Ion Transport in Garnet-Type Solid State Electrolytes. *J. Electroceram.* **2017**, *38*, 168–175.
- (262) Tian, H. K.; Xu, B.; Qi, Y. Computational Study of Lithium Nucleation Tendency in Li₇La₃Zr₂O₁₂ (LLZO) and Rational Design of Interlayer Materials to Prevent Lithium Dendrites. *J. Power Sources* **2018**, *392*, 79–86.
- (263) Aguesse, F.; Manalastas, W.; Buannic, L.; Del Amo, J. M. L.; Singh, G.; Lloldés, A.; Kilner, J. Investigating the Dendritic Growth during Full Cell Cycling of Garnet Electrolyte in Direct Contact with Li Metal. *ACS Appl. Mater. Interfaces* **2017**, *9*, 3808–3816.
- (264) Cao, S.; Song, S.; Xiang, X.; Hu, Q.; Zhang, C.; Xia, Z.; Xu, Y.; Zha, W.; Li, J.; Gonzale, P. M. Modeling, Preparation, and Elemental Doping of Li₇La₃Zr₂O₁₂ Garnet-Type Solid Electrolytes: A Review. *J. Korean Ceram. Soc.* **2019**, *56*, 111–129.
- (265) Li, Y.; Han, J.-T.; Wang, C.-A.; Xie, H.; Goodenough, J. B. Optimizing Li⁺ Conductivity in a Garnet Framework. *J. Mater. Chem.* **2012**, *22*, 15357.
- (266) Park, J. S.; Cheng, L.; Zorba, V.; Mehta, A.; Cabana, J.; Chen, G.; Doeff, M. M.; Richardson, T. J.; Park, J. H.; Son, J. W.; et al. Effects of Crystallinity and Impurities on the Electrical Conductivity of Li-La-Zr-O Thin Films. *Thin Solid Films* **2015**, *576*, 55–60.
- (267) Cheng, L.; Park, J. S.; Hou, H.; Zorba, V.; Chen, G.; Richardson, T.; Cabana, J.; Russo, R.; Doeff, M. Effect of Microstructure and Surface Impurity Segregation on the Electrical and Electrochemical Properties of Dense Al-Substituted Li₇La₃Zr₂O₁₂. *J. Mater. Chem. A* **2014**, *2*, 172–181.
- (268) Schmidt, R. D.; Sakamoto, J. In-Situ, Non-Destructive Acoustic Characterization of Solid State Electrolyte Cells. *J. Power Sources* **2016**, *324*, 126–133.
- (269) Sharafi, A.; Haslam, C. G.; Kerns, R. D.; Wolfenstine, J.; Sakamoto, J. Controlling and Correlating the Effect of Grain Size with the Mechanical and Electrochemical Properties of Li₇La₃Zr₂O₁₂ Solid-State Electrolyte. *J. Mater. Chem. A* **2017**, *5*, 21491–21504.
- (270) Fu, Z.; Gong, Y.; Zhang, L.; Gritton, E.; Godbey, G. L.; Ren, Y.; McOwen, D. W.; Wachsman, E. D. Mechanical Properties of Li₇La_{2.75}Ca_{0.25}Zr_{1.75}Nb_{0.25}O₁₂ Garnet Electrolyte—A Preliminary Study of a Porous Layer Support All-Solid State Battery. In *Meeting Abstracts Electrochemical Society*; Electrochemical Society, 2017.
- (271) Hao, S.; Zhang, H.; Yao, W.; Lin, J. Solid-State Lithium Battery Chemistries Achieving High Cycle Performance at Room Temperature by a New Garnet-Based Composite Electrolyte. *J. Power Sources* **2018**, *393*, 128–134.
- (272) Ohta, S.; Kobayashi, T.; Asaoka, T. High Lithium Ionic Conductivity in the Garnet-Type Oxide Li_{7-X}La₃(Zr_{2-X}, Nb_X)O₁₂ (X = 0–2). *J. Power Sources* **2011**, *196*, 3342–3345.
- (273) Alexander, G. V.; Patra, S.; Sobhan Raj, S. V.; Sugumar, M. K.; Ud Din, M. M.; Murugan, R. Electrodes-Electrolyte Interfacial Engineering for Realizing Room Temperature Lithium Metal Battery Based on Garnet Structured Solid Fast Li⁺ Conductors. *J. Power Sources* **2018**, *396*, 764–773.
- (274) Han, F.; Yue, J.; Chen, C.; Zhao, N.; Fan, X.; Ma, Z.; Gao, T.; Wang, F.; Guo, X.; Wang, C. Interphase Engineering Enabled All-Ceramic Lithium Battery. *Joule* **2018**, *2*, 497–508.
- (275) Ohta, S.; Kobayashi, T.; Seki, J.; Asaoka, T. Electrochemical Performance of an All-Solid-State Lithium Ion Battery with Garnet-Type Oxide Electrolyte. *J. Power Sources* **2012**, *202*, 332–335.
- (276) Tsai, C. L.; Ma, Q.; Dellen, C.; Lobe, S.; Vondahlen, F.; Windmüller, A.; Grüner, D.; Zheng, H.; Uhlenbruck, S.; Finsterbusch, M.; et al. A Garnet Structure-Based All-Solid-State Li Battery without Interface Modification: Resolving Incompatibility Issues on Positive Electrodes. *Sustain. Energy Fuels* **2019**, *3*, 280–291.
- (277) Shao, Y.; Wang, H.; Gong, Z.; Wang, D.; Zheng, B.; Zhu, J.; Lu, Y.; Hu, Y. S.; Guo, X.; Li, H.; et al. Drawing a Soft Interface: An Effective

Interfacial Modification Strategy for Garnet-Type Solid-State Li Batteries. *ACS Energy Lett.* **2018**, *3*, 1212–1218.

(278) Li, Y.; Wang, Z.; Cao, Y.; Du, F.; Chen, C.; Cui, Z.; Guo, X. W-Doped Li₇La₃Zr₂O₁₂ Ceramic Electrolytes for Solid State Li-Ion Batteries. *Electrochim. Acta* **2015**, *180*, 37–42.

(279) Kato, T.; Iwasaki, S.; Ishii, Y.; Motoyama, M.; West, W. C.; Yamamoto, Y.; Iriyama, Y. Preparation of Thick-Film Electrode-Solid Electrolyte Composites on Li₇La₃Zr₂O₁₂ and Their Electrochemical Properties. *J. Power Sources* **2016**, *303*, 65–72.

(280) Liu, B.; Gong, Y.; Fu, K.; Han, X.; Yao, Y.; Pastel, G.; Yang, C.; Xie, H.; Wachsman, E. D.; Hu, L. Garnet Solid Electrolyte Protected Li-Metal Batteries. *ACS Appl. Mater. Interfaces* **2017**, *9*, 18809–18815.

(281) Din, M. M. U.; Murugan, R. Garnet Structured Solid Fast Li⁺ Conductor as Polysulfide Shuttle Inhibitor in Li-S Battery. *Electrochim. Commun.* **2018**, *93*, 109–113.

(282) Xu, S.; McOwen, D. W. D. W.; Wang, C.; Zhang, L.; Luo, W.; Chen, C.; Li, Y.; Gong, Y.; Dai, J.; Kuang, Y.; et al. Three-Dimensional, Solid-State Mixed Electron–Ion Conductive Framework for Lithium Metal Anode. *Nano Lett.* **2018**, *18*, 3926–3933.

(283) Fu, K.; Gong, Y.; Xu, S.; Zhu, Y.; Li, Y.; Dai, J.; Wang, C.; Liu, B.; Pastel, G.; Xie, H.; et al. Stabilizing the Garnet Solid-Electrolyte/Polysulfide Interface in Li–S Batteries. *Chem. Mater.* **2017**, *29*, 8037–8041.

(284) Fu, K. K.; Gong, Y.; Liu, B.; Zhu, Y.; Xu, S.; Yao, Y.; Luo, W.; Wang, C.; Lacey, S. D.; Dai, J.; et al. Toward Garnet Electrolyte–Based Li Metal Batteries: An Ultrathin, Highly Effective, Artificial Solid-State Electrolyte/Metallic Li Interface. *Sci. Adv.* **2017**, *3*, No. e1601659.

(285) Sun, J.; Zhao, N.; Li, Y.; Guo, X.; Feng, X.; Liu, X.; Liu, Z.; Cui, G.; Zheng, H.; Gu, L.; et al. A Rechargeable Li–Air Fuel Cell Battery Based on Garnet Solid Electrolytes. *Sci. Rep.* **2017**, *7*, 41217.

(286) Shao, Y.; Wang, H.; Gong, Z.; Wang, D.; Zheng, B.; Zhu, J.; Lu, Y.; Hu, Y. S.; Guo, X.; Li, H.; et al. Drawing a Soft Interface: An Effective Interfacial Modification Strategy for Garnet-Type Solid-State Li Batteries. *ACS Energy Lett.* **2018**, *3*, 1212–1218.

(287) Xu, S.; McOwen, D. W.; Wang, C.; Zhang, L.; Luo, W.; Chen, C.; Li, Y.; Gong, Y.; Dai, J.; Kuang, Y.; et al. Three-Dimensional, Solid-State Mixed Electron–Ion Conductive Framework for Lithium Metal Anode. *Nano Lett.* **2018**, *18*, 3926–3933.